ABSTRACT

Title of Thesis: THERMAL CYCLING DESIGN ALTERNATIVES FOR THE POLYMERASE CHAIN REACTION

Degree Candidate: Monte Lewis

Degree and Year: Master of Science, 2005

Thesis directed by: Associate Professor Keith E. Herold
Department of Mechanical Engineering

PCR (polymerase chain reaction) is a process by which a small amount of DNA is amplified many times to yield an easily detectable amount. This process is widely used for the detection of bacterial pathogens for biodefense, in basic research, criminal identification, and disease detection in humans. The reaction mixture must be cycled repeatedly between three different temperature levels in PCR. The reaction mixture is first heated at 94 °C, cooled to 54 °C, and then heated to 72 °C. This cycle is repeated 20-40 times.

The main objective of the work reported here is to evaluate alternative heating/cooling schemes for PCR with the ultimate goal of speeding up a PCR reaction. A secondary goal is to arrive at a design that is consistent with battery operation to allow for a portable PCR device. Insight is gained about interactions between the PCR reaction and the engineering system.

The first device analyzed for use as a thermal cycler is a Peltier thermoelectric cooler. A single thermoelectric cooler is characterized. The maximum and average

heating rates and power consumption are determined through experiment. The thermoelectric cooler is evaluated under different conditions and modeled with the lumped capacitance method to reveal the characteristics of the device as a thermal cycler. This Peltier device is used as a heating/cooling system for subsequent work on alternative reaction vessels. A commercially available Peltier thermocycler is also analyzed to determine the heating and cooling rates and power consumption. PCR results are presented that show the time limits of the PCR reaction.

The second device analyzed for use as a thermal cycler is a convective thermocycler. An advantage of the convective thermocycler is it allows for a wide range of vessel geometries. Two variants of convective thermocyclers were built and tested for performance. Heat transfer to a sample is modeled using finite element methods as well as with the lumped capacitance method and corroborated with experiment. Reaction vessels of different sizes and material are modeled in order to better understand the relationship between the air velocity and heating characteristics of the thermal cycler and the reaction volume.

The third device analyzed is a microheater system. The microheater design is arrived at as the preferred design for high speed PCR. Microheaters were fabricated using standard MEMS techniques. Problems encountered in the design, fabrication, and use of these heaters are presented. The microheaters are evaluated for thermal cycling performance under different conditions. Chambers fabricated out of polycarbonate are tested for use as reaction volumes. Two dimensional finite element analysis is used to model these systems and the models are corroborated with experiment. The behavior of liquid in polycarbonate chambers undergoing thermal cycling is investigated. Problems

associated with thermal cycling in polycarbonate chambers is discussed along with possible solutions.

THERMAL CYCLING DESIGN ALTERNATIVES FOR THE POLYMERASE CHAIN REACTION

by

Monte Lewis

Dissertation submitted to the Faculty of the Graduate School of the
University of Maryland, College Park in partial fulfillment
of the requirements for the degree of
Master of Science
2005

Advisory Committee:

Associate Professor Keith E. Herold, Chair
Associate Professor Elisabeth Smela
Assistant Professor Bao Yang

ACKNOWLEDGMENTS

I would like to thank my professor, Dr. Keith Herold, for giving me the opportunity to work for him, for his patience, and for his help in completing this project. I am very thankful to Dr. Jungho Kim for his help on the control system for the microheaters. The USDA funded this work, for which I am grateful. I was very lucky to have worked with our post doc from Ukraine, Andrey Matviyenko who spent many days doing PCR and working on mechanisms for PCR. Nikolai Sergeev and Avi Rasooly also provided valuable input to the project that I am thankful for. I would like to say thank you to Tom Laughran who taught me many things, was always very helpful and responsive, and set an excellent example for cleanroom behavior. Tom also graciously deposited metal on our samples. Nolan Balew and Jon Hummel also provided valuable support in the clean room. I would like to thank the many people I have met in the clean room and provided me with information including Steve Fanning, Samuel Moseley, and Remi Delille. Sayeed Moghaddam and Vytenis Benetis went out of their way to help me in the cleanroom and with the microheater design. I am also thankful to Dr. Elisabeth Smela who allowed the use of her lab equipment and was also an excellent teacher. I would like to thank Lou Hromalo for helping me in several situations. Corey Skurdal also provided valuable input and performed PCR many times. The Terrapin Masters swim team provided me with much needed exercise and camaraderie during my time here for which I am thankful.

TABLE OF CONTENTS

LIST OF TABLES ..... **vi**

LIST OF FIGURES ..... **vii**

SYMBOLS ..... **xiii**

1. INTRODUCTION TO PCR AND THERMOCYCLERS **1**

1.2 PCR reaction and detection reagents 5

1.3 Thermocycler metrics 7

2. TESTING OF PELTIER THERMOCYCLER FOR PCR **10**

2.1 Testing of an independent TEC, apparatus and procedures 10

2.2 Independent TEC testing results 13

2.2.1 Heating flux characteristics of TEC 18

2.2.2 Cooling flux characteristics of TEC 26

2.2.3 Power consumption 29

2.3 Independent TEC testing discussion 29

2.4 Testing of a commercially available Peltier thermocycler, apparatus and procedures 31

2.4.1 Commercial Peltier thermocycler testing results 33

2.4.2 Power consumption of the commercial device 34

2.4.3 PCR results with the commercial device 35

3. ANALYSIS OF CONVECTIVE THERMOCYCLERS FOR PCR **42**

3.1 Testing of a convective thermocycler, apparatus and procedures 42

3.2 Convective thermocycler test results 45

3.2.1 Power consumption of convective thermocyclers 49

3.2.2 Convection characteristics of the thermocycler 50
3.2.3 System response with a test sample 55
3.3 Convective thermocycler options to enhance performance 66
4. ANALYSIS OF MICROHEATERS FOR PCR 77
4.1 Synopsis of work done on microheaters by other groups 77
4.1.1 Comparison of designs 82
4.2 Microheater design 85
4.2.1 Electronic control system design 95
4.3 Microheater fabrication 99
4.3.1 Microheater fabrication equipment and techniques 99
4.3.2 Microheater fabrication sequence 101
4.3.3 Microheater fabrication results 103
4.4 Microheater heat treatment and calibration 106
4.5 Microheater testing 110
4.5.1 Microheater testing results 112
5. MICROCHAMBERS FOR PCR 116
5.1 Microchamber design considerations 124
5.2 Microchamber fabrication equipment and techniques 134
5.3 Microchamber testing 136
5.3.1 Countersunk polycarbonate chambers 137
5.3.2 Glass capillaries 139
5.3.3 Thermally bonded polycarbonate chambers 140
5.3.3.1 Thermally bonded polycarbonate chamber sealing 145

6. SUMMARY, CONCLUSIONS AND FUTURE WORK.....149

6.1 Summary.....149

6.1.1 Testing of Peltier thermocyclers.....150

6.1.2 Testing of convective thermocyclers.....150

6.1.3 Testing of a microheater thermocycler.....151

6.2 Conclusions.....152

6.3 Future work.....157

REFERENCES.....159

LIST OF TABLES

Table 1.1 Primer sequences used in amplification of *B. anthracis* 6

Table 2.1 Properties of aluminum oxide used in the analysis 18

Table 2.2 Comparison of TEC with and without cooling fan 29

Table 2.4 Protocol for elongation time experiment.....35

Table 3.1 Results of air velocity analysis for single and double fan convective thermocyclers 53

Table 3.2 Nusselt number and convection coefficients for single and double fan convective thermocycler 55

Table 3.3 Calculated time constants (τ) for the air velocities within the single and double fan convective thermocycler for a modeled 200 µL polypropylene tube with 10 µL of water 57

Table 3.4 Polypropylene properties 58

Table 3.5 Thermal conductivities of candidate materials for PCR reaction vessels 73

Table 3.6 Biot number for varying polypropylene cylindrical diameters 74

Table 4.1 Comparison of thermocycling devices.....84

Table 4.2 Result of heat treatment on heater and temperature probe.....107

Table 4.3 Comparison of microheater operation with and without heat sink 115

Table 5.1 Model to predict pressure in sealed two-phase system 131

Table 6.1 Comparison of thermocyclers 149

LIST OF FIGURES

Figure 1.1 One cycle of the PCR process....2

Figure 1.2 A PCR cycle showing plateaus at 54, 72 and 94 °C....2

Figure 1.3 Schematic of PCR cycle with dashed areas representing times included in the average power over cycle calculation....8

Figure 2.1 Thermoelectric thermocycler setup....10

Figure 2.2 H-bridge configuration used in the control of the TEC....11

Figure 2.3 Side view of TEC setup....12

Figure 2.4 Simulated PCR cycle for TEC without cooling fan , 13.8 V input....14

Figure 2.5 Simulated PCR cycle for TEC with cooling fan on, 13.8V input....14

Figure 2.6 Steady state heating mode of the TEC without cooling fan and 10.0 V input....15

Figure 2.7 Steady state heating mode of the TEC with cooling fan and 10.0 V input....16

Figure 2.8 Steady state cooling mode of the TEC without cooling fan and 13.8 V input....16

Figure 2.9 Steady state cooling mode of the TEC with cooling fan and 13.8 V input....17

Figure 2.10 Heat flux produced by thermoelectric cooler during heating from 72 to 94 °C and corresponding top and bottom of TEC temperature with 13.8 V input, cooling fan....20

Figure 2.11 Calculated Performance of TEC using hot and cold side temperatures from experiment....21

Figure 2.12 2-D geometry used for cooling and heating model....23

Figure 2.13 Calculated temperature for top of the TEC superimposed on graph of actual temperature for top of TEC for 13.8 V input and cooling fan on....23

Figure 2.14 Heat flux produced by thermoelectric cooler during heating from 72 to 94 °C with 13.8 V input, cooling fan off....24

Figure 2.15 Calculated temperature from 2-D model for top of the TEC superimposed on graph of actual temperature for top of TEC for 13.8 V input and cooling fan off 25

Figure 2.16 Cooling flux produced by thermoelectric cooler during cooling from 94 to 54 °C, 13.8 V Input, cooling fan on 26

Figure 2.17 2-D calculated temperature for top of the TEC superimposed on graph of actual temperature for top of TEC for 13.8 V input and cooling fan on 27

Figure 2.18 Cooling flux produced by TEC during cooling from 94 to 54 °C, 13.8 V input, cooling fan off 28

Figure 2.19 Techne thermocycler analyzed in this section 31

Figure 2.20 Aluminum heating block mounted on top of TECs in Techne thermocycler 32

Figure 2.21 Simulated PCR cycle using commercial Peltier thermocycler 33

Figure 2.22 PCR reaction results for extension time test, 40 s elongation time 36

Figure 2.23 PCR reaction results for extension time test, 30 s elongation time 37

Figure 2.24 PCR reaction results for extension time test, 25 s elongation time 38

Figure 2.25 PCR reaction results for extension time test, 30 s elongation time with 15 s at denaturation and annealing steps..... 39

Figure 2.26 Glass capillaries run with a 1/4000 volumetric concentration of ethidium bromide..... 40

Figure 3.1 Convective thermocycler setup #1 42

Figure 3.2 Heater mounted within vent pipe 43

Figure 3.3 Double fan convective thermocycler setup 43

Figure 3.4 Heater element within double fan convective thermocycle 44

Figure 3.5 Simulated PCR cycle using the single fan convective thermocycler..... 46

Figure 3.6 Simulated PCR cycle using the double fan convective thermocycler 46

Figure 3.7 Cross section of single fan convective thermocycler showing mixing walls located within vent pipe.....52

Figure 3.8 Radial temperature measurements for single fan convective thermocycler with heater and fan at duty cyle = 1.....48

Figure 3.9 Schematic of control volume used for air velocity determination.....50

Figure 3.10 200 µL PCR tube with 10 µL of water used in convective analysis.....55

Figure 3.11 2-D model used for convective analysis of 200 µL polypropylene tube filled with 10 µL of water.....58

Figure 3.12 Experimental results for single fan convective thermocycler with 200 µL tube filled with 10 µL of water placed inside vent pipe.....59

Figure 3.13 2-D model correlation with experimental results for single fan convective thermocycler with 200 µL PCR tube containing 10 µL of water during heating from 52 – 94 °C.....60

Figure 3.14 2-D model correlation with experimental results for single fan convective thermocycler with 200 µL PCR tube during cooling from 94 – 52 °C.....61

Figure 3.15 Experimental results for double fan convective thermocycler with 200 µL polypropylene tube filled with 10 µL of water placed inside vent pipe.....62

Figure 3.16 Lumped capacitance model with experimental results for double fan convective thermocycler with 200 µL PCR tube during heating from 54–94 °C.....63

Figure 3.17 Lumped capacitance model with experimental results for double fan convective thermocycler with 200 µL PCR tube during cooling from 94–54 °C.....65

Figure 3.18 Plot of time constant versus air velocity for cylindrical configuration with constant diameter, length, wall thickness, surface temperature, and air temperature.....67

Figure 3.19 Plot of time constant versus diameter for cylindrical polypropylene configuration.....68

Figure 3.20 Lumped capacitance model of reaction volume temperature for glass capillary of 890 µm outside diameter with 5 µL of water inside.....70

Figure 3.21 Plot of time constant versus diameter for spherical configuration with constant air velocity, and wall thickness 72

Figure 3.22 Biot number versus wall thickness for a poly propylene capillary of outside diameter 890 μm 75

Figure 3.23 Biot number versus wall thickness for a glass capillary of outside diameter 890 μm 76

Figure 4.1 Heater with integrated well as designed by El-Ali et al. 78

Figure 4.2 PCR reaction vessel designed by Zhao et al. 80

Figure 4.3 Microheaters with integrated reaction vessels as designed by Zou et al. 81

Figure 4.4 Flip chip design process used by Zou et al. for fabrication of PCR microheaters 82

Figure 4.5 Schematic of 2-D model used in analysis of heating power 86

Figure 4.6 Response of 3.2 mm diameter polycarbonate chamber of thickness 2 mm with 10 μL of water in it and a heat flux of 20 W/cm^2 86

Figure 4.7 Response of 5 mm diameter polycarbonate chamber of depth 2 mm with a 10 μL sample of water in it and a heat flux of 20 W/cm^2 88

Figure 4.8 Schematic of 5 mm heater 91

Figure 4.9 Exploded view of 5 mm heater with some elements deleted for clarity 92

Figure 4.10 Schematic of 2.5 mm heater 93

Figure 4.11 Exploded view of 2.5 mm heater 94

Figure 4.12 Gold lead mask for 5 mm heater 95

Figure 4.13 Gold lead mask for 2.5 mm heater 95

Figure 4.14 Circuit schematic for microheater control 96

Figure 4.15 Schematic of circuit used to measure temperature of platinum temperature sensor 98

Figure 4.16 Simplified fabrication sequence for microheaters 101

Figure 4.17 Effect of chlorobenzene on photoresist development 102

Figure 4.18 Delamination of heater elements from soda lime glass substrate 104

Figure 4.19 Heater elements from a heater with no discontinuities 105

Figure 4.20 Comparison of 30 μm heater elements with 50 μm temperature sensor 105

Figure 4.21 Points of resistance measurement for 5 mm microheater 107

Figure 4.22 Temperature versus resistance with linear fit for microheater.....108

Figure 4.23 Temperature versus resistance graph with linear fit for microheater temperature sensor 109

Figure 4.24 Comparison of initial calibration of temperature sensor and after 1 week of use 110

Figure 4.25 Microheater test fixture.....111

Figure 4.26 Microheater test fixture with microheater mounted on heat sink 112

Figure 4.27 Heating and cooling characteristics of microheater with cooling fan, no heat sink, 12 V input 113

Figure 4.28 Heating and cooling characteristics of microheater with cooling fan, heat sink, 12 V input 114

Figure 5.1 Silicon reaction chamber fabricated by Daniel et al. 116

Figure 5.2 Simplified fabrication sequence used by Daniel et al. 117

Figure 5.3 Polycarbonate chamber fabricated by Yang et al. 120

Figure 5.4 2-D heat transfer model for polycarbonate chamber 124

Figure 5.5 2-D conduction model of 5 mm square polycarbonate chamber on 5 mm square microheater 125

Figure 5.6 2-D conduction model of 3 mm square polycarbonate chamber on 5 mm square microheater 126

Figure 5.7 2-D conduction model of 3 mm square silicon chamber on 5 mm square microheater 127

Figure 5.8 Schematic of 800 μm capillary on microheater 129

Figure 5.9 Polycarbonate reaction vessel thermally bonded from three 250 μm thick sheets....130

Figure 5.10 Predicted pressure rise inside closed reaction vessel with water and 33% of the volume filled with air....132

Figure 5.11 Predicted bubble volume inside closed reaction vessel with water and 33% of the volume filled with air....133

Figure 5.12 Polycarbonate chamber fabricated from three 250 μm thick sections....134

Figure 5.13 Countersunk polycarbonate chambers created with router bit....135

Figure 5.14 Bubble formation in untreated polycarbonate chambers covered with mineral oil....137

Figure 5.15 2 mm thick polycarbontate after O_2 plasma etch at A)100 W, B) 200 W, C) 250 W....138

Figure 5.16 PCR cycle showing 5 mm square microfabricated heater and temperature inside a 400 μm inside diameter glass capillary filled with ethylene glycol....140

Figure 5.17 PCR cycle showing 5 mm square microfabricated heater and temperature inside a 5 mm square polycarbonate reaction volume filled with ethylene glycol....141

Figure 5.18 Simulated PCR cycle showing 5 mm square microfabricated heater and temperature inside a 3 mm square polycarbonate reaction volume filled with ethylene glycol....142

Figure 5.19 Simulated PCR cycle showing 5 mm square microfabricated heater and temperature inside a 3 mm square polycarbonate reaction volume with a 125 μm thick top and bottom section filled with ethylene glycol....144

Figure 5.20 Simulated PCR cycle showing 5 mm square microfabricated heater and temperature inside a 3 mm square polycarbonate reaction volume with a 125 μm thick bottom section and a 250 μm thick top section filled with ethylene glycol....145

SYMBOLS

A	area, m^2	Bi	Biot number
c	specific heat, J/kg K	c_p	specific heat
D	diameter, m		at constant pressure, J/kg K
f	friction factor; fraction	G	area/length of
h	convection coefficient, W/m^2 K;		thermoelectric device (cm)
	enthalpy, J/kg		
I	electrical current, A	k	thermal conductivity, W/m K
L	length, m	m	mass, kg
N	number	Nu	Nusselt number
P	power, W; Pressure, N/m^2	Pr	Prandtl number
q	heat transfer rate, W	q''	heat flux, W/m^2
R	electrical resistance, Ω; universal gas	Re	Reynolds number
	constant divided by the molecular		
	weight, kJ/kg K		
T	temperature,°C, K	t	time, s; thickness, m
V	voltage, V; volume, m^3; Velocity, m/s	W	percent on time; work, J
w	width, m	x	displacement, m; quality

Greek letters

α	Seebeck coefficient, V/K	Δ	change in
υ	specific volume, m^3/kg	μ	viscosity, kg/s m
ρ	mass density, kg/m^3; electrical	τ	time constant, s
	resistivity, Ω-m		

Subscripts

air	refers to air	*ave*	average
B	beginning	*c*	during cooling; cold
D	diameter		side; characteristic
E	end	*h*	during heating, hot side
i	initial condition; inlet condition	*l*	liquid
max	maximum	*min*	minimum
n	point n	*o*	outlet condition
P	parallel	*p*	polypropylene
RT	thermometer resistance	*S*	series
s	surface; solid	*t*	thermal; thermometer
tot	total	*v*	vapor
w	water	*wl*	liquid water
wv	water vapor	∞	free stream conditions

Overmarks

$\dot{}$	per unit time, /s	$\bar{}$	surface average conditions, time mean

1. INTRODUCTION TO PCR AND THERMOCYCLERS

PCR is a process by which a small amount of DNA is amplified many times to yield an easily detectable amount. This process is widely used for the detection of bacterial pathogens for biodefense (Draghici, Khatri et al. 2005; Hindson, Makarewicz et al. 2005). PCR is also utilized in other applications such as basic research, criminal identification, and disease detection in humans (Aryee, Bailey et al. 2005; Gill 2005). DNA, primers that dictate what part of the DNA is to be copied, nucleotides that form the building blocks for copying, buffer, polymerase that is the machine for copying, and magnesium ions are needed for the reaction (Cadoret, Rousseau et al. 2005). Three temperature levels are required in a typical PCR reaction. The first step involves heating to around 94 °C. The double stranded DNA is denatured, or split into two single strands during this step. The second step involves cooling to approximately 54°C to allow the primers to attach to the single-stranded DNA. The primers are what determine which section of DNA will be copied. They are designed such that they straddle a predetermined specific site on the DNA based on the sequence of the DNA. The third step is performed at around 72 °C. The actual copying of the DNA is performed by the DNA polymerase during this step. The DNA polymerase attaches to the primer site and copies DNA using the nucleotides that are in solution as building blocks. This cycle is repeated approximately 30 times (Nam, Srinivasan et al. 2005). The steps in the PCR cycle are illustrated graphically in Figure 1.1. The temperature profile of a PCR cycle is shown in Figure 1.2.

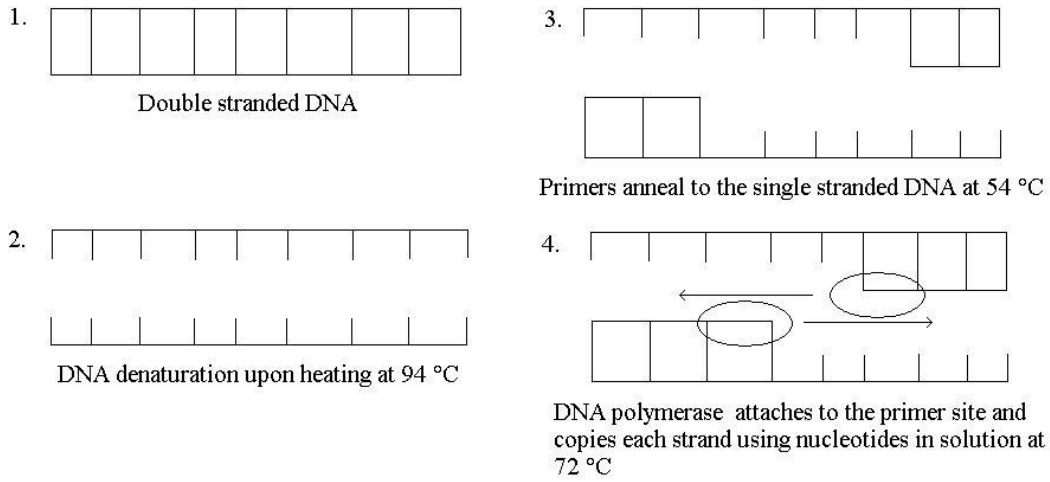

Figure 1.1 One cycle of the PCR process (Vierstraete 2004)

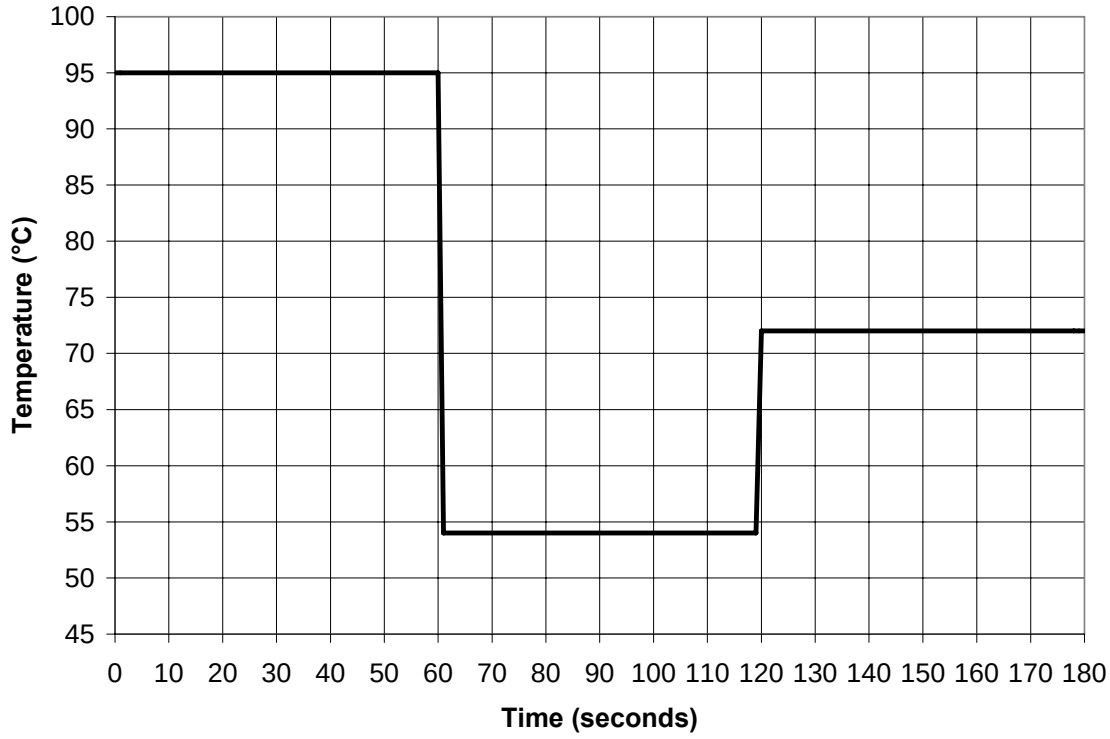

Figure 1.2 A PCR cycle showing plateaus at 54, 72, and 94 °C

A typical PCR reaction in a commercial thermocycler takes between 30 minutes (LightCycler) and 2 hours (typical Peltier systems). This time duration is acceptable for some applications, however, many other applications exist where a rapid reaction is desirable such as clinical applications where treatment depends on the result. The primary objective of this thesis was to investigate system alternatives for high speed PCR. A secondary objective was to minimize power consumption to allow eventual portable operation with battery power. A series of alternative designs were tested in this effort and each was found to have a set of unique and useful characteristics.

The cycle time can vary based on the situation. The cycle time is strongly dependent upon the characteristics of the thermocycler. If the thermocycler takes a long time to reach the setpoint, then this must be accommodated. If heat conduction or convection is slow through the reaction chamber in spite of a fast heater, then the cycle time would also be longer. PCR reactions run in this lab in commercially available Peltier type thermocyclers are usually run for two hours. This type of thermocycler has an aluminum heating block that weighs 41 g. This block takes time to heat up and slows the heating of the actual reaction volume. The commercially available convective LightCycler has been reported to produce PCR results in as little as 20 minutes (Nitsche, Steur et al. 1999). One reason PCR occurs so rapidly in this device is that the reaction volume heats up very quickly. Another factor that influences the speed of a PCR reaction is the length of DNA strand that is to be copied. Shorter strands take less time to copy then longer strands. The insertion rate for nucleotides during primer extension (72 °C) is 50 base pairs /s (Scheinert, Behrens et al. 2005). A base pair (bp) is simply one link between the two single strands of DNA. If the DNA fragment to be copied is only 100

bp then it would require only two seconds at 72 °C to be copied. If the DNA fragment was 400 bp then it would require 8 seconds to be copied. The type of DNA polymerase that is used can significantly alter the reaction time. Hot Start TAQ DNA polymerase requires 15 minutes of heating at 95 °C to become effective. This type of polymerase is commonly used in PCR reactions because it reduces the occurrence of nonspecific amplicons (Kermekchiev, Tzekov et al. 2003). The term amplicon refers to the DNA segments produced from the PCR reaction. Other types of DNA polymerase may not be as specific, but they do not require this 15 minute heating time. In conclusion, the cycle time is influenced by the thermocycler, the reaction volume, the length of the DNA segment to be copied, and the type of DNA polymerase used.

The amplified DNA may be detected in a number of ways. One way is by taking the sample and moving it through a gel with the application of an electric field. Smaller DNA segments migrate through the gel more quickly while larger DNA fragments move more slowly. The DNA fragment is detected by determining how far it migrates through the gel. The distance migrated through the gel is revealed by illuminating the DNA under a UV light source. The UV light causes fluorescent dye that is added to the DNA to fluoresce, thus enabling one to see the location of the DNA fragment. Another method of detection involves the use of probes that have the complementary sequence to the single strand of DNA that is being copied. If probe locations are occupied with double stranded DNA, then it is known that PCR occurred on that particular piece of DNA (Lane, Everman et al. 2004).

PCR requires that the reaction volume undergo changes in temperature, therefore a thermal cycler is needed to perform this operation. Thermal cyclers come in a variety

of shapes and sizes, but generally may be broken down into two branches: convective thermocyclers and conductive thermal cyclers with other types being reported such as microwave assisted (Fermer, Nilsson et al. 2003) and infrared (Lee, Tsai et al. 2004). Convective thermocyclers operate on the principal of flowing air past a reaction vessel in order to increase or decrease the temperature of the reaction vessel. These units consist of a reaction chamber, housing, heater, fan, and control system (Wittwer, Fillmore et al. 1989). The other type of thermocycler relies on conduction from a heated plate to drive the reaction. The heated plate could take on a variety of shapes and sizes varying from a thermoelectric cooler to a microfabricated heater. The purpose of this thesis is to investigate the properties of these different types of thermocyclers.

1.2 PCR reaction and detection reagents

PCR was run many times to determine the efficacy of the thermocyclers tested. Several reagents are necessary to run the reaction. The DNA was genomic DNA from non-infectious *B. anthracis* (Sterne strain) which is the strain used to make vaccine. Hot start TAQ DNA polymerase, 10 X buffer solution, and 25 mM $MgCl_2$ solution supplied by Qiagen were used in all PCR runs. The dNTPs, which are the building blocks the DNA polymerase uses to copy the target DNA, were obtained as a 10 mM solution from Fisher Scientific. Primers that determine which section of DNA is to be copied were designed and ordered from Operon. The gene amplified was the piplc gene of *B. anthacis*. Table 1.1 shows the exact sequence of the primers used and the amplicon length that was expected based on the designated primers.

Table 1.1 Primer sequences used in amplification of *B. anthracis*

Primer	Sequence	Amplicon length
piplc-R	ATA TTT ATC ACA TTT GTA TTT GCT TTA CAT GA	879
piplc-F	CTT CTT GAT ACA ATA ATG GTG ACC ACT	
piplc-R2	ATG AAA CGA TGA ACA ATA GTG AGG A	216

The R and F suffixes at the end of the primer name in the first column of Table 1.1 designate whether the primer was a forward primer or a reverse primer. Forward primers attach to one end of the single stranded DNA segment to be copied while reverse primers attach to the other end of the complementary strand. Copying proceeds as shown in Figure 1.1. The first two primers listed in Table 1.1 were used to amplify a segment of DNA 879 bp long. The third row of Table 1.1 is the reverse primer that was used with the forward primer to produce an amplicon of length 216 bp. Distilled water was used in all reactions. Bovine serum albumin was also added to the reactions. Bovine serum albumin helps to coat the reaction vessel and stop protein adsorption to the surface (Liu, Rauch et al. 2002).

One method used to detect the PCR products was gel electrophoresis. A QS710 horizontal gel electrophoresis unit was obtained from Fisher Scientific. The power supply used with the gel electrophoresis unit was a Buchler DC power supply, model 31153. A Kodak EDA 290 camera stand was mounted on top of a Foto Prep I by Fotodyne UV light source to take pictures of the gel. Kodak 1D version 3.6 was the software used to take the pictures. Omni Pur PCR plus agarose was used to separate the PCR products. The buffer solution used in the electrophoresis unit was TBE Omni Pur 10 X powder. Ethidium bromide was used to attach to the double stranded DNA during gel electrophoresis. Ethidium bromide fluoresces under UV light when attached to

double stranded DNA. Exact gene 100 bp PCR DNA ladder was used to determine the length of PCR amplicons.

Another method used to detect the occurrence of PCR was by adding ethidium bromide to the PCR solution at a concentration of 1:4000 by volume. This method worked well for illuminating PCR product in glass capillaries and sped up the PCR process by skipping the time consuming gel electrophoresis step.

1.3 Thermocycler metrics

Metrics that will be used to discuss the performance of the thermocyclers are heating rate, cooling rate, average heating rate, average cooling rate, and power consumption. The maximum heating rate is defined as the maximum rate of change of temperature when the heater is active during heating within the temperature range of a typical PCR reaction (54 to 94 °C). The heating rate is based on the surface temperature of the heater, or in the case of the convective thermocycler, the air temperature.

$$\dot{T}_h = \left.\frac{dT}{dt}\right|_{\max} \tag{1.1}$$

where T is the temperature and t represents time. The cooling rate is defined as the maximum rate of decrease in temperature during cooling from 94 to 54 °C.

$$\dot{T}_c = \left.\frac{dT}{dt}\right|_{\min} \tag{1.2}$$

The average cooling and heating rate are defined as follows

$$\bar{T}_h = \frac{T_2 - T_1}{t_2 - t_1},\ \bar{T}_c = \frac{T_2 - T_1}{t_2 - t_1} \tag{1.3}$$

The average rates are influenced by the control system implemented to control the temperature of the heater, unlike the maximum heating and cooling rates, which are maximum values calculated when the heater was less inhibited by the control system. The average heating rate would be much faster if the heater was on at full power during the entire interval between T_2 and T_1. This is not the case, however, because the control system intervenes before the heater temperature reaches the set point in order to avoid overshoot.

The energy consumption can be reported in several ways. The maximum energy consumption per unit time during heating and cooling is one of those ways. During the heating stages where the PCR reaction increases in temperature, the heater is on at full power. This means that the power required is given by

$$P = VI \tag{1.4}$$

where P is the power, V is the voltage, and I is current draw of the device.

The power requirement varies throughout the cycle, so the average power over a cycle can be used to characterize the system. The average power over a cycle includes the time required for heating and cooling as well as five seconds of each plateau period as shown in Figure 1.3.

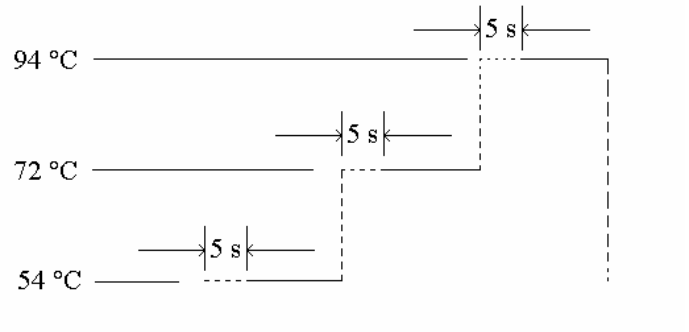

Figure 1.3 Schematic of PCR cycle with dashed areas representing times included in the average power over cycle calculation

The average power is defined in this way in order to compare different heaters. All of the heaters tested had at least a five second plateau period, so this method would compare them with the same standard. The average power over a cycle could be increased or decreased if the energy of a very long plateau was included in the calculation. The average power over a cycle is given by the following equation

$$P_{ave/cycle} = \frac{1}{N}\sum_{0}^{N} P_n t \tag{1.5}$$

where $P_{ave/cycle}$ is the average power over a cycle, N is the number of seconds in the cycle, t is the time of each period, and P_n is the power used by the system during period n.

Some of the systems described in this thesis were controlled using a pulse width modulation scheme where the power was applied during some fraction of each control period (period used here was 1 sec). This control scheme is referred to as pulse width modulation (PWM). In this case, P_n is given by

$$P_n = VIW \tag{1.6}$$

where W is the time per period that the heater was on.

2. TESTING OF PELTIER THERMOCYCLER FOR PCR

A thermoelectric cooler (TEC) was tested to determine its efficacy for performing PCR. The thermoelectric cooler was mounted on an aluminum heat sink with an attached cooling fan. The TEC was tested for power consumption, heating and cooling rate, and heating and cooling flux. A commercially available thermocycler using four thermoelectric coolers with an aluminum block to hold reaction vessels was also tested to determine the same properties.

2.1 Testing of an independent TEC, apparatus and procedures

A single TEC was tested using the setup shown in Figure 2.1. A Mastech power supply was used as the voltage source. A Type T thermocouple was used to monitor the temperature of the surface of the heater. The InstruNet was used as the data acquisition and controller for the setup.

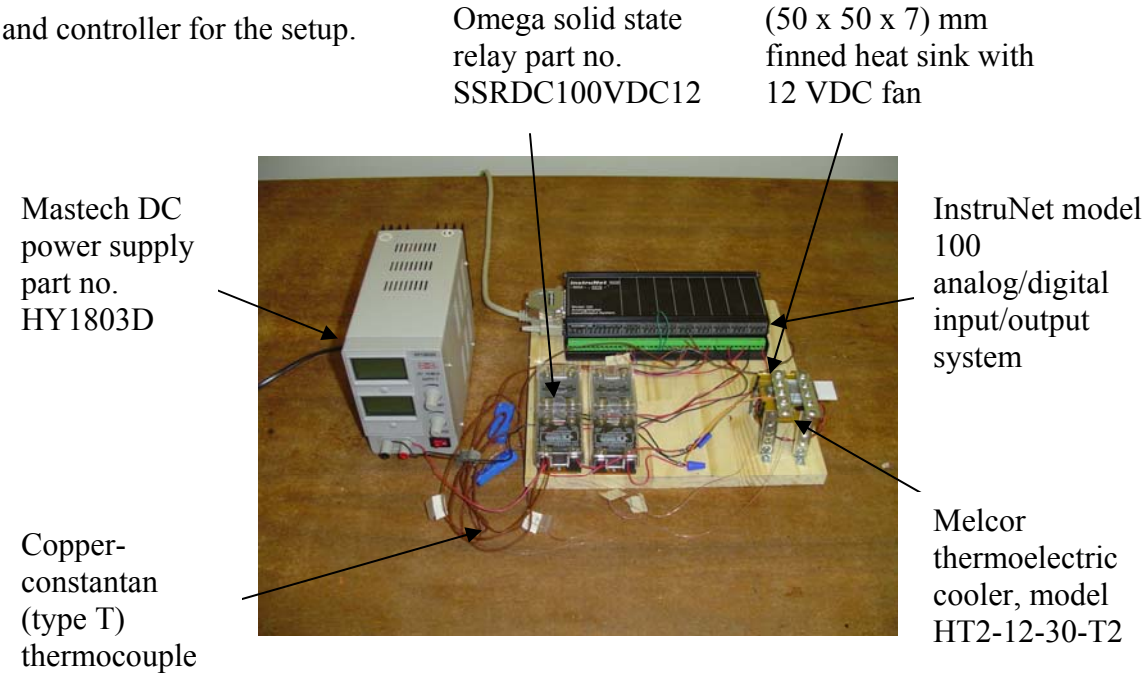

Figure 2.1 Thermoelectric thermocycler setup

The thermoelectric cooler (TEC) was controlled with a Visual Basic program interfaced with the InstruNet model 100 analog/digital input/output system. The TEC was controlled with a pulse width modulation scheme with a pulse frequency of 1 Hz. The program calculated the appropriate pulse width and controlled the relays accordingly via the InstruNet interface. Four solid state relays were utilized in an H-bridge configuration allowing the direction of the current to be switched based on whether the TEC was in heating or cooling mode as shown in Figure 2.2.

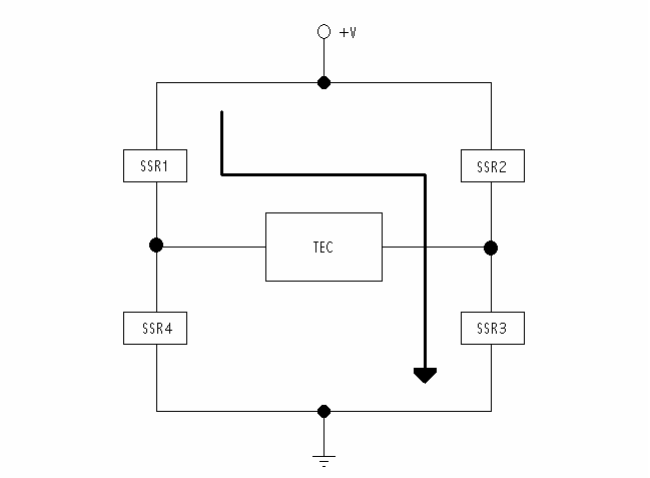

Figure 2.2 H-bridge configuration used in the control of the TEC. The components labeled SSRi are solid state relays. Arrow on figure shows current flow in heating mode.

A forward current flows through the TEC when SSR1 and SSR3 are opened via a signal from InstruNet (SSR2 and SSR4 remain closed). This is the heating mode of operation. The TEC was put in cooling mode by closing SSR1 and SSR3 and opening SSR2 and SSR4. This configuration allowed current to flow through the TEC in the opposite direction.

The thermoelectric cooler was placed on the heat sink as shown in Figure 2.3. The bottom of the TEC was coated with synthetic grease to aid in heat transfer between the heat sink and the TEC. A glass slide, representing an in situ PCR configuration, was mounted on top of the TEC and held in place with two metal strips. The thermocouple was attached to the slide and held in place with a piece of tape. The purpose of this thermocouple was to control the temperature of the slide. Another thermocouple was taped to the heat sink. In some tests, thermocouples were attached to the top and bottom surfaces of the TEC with glue in order to monitor the temperature of those two surfaces. Voltage and current readings were obtained from the digital display on the power supply (Mastech HY1803D). The TEC was tested over the range 9 – 13.8 VDC to assess the effect on power consumption.

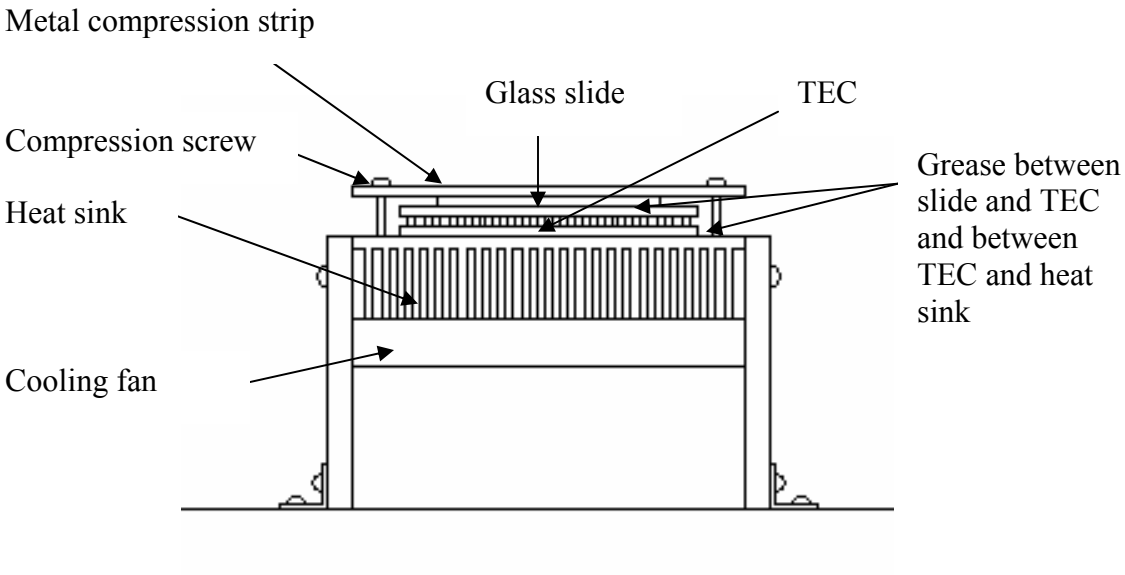

Figure 2.3 Side view of TEC setup

The data acquisition program recorded data once per second. Data recorded included the temperature of the slide and top of TEC, the pulse width, time, and set point

temperature (set point temperature varied during the run according to a programmed input function). Using the recorded data, heating rate, cooling rate, and power consumption were calculated. Only the power used by the heater was included in the calculations for power consumption. Power consumed by the heat sink cooling fan, the computer, and power supply were not included. The heating and cooling rates were calculated as described in the thermocycler metrics section.

2.2 Independent TEC testing results

The TEC was tested with two different configurations to determine its behavior under different conditions. The first condition was with the cooling fan on the heat sink on. The fan was run continuously and was never turned off. The second condition was with the fan on the heat sink off at all times.

The maximum heating rate for the TEC was 5.78 K/s with an input voltage of 13.8 V without the heat sink fan turned on as shown in Figure 2.4. The top of TEC curve in Figure 2.4 also shows that the average heating rate for heating between 72 and 94 °C was 2.0 K/s while the average heating rate between 54 and 72 °C was 1.4 K/s. The maximum cooling rate for this setup was 5.2 K/s. The average cooling rate between 94 and 54 °C was 4.3 K/s.

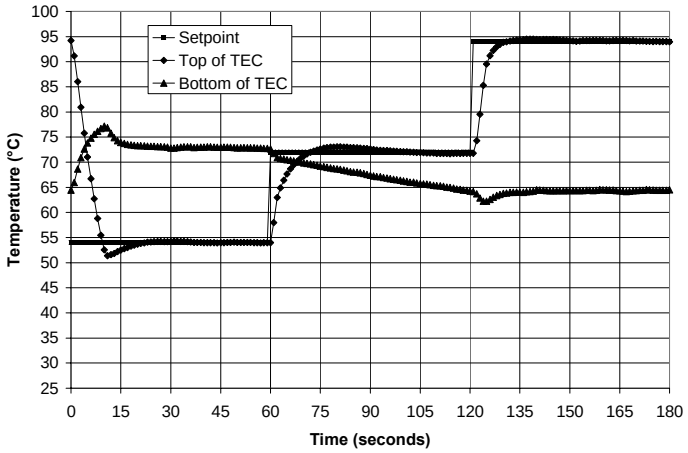

Figure 2.4 Simulated PCR cycle for TEC without cooling fan , 13.8 V input

The TEC was next tested with the cooling fan on the heat sink on. The top of TEC trace in Figure 2.5 was used to calculate the maximum heating and cooling rates as well as the average rates. The maximum heating rate was 5.2 K/s. The average heating rate between 54 and 72 °C was 1.8 K/s while the average heating rate between 72 and 94 °C was 1.3 K/s. The maximum cooling rate of the TEC with cooling fan was 6.6 K/s. The average cooling rate was 5.8 K/s.

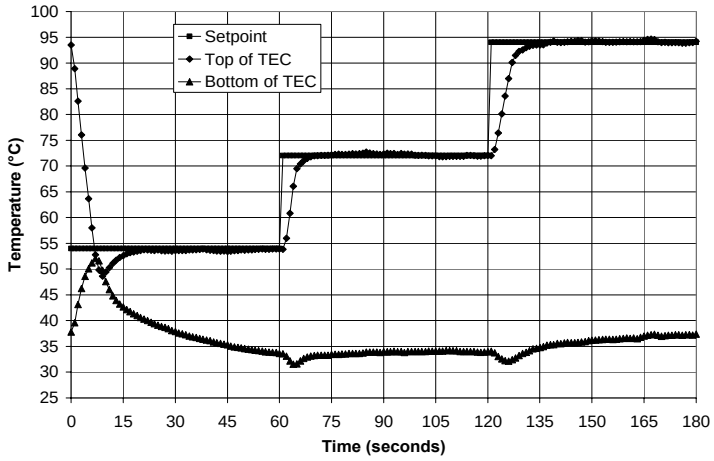

Figure 2.5 Simulated PCR cycle for TEC with cooling fan on, 13.8V input

The TEC was next tested to determine its behavior at steady state. The TEC was allowed to reach steady state while receiving full power (duty cycle = 1) and the results were recorded. The TEC was powered with 10 V during this testing. The results for the case where the TEC was allowed to reach steady state in heating mode with no cooling fan are shown in Figure 2.6. Heating mode means that the top of the TEC was hot while the side against the heat sink was cold.

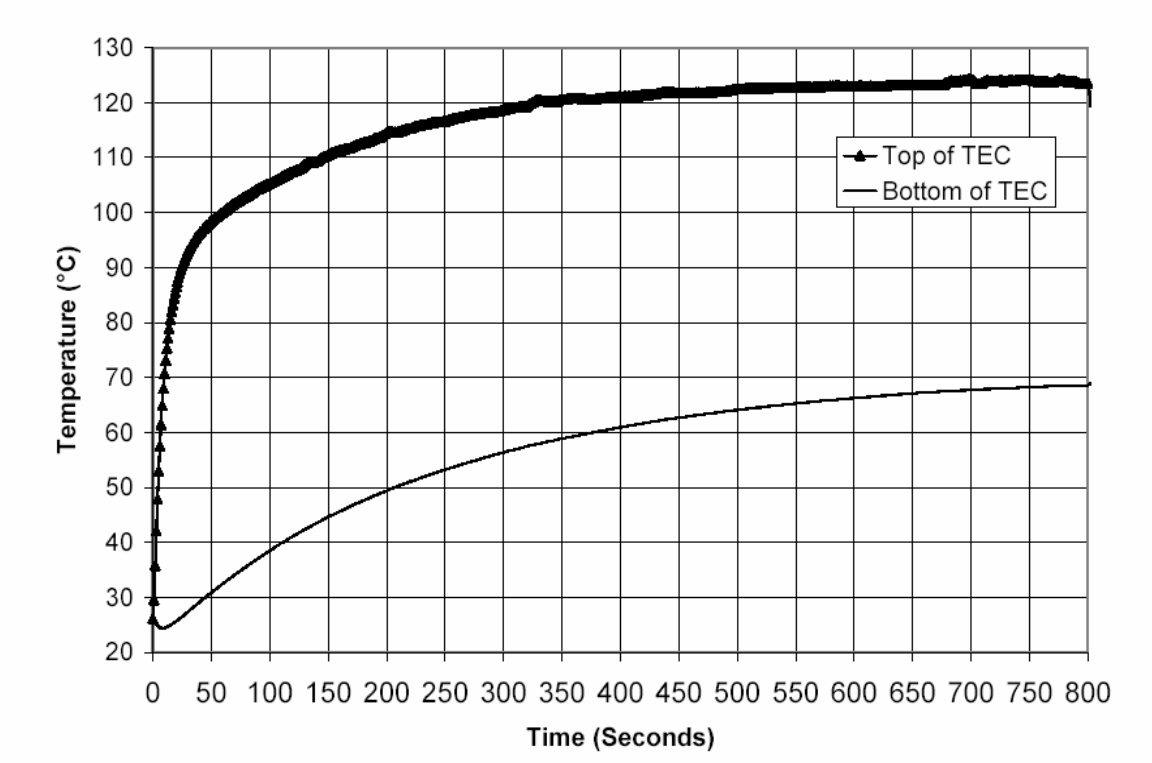

Figure 2.6 Steady state heating mode of the TEC without cooling fan and 10.0 V input

The final temperature differential between hot and cold side was 55 K for the case where the TEC was run in heating mode at steady state. The cold side temperature grew to approximately 70 °C by the end of the test.

The TEC was run in heating mode at steady state with the cooling fan on. The results of the test with a 10.0 V input are shown in Figure 2.7. The temperature of the

cool side was limited to 40 °C. The final temperature differential between hot and cold side was 63 K as shown in Figure 2.7.

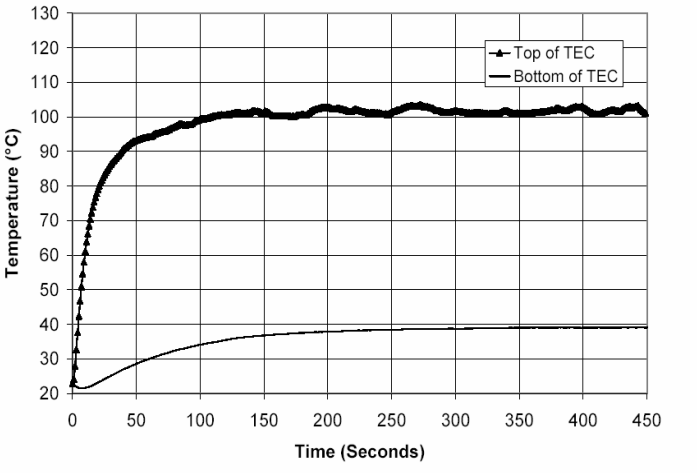

Figure 2.7 Steady state heating mode of the TEC with cooling fan and 10.0 V input

The TEC was next operated at steady state conditions in cooling mode with a 13.8 V input. The top of the TEC was the cold side during cooling while the hot side was against the heat sink. The TEC was supplied with full power during this test and no control system was used. The results were recorded until the system reached steady state.

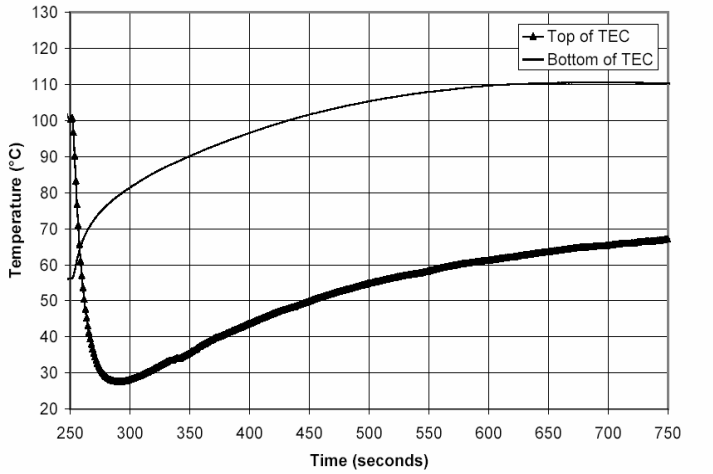

Figure 2.8 Steady state cooling mode of the TEC without cooling fan and 13.8 V input

The steady state cooling mode of the TEC is shown in Figure 2.8. The final temperature differential between hot and cold side was 42 K. It is noted that the cold side trace in Figure 2.8 does not appear to be at steady state because this test was terminated early. However, with the exception of an accurate measurement of the steady state temperature difference, this test demonstrated the key aspects of interest.

A similar test with the cooling fan on is shown in Figure 2.9. The test shows the cooling characteristics of the TEC from 94 °C. The test was run until steady state was reached, as can be seen from the graph. The cold side of the TEC decreased to almost 0 °C. A temperature differential between top and bottom of approximately 50 K was established.

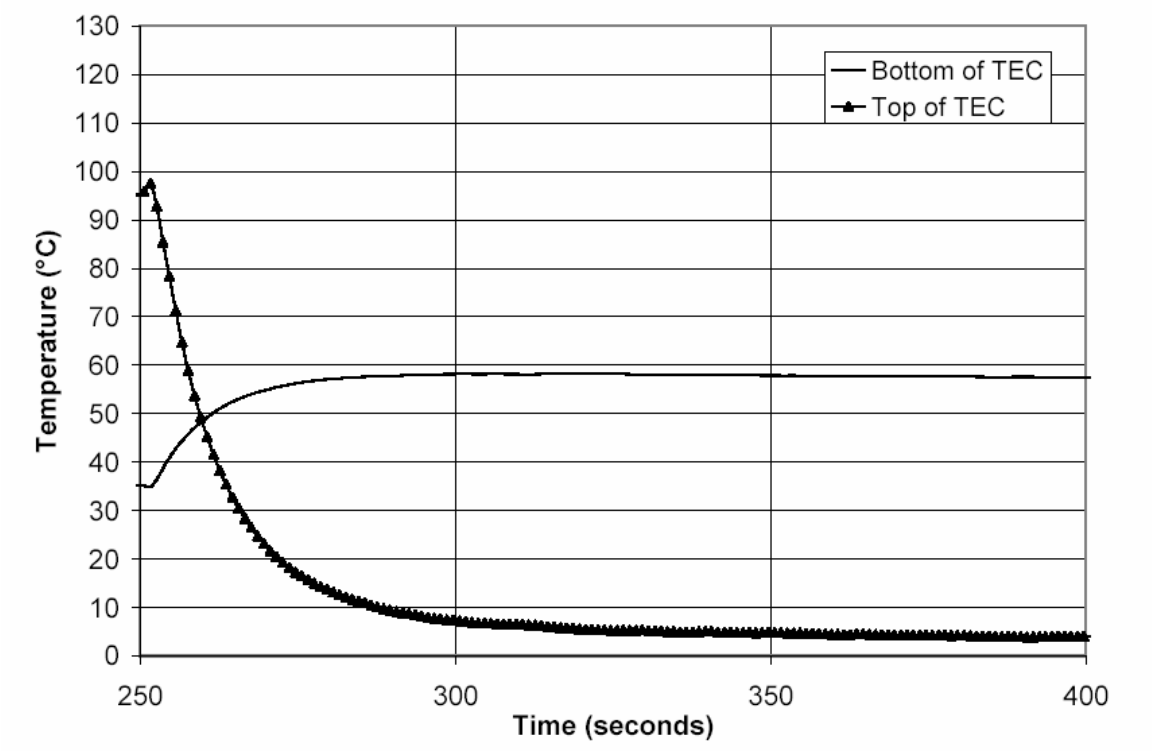

Figure 2.9 Steady state cooling mode of the TEC with cooling fan and 13.8 V input

2.2.1 Heating flux characteristics of TEC

Modeling was done to better understand the heat flux characteristics of the TEC. The data from the thermocouple placed on top of the TEC was used to calculate the heat flux as a function of time during the heating and cooling modes of the TEC. The heating of the top surface of the TEC which is made of aluminum oxide, also known as alumina, is a transient problem, therefore transient methods must be used. The lumped capacitance model is useful because it does not consider heat conduction within the solid. The lumped capacitance method utilizes an energy balance around the solid. This approach allows one to solve the transient problem easily. The lumped capacitance is most accurate in situations where the Biot number is much less than one. If the Biot number is much less than one, then convection from the surface occurs much more readily than conduction within the solid, therefore conduction within the solid may be ignored (Incropera and DeWitt 1996). Radiation effects were ignored in this case and the convection coefficient was assumed to be constant with time. The lumped capacitance method was selected to model this transient problem because the Biot number in this case is 1.26×10^{-4}, assuming that the convection coefficient is 5 W/m^2K, the characteristic length is 1 mm, and aluminum oxide has the properties shown in Table 2.1.

Table 2.1 Properties of aluminum oxide used in the analysis (Accuratus 2005)

Property	Aluminum Oxide
Thermal Conductivity (W/m K)	25
Density (kg/m^3)	3720
Specific Heat (J/kg K)	880

The use of the lumped capacitance method greatly simplifies the problem. For the conditions of this problem, the lumped capacitance model has an analytical solution as (Incropera and DeWitt 1996)

$$\frac{T - T_\infty}{T_i - T_\infty} = \exp(-at) + \frac{b/a}{T_i - T_\infty}(1 - \exp(-at)) \tag{2.1}$$

where a and b are given by

$$a = \frac{hA_S}{\rho Vc} \text{ and } b = \frac{q_s'' A_s}{\rho Vc} \tag{2.2}$$

Equations 2.1 and 2.2 were solved implicitly for the heat flux using temperature data from the test. This was possible because the temperature at the beginning and end of each second was known and could be inserted into the equation for T and T_i. All of the other variables are known, except for q_s''. The properties used in the equation are the alumina properties listed in Table 2.1. The other variables were

A_s=0.0009 m^2 (0.030 x 0.030) m^2, surface dimensions of alumina

V=9 x 10^{-7} m^3 (0.030 x 0.030 x 0.001) m^3, volume of alumina

The heat flux produced by the TEC during heating from 72 to 94 °C with cooling fan as calculated with the lumped capacitance method is graphed in Figure 2.10 along with the corresponding temperature of the top and bottom of the TEC. The TEC was on at full power for the first five seconds of the cycle meaning that the duty cycle was 100%, after that the duty cycle was controlled with the control system. The maximum heat flux within the 72 to 95 °C range with a 13.8 V input and cooling fan on was 1.23 W/cm^2. The maximum heat flux occurred at t = 3 seconds. The heat flux decreased for the next two seconds despite the fact that the TEC was on at full power.

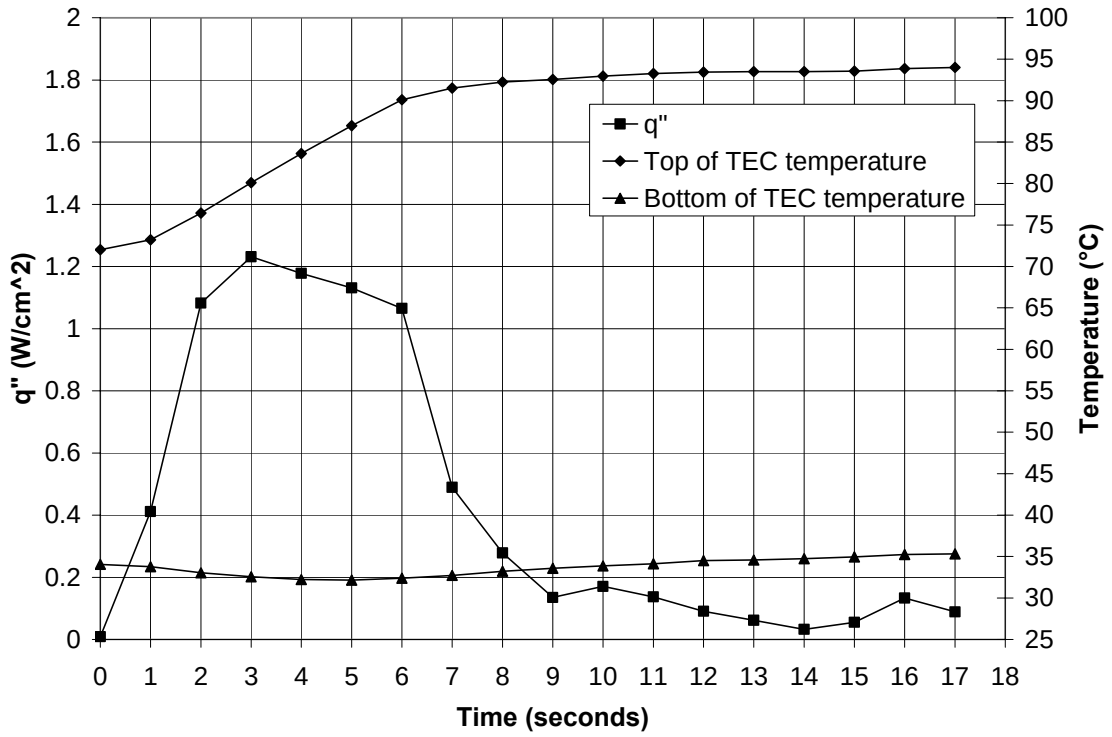

Figure 2.10 Heat flux produced by thermoelectric cooler during heating from 72 to 94 °C and corresponding top and bottom of TEC temperature with 13.8 V input, cooling fan.

The reason the heat flux increased to a maximum and then began to decrease, despite the fact that the TEC was on at full power can be attributed to the characteristics of the TEC. The relevant governing equations of a TEC are given by (Melcor 2005)

$$q_c = 2N(\alpha I T_C - \frac{I^2 \rho}{2G} - k\Delta T G) \tag{2.3}$$

$$V = 2N(\frac{I\rho}{G} + \alpha\Delta T) \tag{2.4}$$

$$q_h = \dot{W} + q_c \tag{2.5}$$

Where q_c is the heat pumped at the cold surface of the TEC, q_h is the heat pumped at the hot surface of the TEC, N is the number of thermocouples in the TEC, α is the Seebeck

coefficient, I is the electrical current consumed by the TEC, T_c is the cold side temperature, ρ is the resistivity of the bismuth telluride which makes up the TEC junctions, G is the area divided by the length of a thermoelectric element, k is the thermal conductivity of the bismuth telluride, ΔT is the difference in temperature between the hot side and the cold side of the TEC, V is the voltage supplied to the TEC, and $\dot{W}$ is the power supplied to the TEC via the power supply.

These equations may be used to estimate the performance of the TEC and determine trends in its performance. The calculated heating and cooling fluxes as well as the current for the TEC were determined by inserting the recorded values for the hot and cold side temperatures into equations 2.3-2.5 with the supply voltage value of 13.8 V. The material properties of the bismuth telluride are variable with temperature and were obtained from the manufacturer (Melcor 2005). The results of the analysis are shown in Figure 2.11.

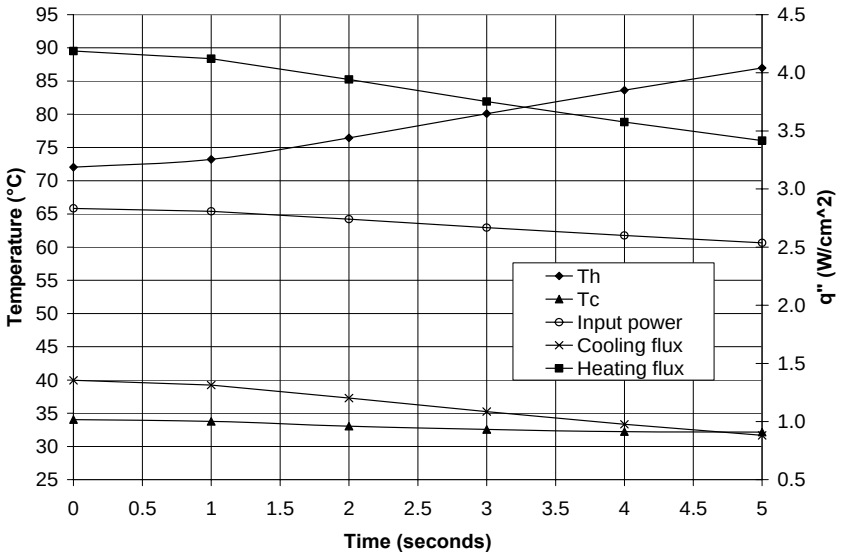

Figure 2.11 Calculated Performance of TEC using hot and cold side temperatures from experiment

The hot and cold side temperatures are plotted on the left axis while the heating flux, cooling flux, and input power per unit area are plotted against the right axis. The results indicate that as the difference in temperature between the hot and cold side of the TEC increases, the heat flux, input power, and cooling flux all decrease. The reason for this is clear looking at Equations 2.3-2.5. The value of q_c decreases as the temperature difference increases because T_c decreases and ΔT increases. The power decreases also because the current decreases as the difference in temperature between the hot and cold side increases.

The reason that the heat flux increases and then decreases, even though the TEC was operating at full power is because as the temperature difference between top and bottom increases, the heating flux decreases as the above analysis shows. The initial ramp of the heating flux may be attributed to transient operation of the device while decreases of the heat flux after the first five seconds may be attributed to the fact that the input power to the device was reduced by the control system.

The maximum heat flux calculated by the Melcor model was 3 times greater than the actual heat flux. Melcor recommends that an insulating boundary be placed around the TEC. The TEC was not insulated in this case leading to losses to convection. The error could also be caused by the model not relating to transient conditions well. The model was useful for looking at trends in the heating and cooling flux, however.

The heat flux information obtained from the above analysis was then applied to the bottom surface of a system model using a two dimensional finite element heat transfer program called Finite Element Heat Transfer (FEHT). The nodal temperatures on the top surface of the model were then compared with the experimental data in order to verify

that the heat flux information was correct. The 2-D model geometry is shown in Figure 2.12. The alumina plate is 30 x 30 x 1 mm.

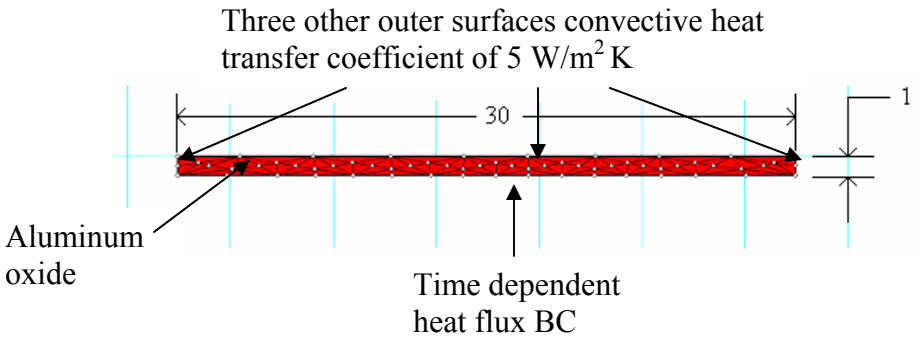

Figure 2.12 2-D geometry used for cooling and heating model. All dimensions in mm.

The results, superimposed on the graph for the experimental results, are shown in Figure 2.13. The calculated surface temperatures differ by at most 1.7 K from the measured values. This result indicates that the lumped capacitance method is a valid method for calculating the heat flux for transient heating.

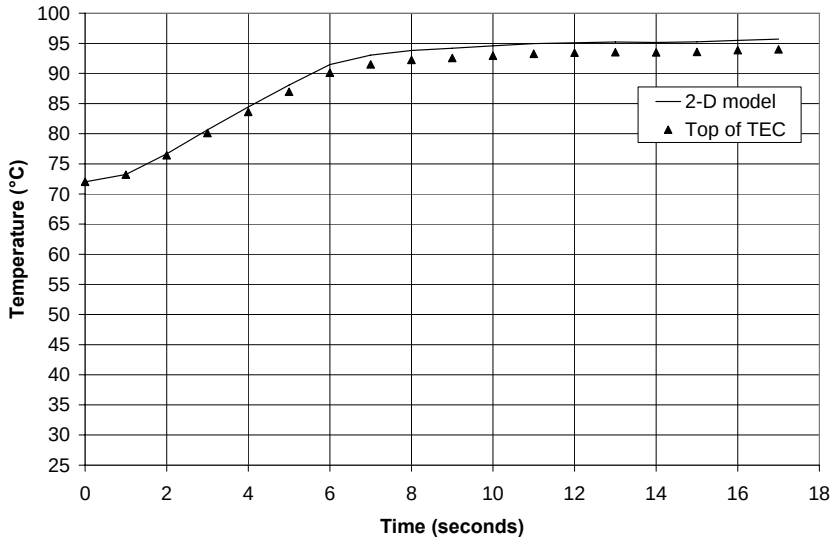

Figure 2.13 Calculated temperature for top of the TEC superimposed on graph of actual temperature for top of TEC for 13.8 V input and cooling fan on.

A similar calculation was performed to analyze the heating characteristics of the TEC with the heat sink cooling fan off and a 13.8 V input. The calculated heat flux is shown in Figure 2.14. The maximum heat flux for the TEC during heating from 72 to 94 °C was 1.92 W/cm^2 with the heat sink fan off and a 13.8 V input.

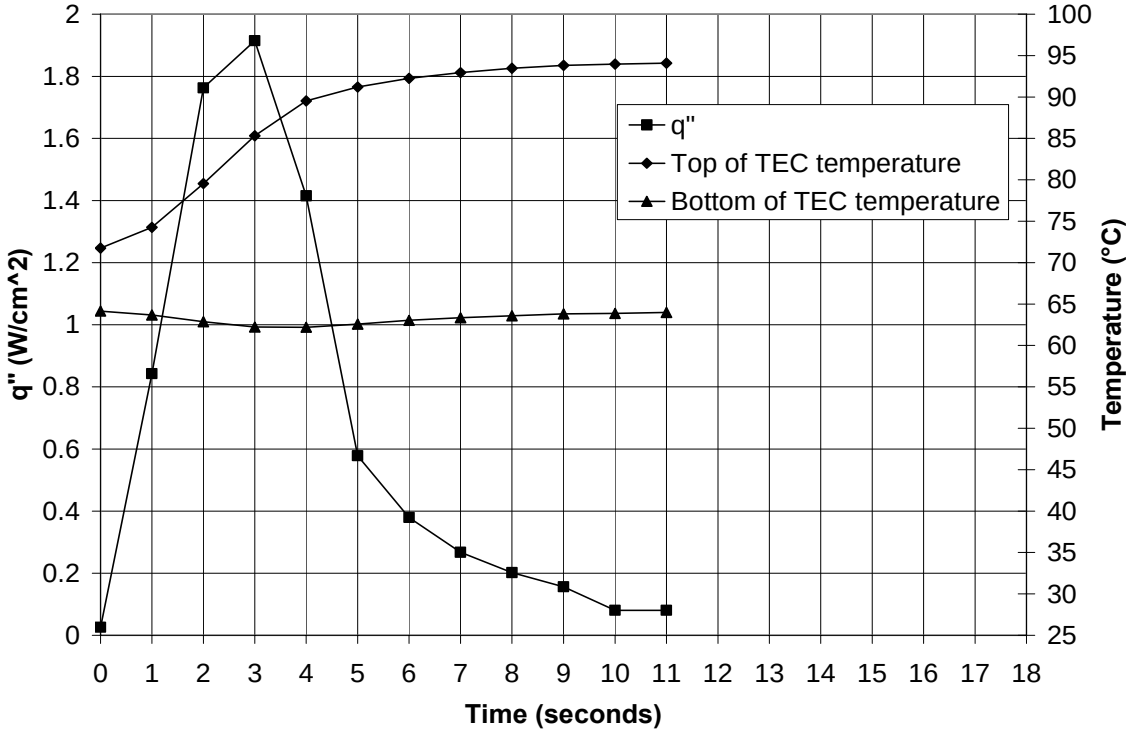

Figure 2.14 Heat flux produced by thermoelectric cooler during heating from 72 to 94 °C with 13.8 V input, cooling fan off

The heat flux for the case without the cooling fan on and a 13.8 V input reacts differently then the case where the cooling fan was on. The heat flux for the case without cooling fan increases for the first three seconds. The TEC was being operated with a 100 % duty cycle during this time. The TEC was pulsed after the three second point. This differs from the case with the cooling fan on, where the heat flux increased and then decreased, despite the fact that the TEC was on at full power. The temperature of the

heat sink in the case with no cooling fan was 30 K warmer than the case with heat sink fan on. The fact that the heat sink was warmer and the temperature difference between top and bottom of TEC was less, created a higher heat flux and made it possible for the heat flux to not decrease when on at full power as explained in the discussion of Figure 2.10.

The heat flux calculated in Figure 2.14 was input into the 2-D model and the simulation was run to predict temperature. The calculated values are superimposed on the temperature data in Figure 2.15. The maximum error between the model and actual temperatures was 1.8 K.

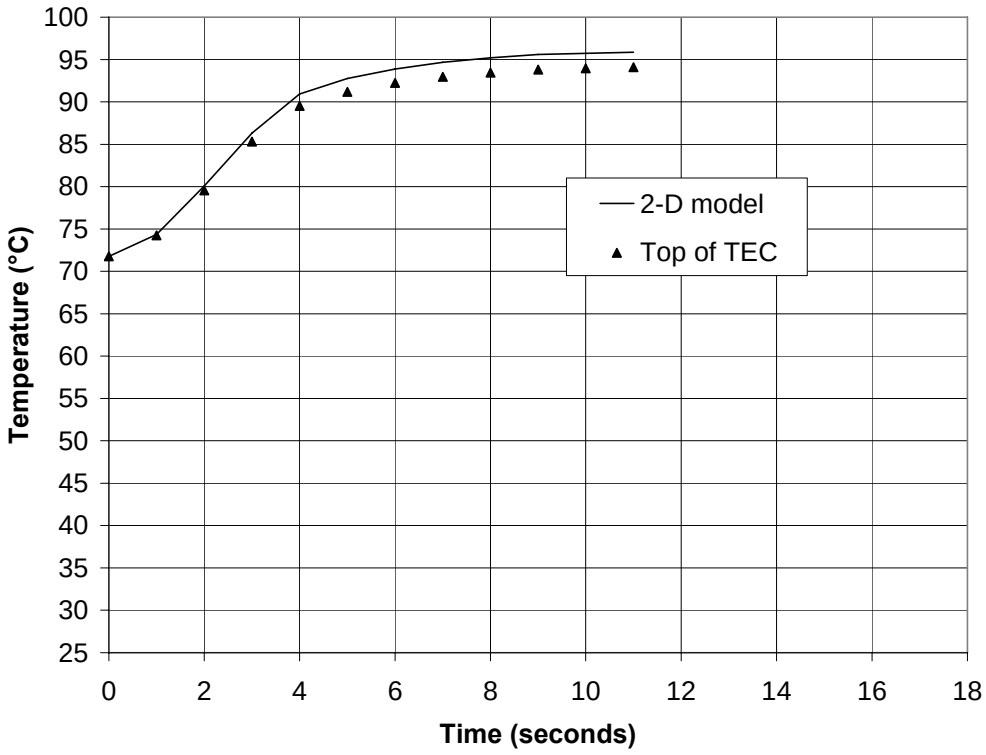

Figure 2.15 Calculated temperature from 2-D model for top of the TEC superimposed on graph of actual temperature for top of TEC for 13.8 V input and cooling fan off.

2.2.2 Cooling flux characteristics of TEC

The cooling flux of the TEC was analyzed with the same method as used to determine the heating flux of the TEC. The 2-D model and the properties for the material were the same. The first case analyzed was the case with the cooling fan. The results from the test are shown in Figure 2.16.

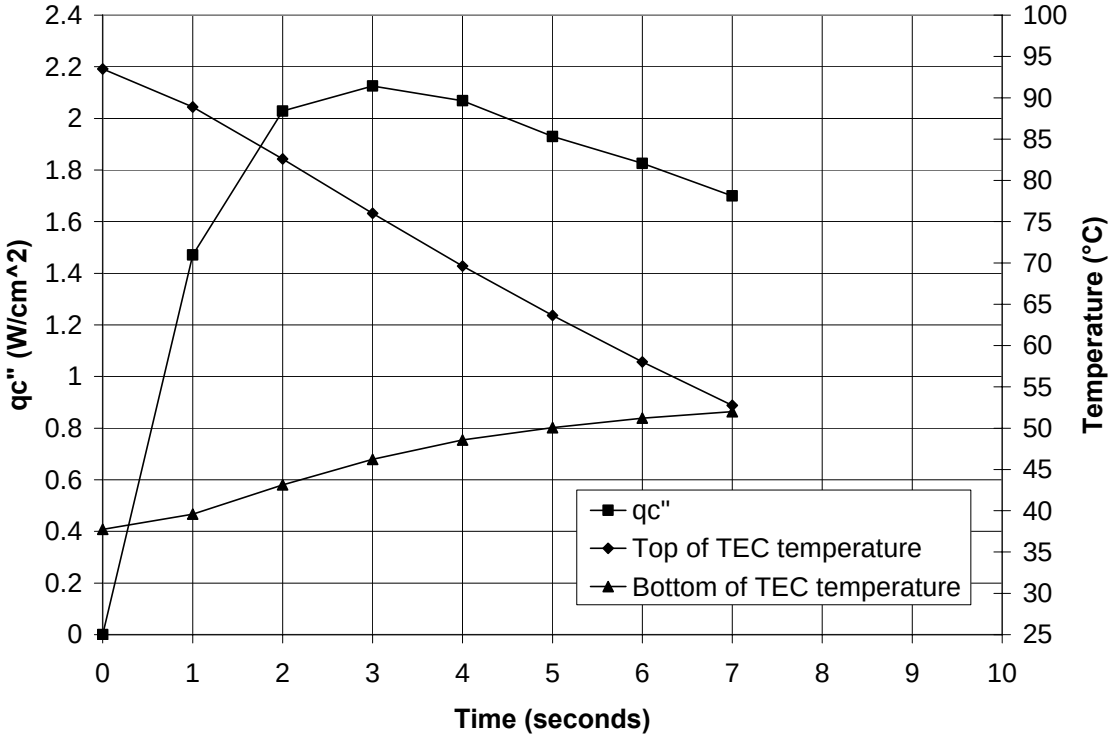

Figure 2.16 Cooling flux produced by thermoelectric cooler during cooling from 94 to 54 °C, 13.8 V Input, cooling fan on

Figure 2.16 shows the cooling flux characteristics of the TEC as calculated with the lumped capacitance method. The maximum cooling flux produced by the TEC was 2.1 W/cm^2 for the case with cooling fan on and a 13.8 V input. The TEC was on at full power through t= 6 s. The cooling flux increases, reaches a peak, and then decreases as the temperature difference between the top and bottom of the TEC decreases. This is the

exact opposite behavior observed in the case where the TEC was in heating mode. The cooling flux increased as the difference between the top and bottom of the TEC decreased in the heating mode case. The equations governing the behavior of the TEC may once again be used to understand the operation of the TEC. In the heating mode case, the value of ΔT increases because $\Delta T = T_h - T_c$. The value of ΔT is increasing in the cooling mode case also because the difference in temperatures at t = 0 seconds is a negative number. As time proceeds, the value of ΔT becomes less negative, so it is indeed increasing. Thus, what appears to be a contradiction between the heating mode and the cooling mode case is actually the same case, so it makes sense that the cooling flux decreases as the hot and cold side temperatures get close to one another.

The tabulated cooling flux results were next put into the 2-D model as a time dependent heat flux on the bottom surface of the alumina. The results of that analysis are shown in Figure 2.17.

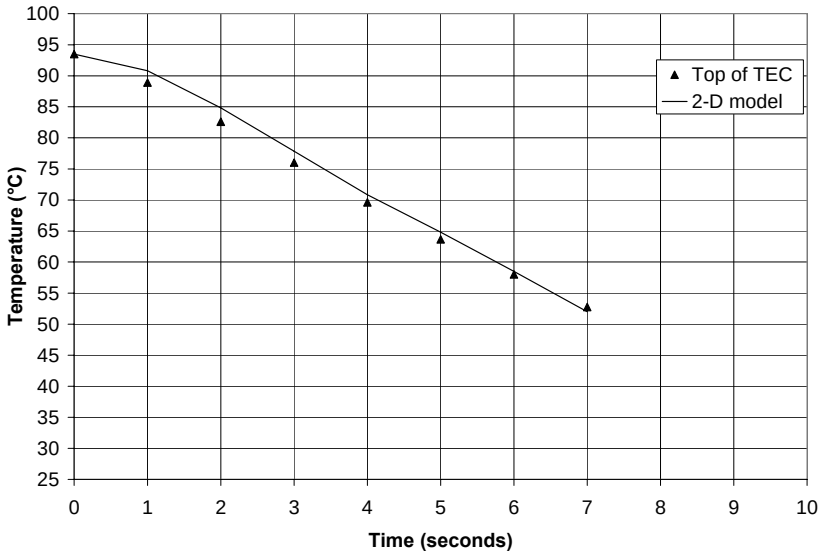

Figure 2.17 2-D calculated temperature for top of the TEC superimposed on graph of actual temperature for top of TEC for 13.8 V input and cooling fan on

The maximum error between the measured values of temperature and the calculated temperature was 2.2 K, indicating that the lumped capacitance model is an acceptable model for this system.

A similar procedure was used to calculate the cooling flux produced by the TEC during cooling with the cooling fan off. The results are shown in Figure 2.18.

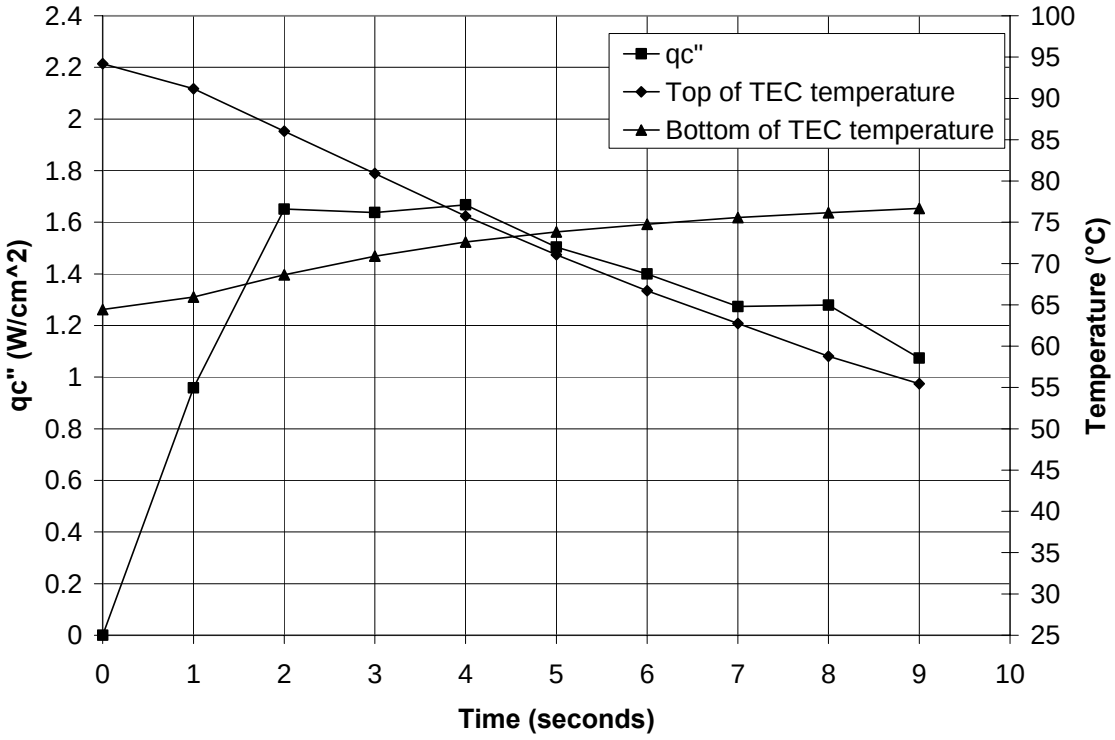

Figure 2.18 Cooling flux produced by TEC during cooling from 94 to 54 °C, 13.8 V input, cooling fan off

The maximum cooling flux for this period was 1.7 W/cm^2. The cooling flux in the case with the cooling fan behaves in a similar manner to the case with cooling fan on. The maximum cooling flux is 0.4 W/cm^2 lower in the case with no cooling fan, however.

The reason for this is because the heat sink is initially 18 K higher than the cooling fan case meaning that ΔT is greater for the no cooling fan case.

2.2.3 Power consumption

The voltage and current consumed by the TEC were monitored via the display on the power supply and a multimeter placed in series with the TEC.

The test used to determine the power and average power consisted of the TEC mounted on the heat sink with the cooling fan on in one case and off in the other case. Thermal grease was used between the TEC and heat sink. Control was provided by a thermocouple placed on top of the TEC. The input voltage to the TEC for this test was 13.8 V. As the TEC was heated, the current was monitored on the power supply display.

The peak power for the TEC with and without cooling fan on was 23.7 W. The average power over cycle for the TEC with cooling fan was 11.3 W. The average power over cycle for the TEC without cooling fan was 7.9 W.

2.3 Independent TEC testing discussion

The results of the testing of the TEC are summarized in Table 2.2.

Table 2.2 Comparison of TEC with and without cooling fan

	Max Heating rate (K/s)	Average heating rate (K/s)	Max Cooling rate (K/s)	Average cooling rate (K/s)	Max heating flux (W/cm^2)	Max cooling flux (W/cm^2)	Max Power consumption (W)	Average power consumption over cycle (W)
TEC with cooling fan	5.2	1.8	6.6	5.8	1.2	2.1	23.7	11.3
TEC without cooling fan	5.8	2.0	5.2	4.3	1.9	1.7	23.7	7.9

The cooling fan produced a difference in the heating and cooling rates of the TEC. The maximum and average heating rate were greater for the case without the cooling fan. The reason for this is that the difference between the hot and cold side temperatures of the TEC was less for the case without the heat sink fan on. This allowed the top of the TEC to heat up more rapidly. The average and maximum cooling rates for the TEC with cooling fan on were 1.5 K greater. This occurred because the difference between hot and cold side temperatures was less for the case with cooling fan on.

The differences in heating and cooling rates translate into time for each cycle of PCR. Using the TEC without the cooling fan would save 2.2 seconds in heating time for each PCR cycle. Multiplying this value by 35 gives a total time saving of 77 seconds. Using the TEC with cooling fan would save 2.5 seconds for each PCR cycle. Multiplying this by 35 cycles gives a total time saving of 88 seconds for an entire PCR run with 35 cycles. There is little benefit in using the cooling fan considering the time savings.

The real savings in not using the cooling fan comes in power consumption. The average power over cycle for the case without cooling fan was 3 W less than the case with cooling fan on. The reason for this is because the average temperature of the TEC remained warmer during operation without cooling fan. This made it possible to heat the top surface of the TEC using less power. More power was required for cooling, but overall the case with no cooling fan used less power.

A disadvantage of not using the fan on the heat sink was that the heat sink got progressively warmer with each PCR cycle. This made the system slightly more difficult to control.

The cooling fan on the heat sink produced an effect on the performance of the TEC at steady state. The bottom of the TEC remained 29.4 K cooler in the case with the heat sink fan on. The temperature differential between the hot and cold side of the TEC with cooling fan was 17 K more than the TEC with no cooling fan. These results indicate that the cool side of the TEC will rise above ambient during steady state operation. The cooling fan keeps the bottom of the TEC cooler because it increases the convection coefficient between the heat sink and the air.

2.4 Testing of a commercially available Peltier thermocycler, apparatus and procedures

A commercially available thermocycler was tested to determine the characteristics of the device. The thermocycler was a Techne Techgene thermocycler, model FTGene5D rated at 120 or 230 V and 250 W shown in Figure 2.19.

Figure 2.19 Techne thermocycler analyzed in this section

The thermocycler was cooled and heated via 4 Marlow Industries Inc. TECs, part number SP1975. On the bottom surface of the TECs was a 10.1 X 9.6 cm aluminum heat sink with a fin height of 4.5 cm. On the top surface of the TEC an aluminum heating block weighing 40.7 g was mounted. The dimensions of the heating block were 5.7 x 5.4 x 0.3 cm. The heating block had wells protruding from the surface. The wells were 11.9 mm high, had a diameter of 7.6 mm, and had a wall thickness of 0.8 mm. The heating block contained 20 wells making it possible to do 20 different PCR reactions in one run as shown if Figure 2.20.

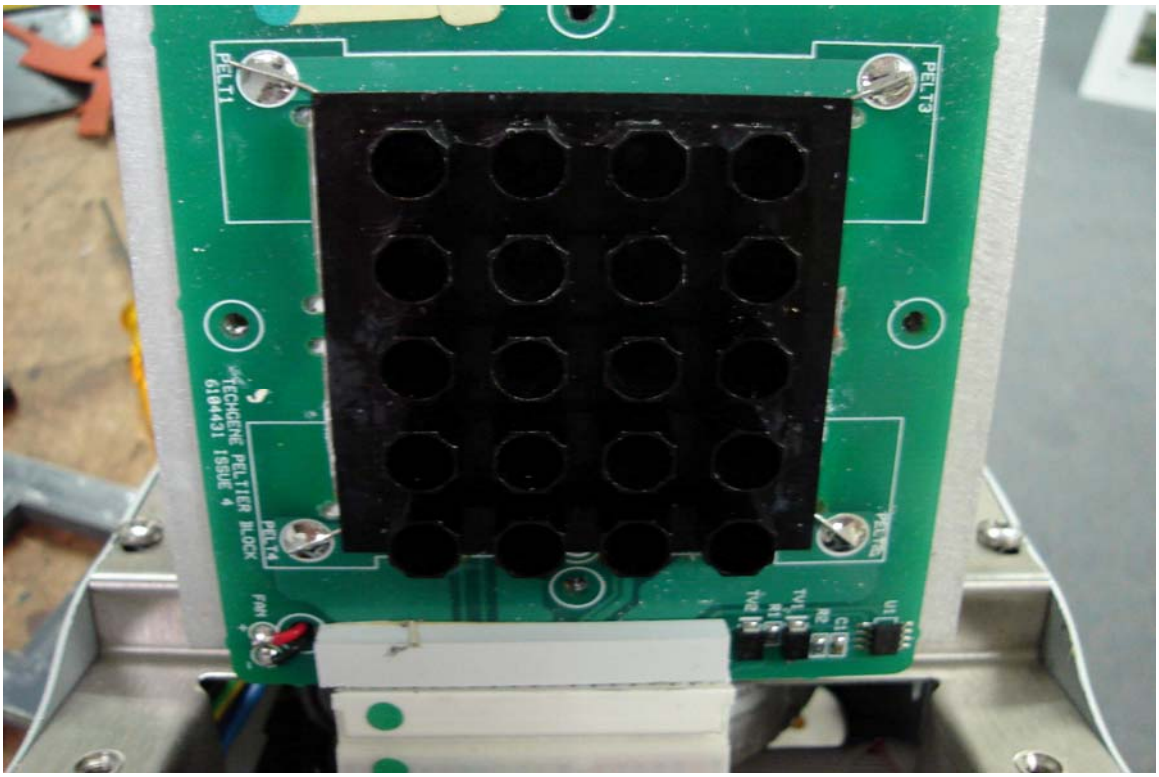

Figure 2.20 Aluminum heating block mounted on top of TECs in Techne thermocycler

The thermocycler was tested using T type thermocouples. 10 µL of water was inserted into a 200 µL tube. A thermocouple was then inserted into the solution and the lid of the PCR tube was closed. This assembly was then inserted into one of the wells located in the heating block. The thermocouple inside the tube measured the response of

the reaction vessel to the heating of the block. Another empty 200 µL tube was used to measure the temperature of the heating block. A thermocouple was wedged between the empty tube and the well in order to determine the temperature of the block. The lid of the thermocycler was closed during the experiment.

The power to the device was measured by severing the power cable and inserting a multimeter in series with the thermocycler to measure the current. The input voltage to the device was 120 VAC.

2.4.1 Commercial Peltier thermocycler testing results

The commercial Peltier thermocycler was tested for heating and cooling rate. The results of that test are shown in Figure 2.21.

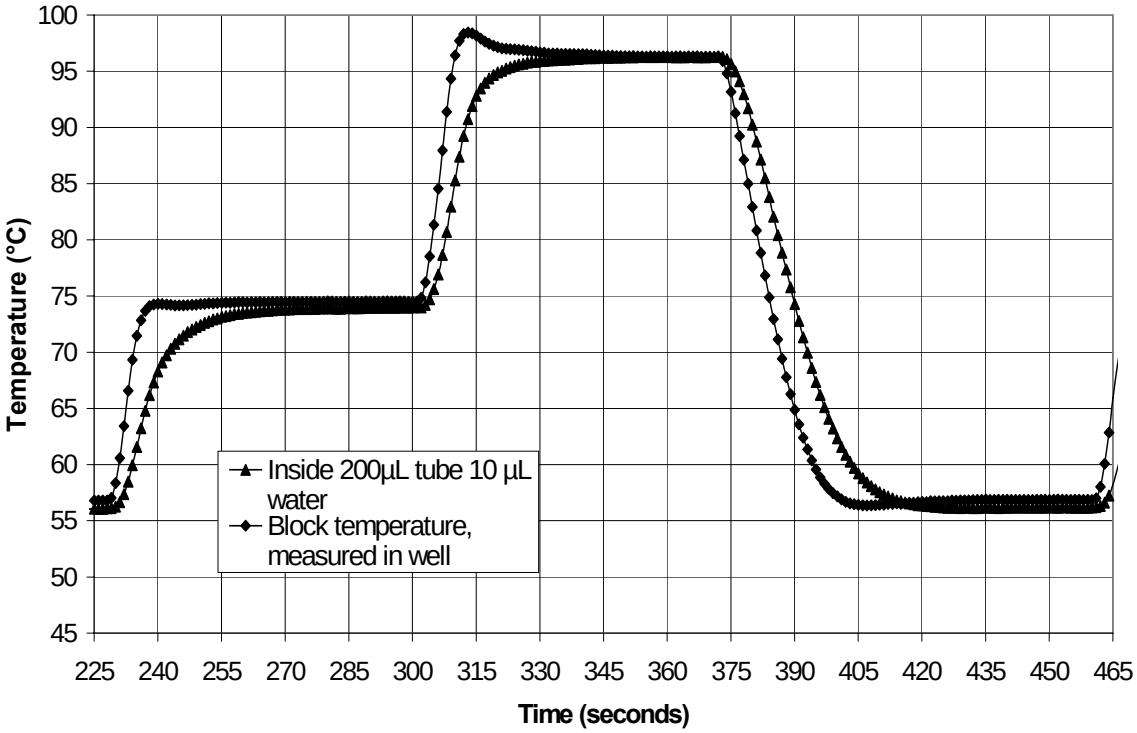

Figure 2.21 Simulated PCR cycle using commercial Peltier thermocycler

The setpoint temperatures for this test were 94, 54, and 72 °C. The temperatures that were measured via the thermocouples were all 2 K higher than these values. The error in measurement is likely in the thermal cycler. The thermocouple is inserted into a hole in the aluminum block and then glued into place. There may have been some air gaps or other resistance present in this setup. The maximum heating rate within the well of the heating block for the commercial device was 3.6 K/s. The maximum cooling rate turned out to be 2.0 K/s. The average heating rate for the block of this device during heating between setpoints 72 and 94 °C was 2.8 K/s and 1.8 K/s for heating between setpoints 54 and 72 °C/s. The average cooling rate for this device was 1.4 K/s.

2.4.2 Power consumption of the commercial device

The commercial Peltier unit was tested to determine the power requirements of the device. The unit operated on 120 VAC. The current consumed by the device varied during the different stages of operation. The current supplied to the device during heating from 72 to 94 °C varied from 2.2 to 1.2 A with the largest current consumption at the beginning of heating and the smallest current as the unit reached the setpoint. This makes sense because it is expected that the control system of the device would scale the power down as the setpoint temperature was reached. Current during heating between 54 and 72 °C peaked at 2.0 A during the initial phase of heating and decreased to 0.3 A as the device neared the setpoint. During cooling, the current in the device ranged from 1.8 A to1.1 A as the setpoint was reached. The current consumed by the device at the 94 °C plateau was 0.4 A, 0.3 A at the 72 °C setpoint, and 0.3 A at the 54 °C setpoint.

Considering these values gives a maximum power requirement of 264 W with an average power over cycle of 145.0 W.

2.4.3 PCR results with the commercial device

PCR was run in the commercial device many times. The results presented in this section are just a representative sample of those efforts. An experiment was run that demonstrated the effect of elongation time on PCR results. As was discussed in Section 1.2, two different sets of primers were used. One primer set was for amplifying a piece of DNA 879 bp long while the other primer set was for a 216 bp amplicon. The elongation time was adjusted until the smaller section of DNA was amplified, but the longer section was not. The protocol for these experiments is shown in Table 2.4.

Table 2.4 Protocol for elongation time experiment

	879 bp amplicon reaction mixture (µL)	216 bp amplicon reaction mixture (µL)
Buffer	3.0	3.0
MgCl2	1.0	1.0
dNTP	4.5	4.5
Primers	1.5	1.0
DNA	1.0	1.0
Taq Polymerase	0.3	0.3
Albumine	3.0	3.0
Water	10.7	11.2
Total	25.0	25.0

PCR was run in either 500 or 200 µL polypropylene PCR tubes with the heated lid on the Techne thermocycler on to prevent solution evaporation. The PCR cycle for the first case consisted of a 95 °C activation period for 15 minutes followed by 35 cycles of 30 seconds at 94 °C, 30 seconds at 54 °C, and 40 seconds at 72 °C. A 15 minute final elongation step at 72 °C completed the PCR run. The Techne control system only counts the plateau

time in the cycle time. For example, 30 seconds at 72 °C means that the thermocycler plateaued at that temperature for 30 seconds. The time required to heat the block from 54 to 72 °C is not included. The results of this test are shown in Figure 2.22.

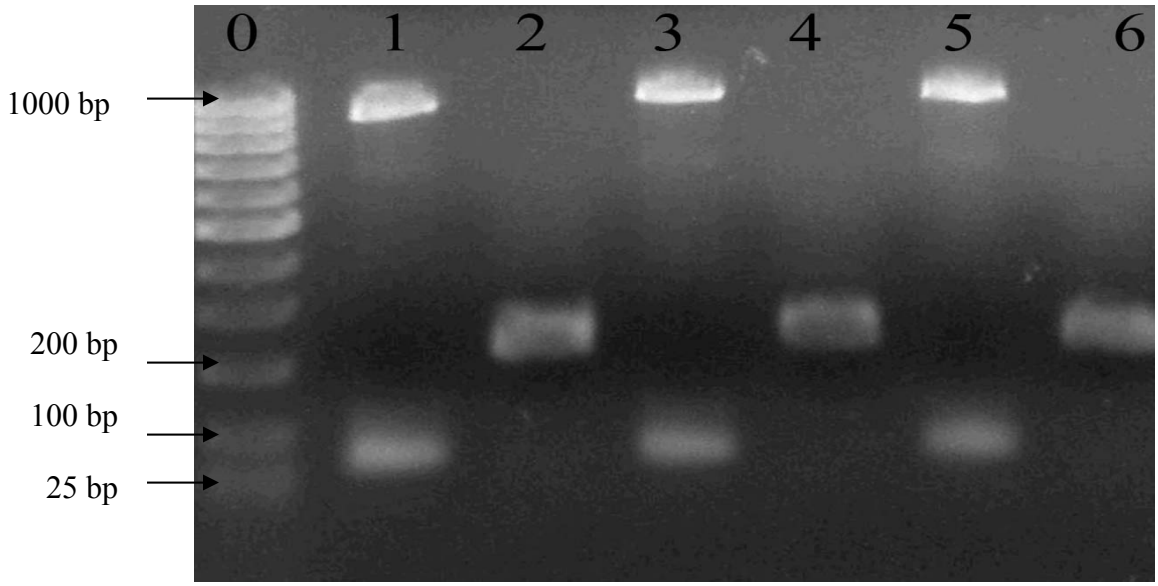

Lane	Description
0	DNA ladder
1	500 µL tube, 10 µL solution, 879 bp amplicon
2	500 µL tube, 10 µL solution, 216 bp amplicon
3	200 µL tube, 5 µL solution, 879 bp amplicon
4	200 µL tube, 5 µL solution, 216 bp amplicon
5	200 µL tube, 5 µL of solution, 879 bp amplicon
6	200 µL tube, 5 µL of solution, 216 bp amplicon

Figure 2.22 PCR reaction results for extension time test, 40 s elongation time

The results indicate that 40 seconds at 72 °C was sufficient to elongate both the 216 and 879 bp DNA fragment. The DNA ladder may be used to determine the length of the PCR amplicon. The DNA ladder is a 1000 bp ladder in 100 bp increments. This means that the line in lane 0 closest to the bottom of the picture is 25 bp, the next line is 100 bp, the next line is 200 bp, the next line is 300 bp, all the way up to the first line that is the 1000 bp marker.

The next test run in this sequence of tests to determine the amplification rate of these two amplicons was to decrease the elongation time to 30 seconds, decrease the denaturation time to 20 seconds, and decrease the annealing time to 20 seconds. The results of that test are shown in Figure 2.23.

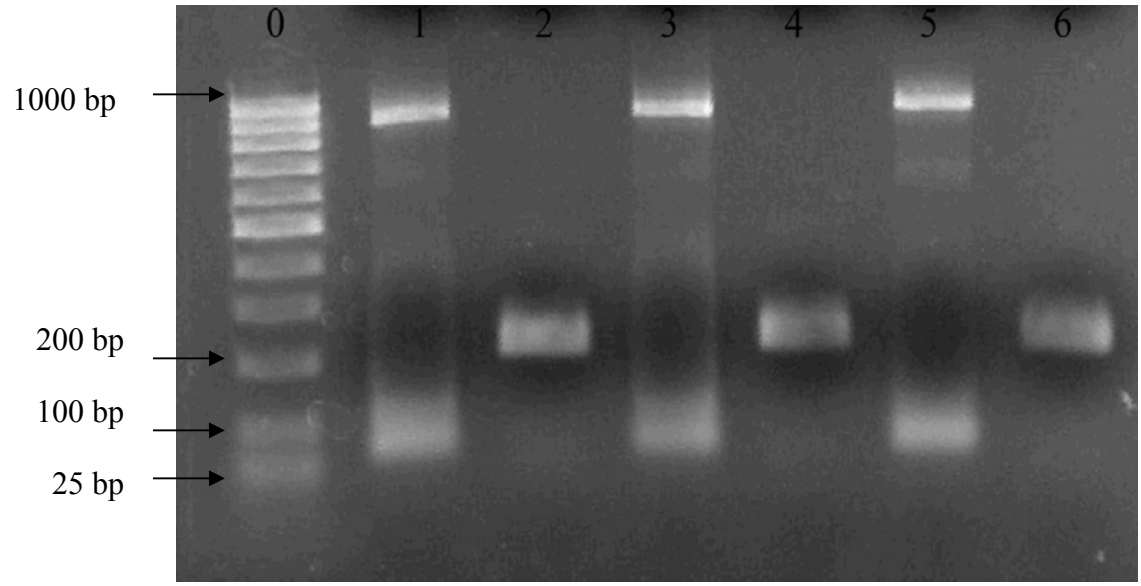

Lane	Description
0	DNA ladder
1	500 µL tube, 10 µL solution, 879 bp amplicon
2	500 µL tube, 10 µL solution, 216 bp amplicon
3	200 µL tube, 5 µL solution, 879 bp amplicon
4	200 µL tube, 5 µL solution, 216 bp amplicon
5	200 µL tube, 5 µL of solution, 879 bp amplicon
6	200 µL tube, 5 µL of solution, 216 bp amplicon

Figure 2.23 PCR reaction results for extension time test, 30 s elongation time

The results indicate that decreasing the elongation time to 30 seconds has no effect on either amplicon. It is expected that as the elongation time continues to be decreased, the longer amplicon will fail to be copied. Decreasing the denaturation and elongation times from 30 to 20 seconds also had no effect on the reaction as a signal was received for each tube.

The third step in this test consisted of decreasing the denaturation and annealing times to 15 seconds and decreasing the elongation time to 25 seconds. The results of that test are shown in Figure 2.24.

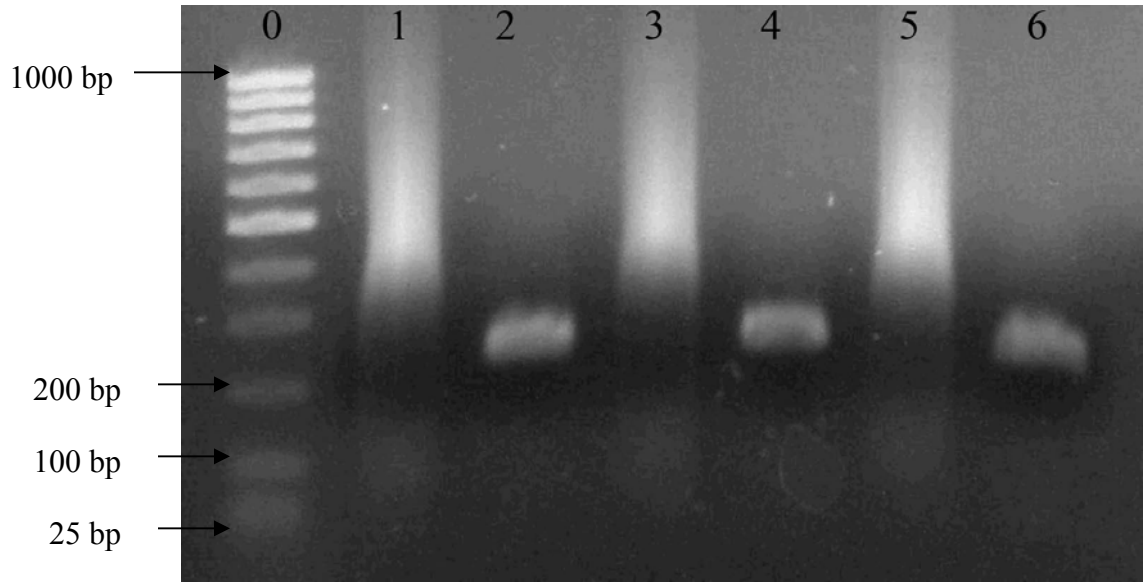

Lane	Description
0	DNA ladder
1	500 µL tube, 10 µL solution, 879 bp amplicon
2	500 µL tube, 10 µL solution, 216 bp amplicon
3	200 µL tube, 5 µL solution, 879 bp amplicon
4	200 µL tube, 5 µL solution, 216 bp amplicon
5	200 µL tube, 5 µL of solution, 879 bp amplicon
6	200 µL tube, 5 µL of solution, 216 bp amplicon

Figure 2.24 PCR reaction results for extension time test, 25 s elongation time

The lack of a clear signal for any of the 879 bp amplicons in Figure 2.24 indicates that the 25 second elongation time was a problem for the longer amplicon. Theoretically, the copying rate for DNA polymerase is 50 bp/s, which would mean that it would be possible to copy a 1250 bp segment in this time. The experiment that was run in this case indicates that the rate of copy is around 29 bp/s.

An experiment was run to determine if the results shown in Figure 2.24 were due to the decrease in annealing and denaturation times, or by the decrease in extension time.

The denaturation and annealing time in this step remained at 15 seconds while the elongation time was increased to 30 seconds, 5 seconds greater than the previous test. The results of the test are shown in Figure 2.25.

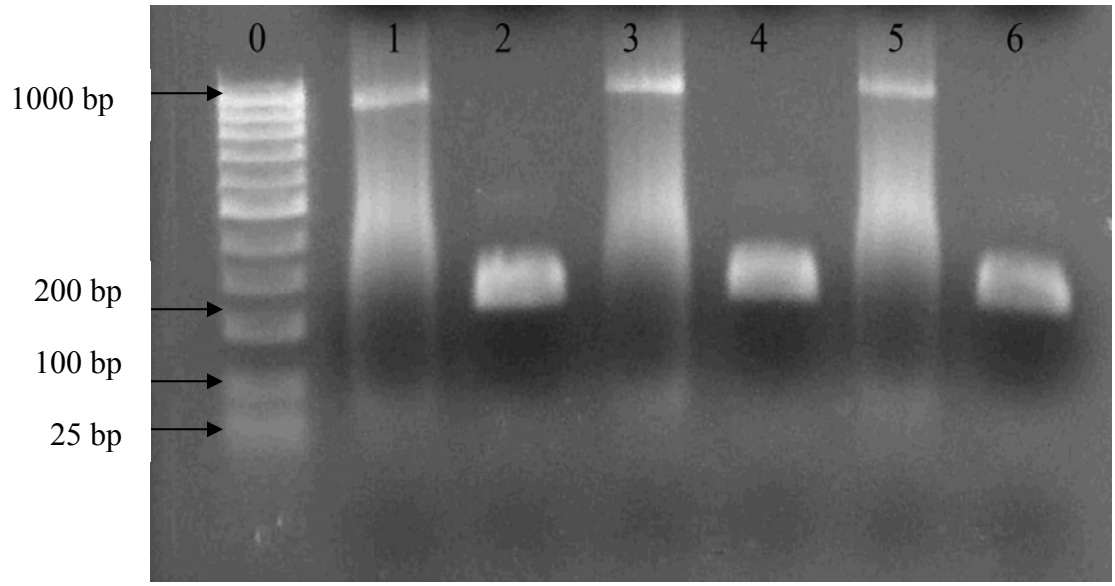

Lane	Description
0	DNA ladder
1	500 µL tube, 10 µL solution, 879 bp amplicon
2	500 µL tube, 10 µL solution, 216 bp amplicon
3	200 µL tube, 5 µL solution, 879 bp amplicon
4	200 µL tube, 5 µL solution, 216 bp amplicon
5	200 µL tube, 5 µL of solution, 879 bp amplicon
6	200 µL tube, 5 µL of solution, 216 bp amplicon

Figure 2.25 PCR reaction results for extension time test, 30 s elongation time with 15 s at denaturation and annealing steps

The results indicate that with an elongation time 5 s longer, the longer amplicon was copied, even with the shorter denaturation and annealing steps. This result shows that the limiting factor in PCR is the elongation phase. The copying speed of DNA polymerase is a limiting factor in PCR speed.

Another method of visualizing PCR reaction success is by running the reaction with ethidium bromide in the solution at a volumetric concentration of 1:4000 in a glass

capillary. This eliminates the need to use gel electrophoresis to determine if the reaction occurred. If the reaction occurred, the solution will fluoresce when placed in a UV light enclosure. If it did not occur, then no fluorescence will be seen. Ethidium bromide is a substance that fluoresces when exposed to UV light. Ethidium bromide has the ability to attach itself to the DNA molecule (D'Amico, Paiotta et al. 2002). The ethidium bromide undergoes an increase in flourescense when bound to the DNA molecule (Pyun and Park 1985). The concentration of ethidium bromide must be just right. If a large concentration of ethidium bromide is used, then it will be impossible to distinguish between a successful reaction and an unsuccessful reaction because ethidium bromide fluoresces under UV light by itself. If too small an amount is used then no fluorescence will be seen if the reaction occurred or if if did not. A picture of three capillaries in the UV light hood is shown in Figure 2.26.

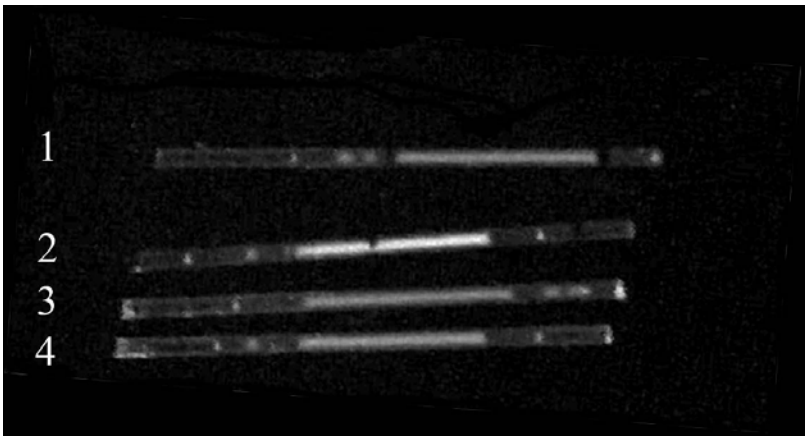

Figure 2.26 Glass capillaries run with a 1/4000 volumetric concentration of ethidium bromide. 1) PCR solution before amplification, 2) PCR solution after amplification in commercial thermocycler, 3,4) Unsuccessful reactions on microheater

The fluorescence is easily detectable in the successful PCR reaction, labeled 2 in Figure 2.26. There is no fluorescence in the reaction mixture before PCR, labeled 1, and the two unsuccessful reactions run on the microheater, labeled 3 and 4 in Figure 2.26.

3. TESTING OF A CONVECTIVE THERMOCYCLER FOR PCR

A convective thermocycler was built in the lab to test the possibility of using a device that directs an air flow past a sample to perform the heating and cooling for the PCR reaction. The heating and cooling rate, heating and cooling flux, and power consumption were monitored.

3.1 Testing of a convective thermocycler, apparatus and procedures

Two different configurations of the convective thermocycler were built. The first variation is shown in Figures 3.1 and 3.2.

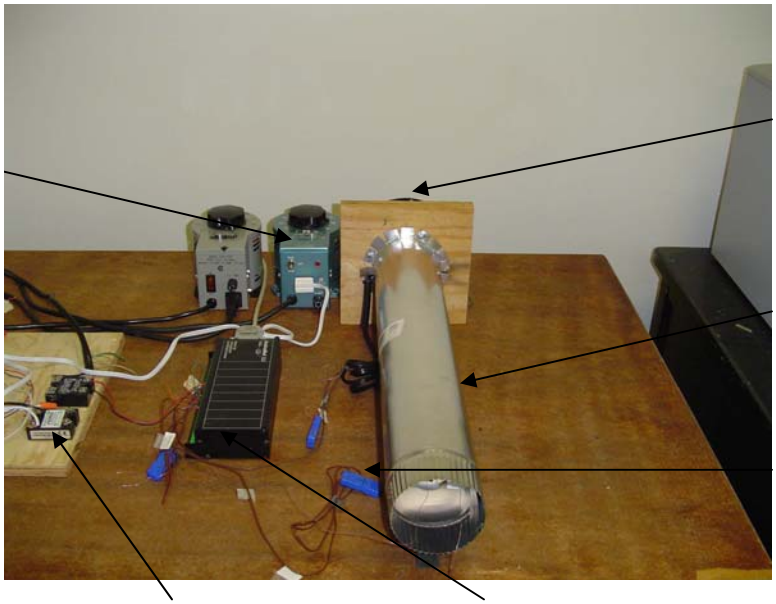

Figure 3.1 Convective thermocycler setup #1

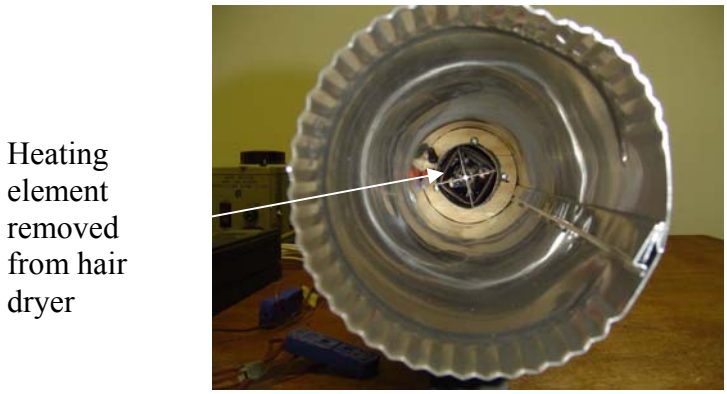

Figure 3.2 Heater mounted within vent pipe

The second configuration was designed with two fans. One of the fans was used for flowing air over the heating element while the other fan was used for cooling. The purpose of this was to speed cooling. This double fan convective thermocycler is shown in Figures 3.3 and 3.4.

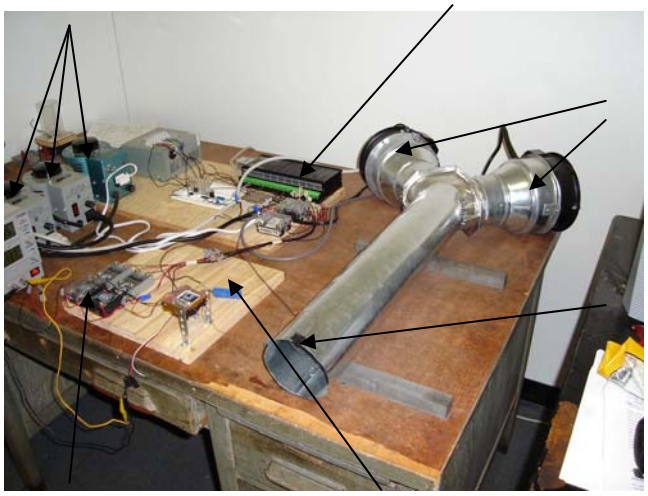

Figure 3.3 Double fan convective thermocycler setup

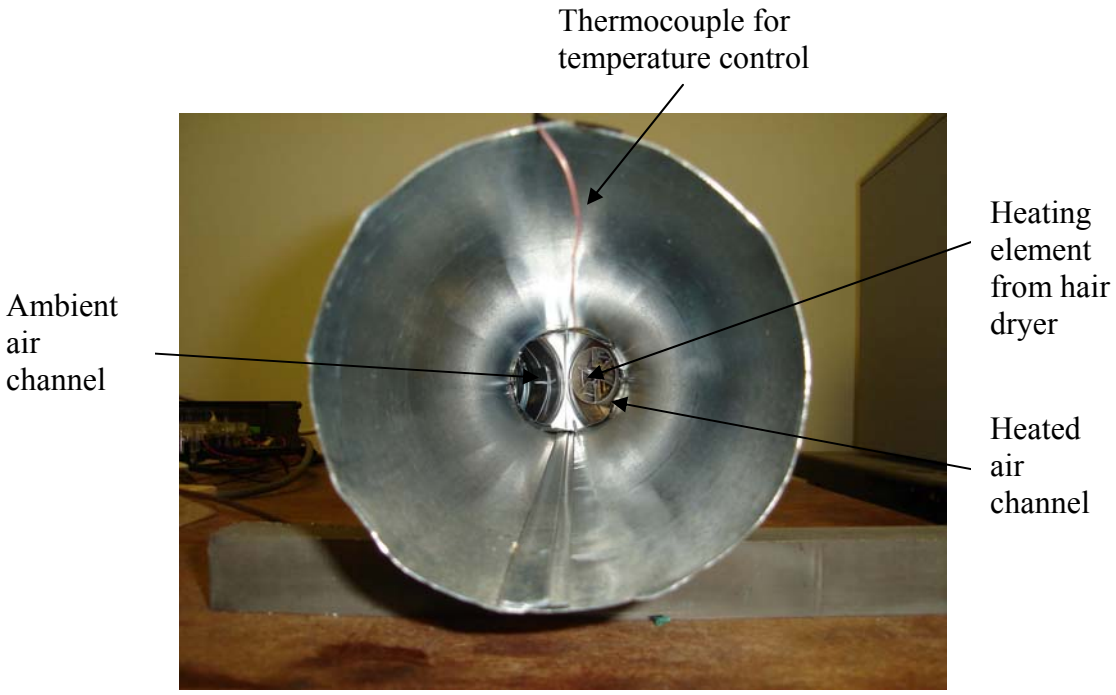

Figure 3.4 Heater element within double fan convective thermocycler

There are several similarities between the two convective thermocycler designs. The convective thermocyclers described in this section were controlled with pulse width modulation (PWM), similar to the thermoelectric cooler (TEC) described in Chapter 2. A Visual Basic program was written to control the system. The software used a proportional-integral-derivative (PID) controller scheme to control the fractional on-time of the heater during each control period (1 sec control period used in this work). The pipe centerline air temperature near the outlet was measured and was compared against the setpoint to act as the controller input signal.

The fan on the single fan convective thermocycler was used to drive air through the device. The air is heated as it flows past the heating element. The fan speed in the single fan unit was also controlled with PWM in heating mode. The fan power was turned on only 50% of the time to yield a reduced fan speed. During cooling, the heater

was turned off and the fan was run at full power to introduce the maximum flow of cooling air.

The double fan convective thermocycler operated in much the same way as the single fan convective thermocycler. The heater was controlled in an identical manner. The difference between the two designs was that the double fan convective thermocycler used two fans. The first fan was run at reduced speed as described above for the single fan unit and was responsible for driving ambient air over the heating element to create a stream of hot air in the main channel (second fan was off during heating). The second fan was responsible for providing the cooling air flow. It was run at full speed during cooling mode (the heating fan was turned off during cooling).

The software recorded data at a frequency of 1 Hz. The data recorded was the pulse width, setpoint, and temperature at the outlet of the heater. An Extech Instruments multimeter, model 22-816 was used to measure the voltage and current output of the variable transformer.

The thermocouple for measuring the temperature of the air in the thermocycler was placed along the axis of the pipe at a point 7.6 cm upstream from the end of the pipe.

3.2 Convective thermocycler test results

The maximum heating rate for the single fan convective thermocycler was 2.0 K/s. The maximum cooling rate was 1.8 K/s. A single simulated PCR cycle using the single fan convective thermocycler is shown in Figure 3.5.

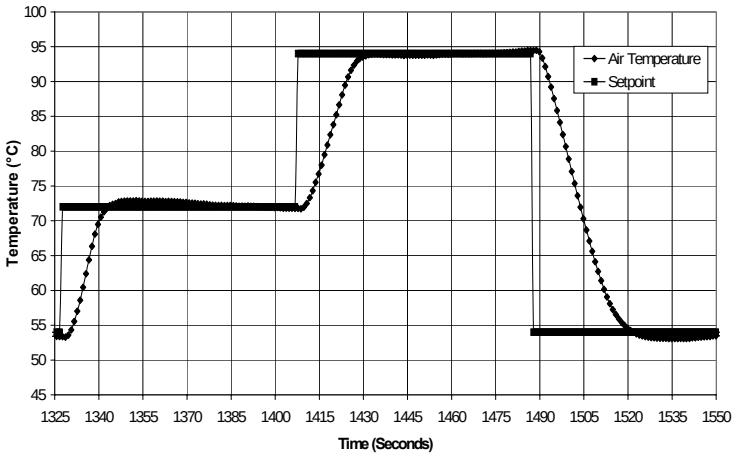

Figure 3.5 Simulated PCR cycle using the single fan convective thermocycler

The average heating and cooling rates were also calculated. The average heating rate for heating between 54 and 72 °C for this setup was 1.2 K/s. The average heating rate between 72 and 94 °C was 0.9 K/s. The average cooling rate for the single fan convective thermocycler was 1.2 K/s.

The double fan convective thermocycler was tested to determine the heating and cooling rates. The results of the test are shown in Figure 3.6.

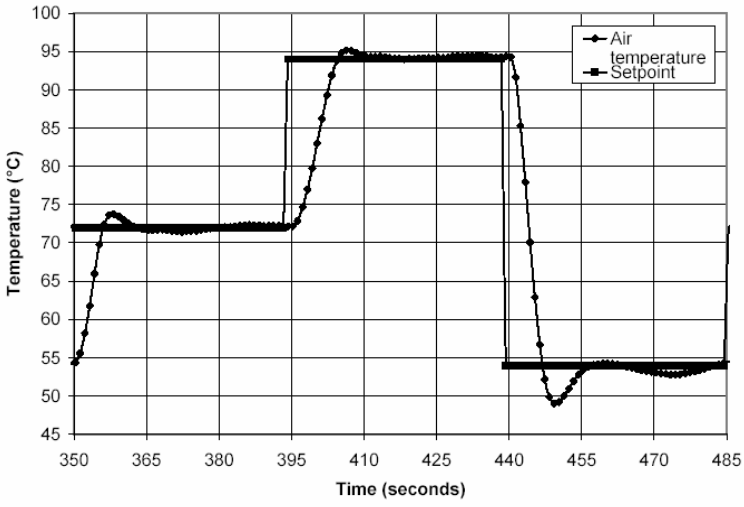

Figure 3.6 Simulated PCR cycle using the double fan convective thermocycler

The maximum heating rate of the double fan convective thermocycler was 4.2 K/s. The maximum cooling rate for this setup was 7.9 K/s. The average heating rates were 2.6 K/s for heating between 54 and 72 °C and 2.0 K/s for heating between 72 and 94 °C. The average cooling rate was 5.3 K/s. The heating rates are higher because the relative flow rate and power input were set to obtain higher rates for the double fan unit. Cooling rates are higher because the cooling fan flow rate is higher due to a more open flow path obtained when the heater element is not present in the cooling flow path. These characteristics were the motivation in designing the double fan unit.

One of the important characteristics of a convective thermocycler is temperature uniformity across the area where the reaction will be occurring. The temperature should be as uniform as possible to ensure a quality PCR reaction. The single fan convective thermocycler was tested for temperature uniformity. Different ideas were tried in order to make the radial temperature profile as even as possible. 2 in. thick foil and fiberglass duct insulation was used in one test to cover the outside of the duct. This was done in order to reduce the amount of heat loss through the walls of the duct, thus making the wall temperature closer to the duct midpoint temperature.

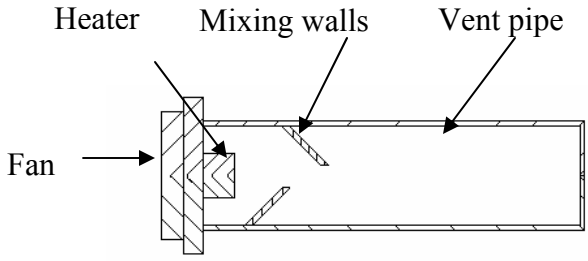

Figure 3.7 Cross section of single fan convective thermocycler showing mixing walls located within vent pipe

Another variant of the convective thermocycler was to place mixing walls within the duct in an attempt to make the flow within the tube more turbulent, thereby enhancing mixing as shown in Figure 3.7.

Another tactic that was tested to make the temperature profile more uniform was to add an additional vent pipe 61 cm long to the end of the convective thermocycler. The result of the testing is shown in Figure 3.8.

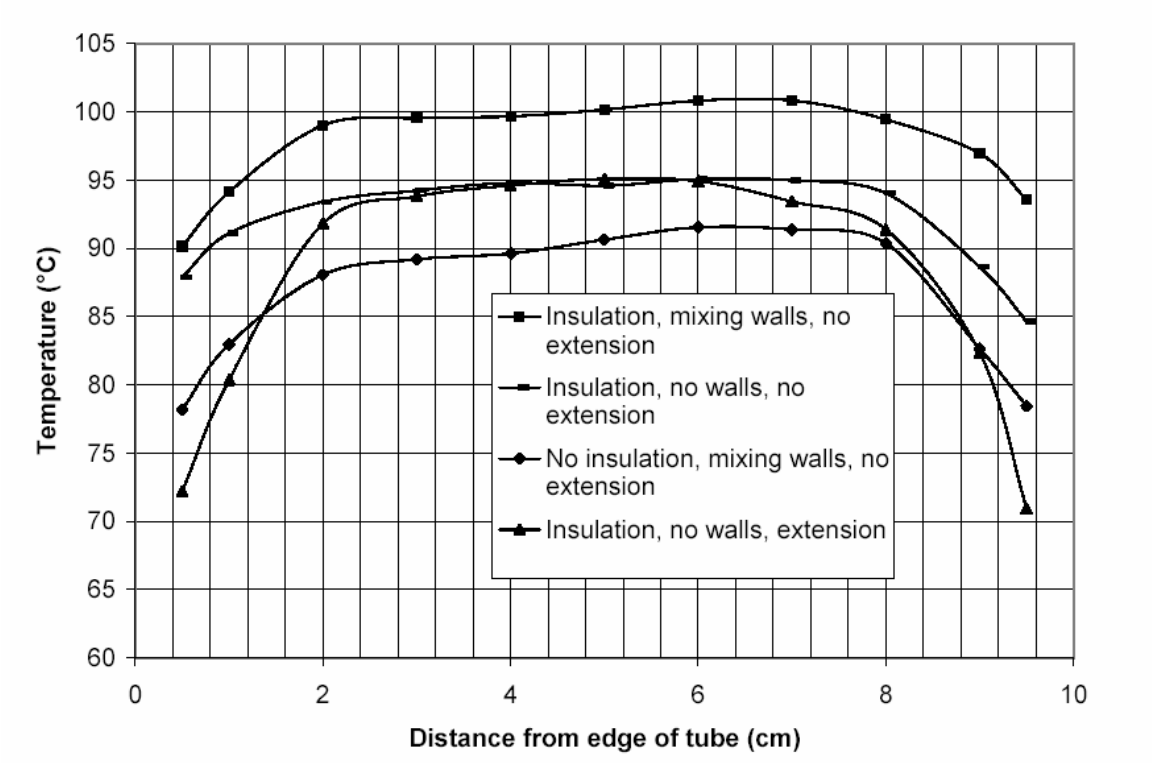

Figure 3.8 Radial temperature measurements for single fan convective thermocycler with heater and fan at duty cyle = 1

The configuration that provided the best results in terms of temperature uniformity was the case where the pipe was covered with insulation, mixing walls were inserted into the pipe, and no extension was used. The standard deviation for this case was 3.5 K, compared to 3.6 K for the case with insulation, no mixing walls, and no extension. The worst case scenario was the case with the extension, no insulation, and no walls. This case had a standard deviation of 9.3 K. The effect of the mixing walls on the temperature

uniformity was very small, as can be seen by comparing the standard deviations for the top two traces in Figure 3.8. Only 0.1 K separated the standard deviations of these two cases. There was a large drop off in the standard deviation in temperature profile for the case with mixing walls, no extension or insulation. The standard deviation for that case was 5.1 K, indicating that the insulation was more important than mixing walls in maintaining temperature uniformity.

3.2.1 Power consumption of convective thermocyclers

For the single fan unit, the power input to the fan was 108 VAC and 0.6 A. The power supplied to the heater element was 78.4 VAC at 7.7 A. For the double fan convective thermocycler, the heater was supplied with of 118.2 VAC which drew a current of 11.6 A. The cooling and heating fans were supplied with 82.3 VAC each of which drew a current of 0.4 A.

The power consumption of the single fan convection cycle was found by multiplying the current, voltage and duty cycle. The power required to run the fan was not taken into account for this calculation because the power required by the fan is small compared to the power required by the heater. The power required to run the fan at full power is only 10% of the power required to run the heater at full power for the single fan convective thermocycler. The single fan convective thermocycler heater required 604 W to operate when it was not pulsed. The average power over a cycle shown in Figure 3.5 was 255 W.

The power consumption for the double fan convective thermocycler was found similarly. The power required for the heating and cooling fans was not taken into

account for this calculation. The power required to run the fan at full power is only 2.4% of the total power required to run the heater of the double fan convective thermocycler at full power. The double fan convective thermocycler required 1371 W of power when not pulsed. The average power over cycle shown in Figure 3.6 was 645 W.

It is noted that the power requirements of these convective thermocylers is quite high due to the fact that a large volumetric flow rate of heated air is dumped to the room. Air heating/cooling requires significant air velocities to maintain high heat transfer coefficients and such designs suffer from poor energy performance (high power requirements) unless some recycling scheme is used to recycle the hot air instead of throwing it away. In early designs, energy recycling was attempted but it was found that such designs impacted the cycling speed. Air heating/cooling designs were found to provide reasonably fast heating and cooing but at the cost of large power requirements.

3.2.2 Convection characteristics of the thermocycler

The velocity of the air within the two convective thermocyclers was found in order to determine the heating power produced at the tube outlet. A control volume analysis was used to determine the velocity of the air in the tube. A schematic of the model used is shown in Figure 3.9.

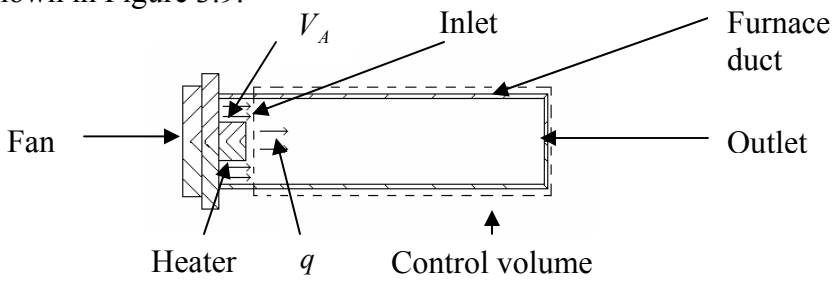

Figure 3.9 Schematic of control volume used for air velocity determination

where V_A is the air velocity produced by the fan and q is the energy per unit time transferred to the control volume by the heater. The control volume energy rate balance reduces to (Moran and Shapiro 1999)

$$0 = -q_{CV} + \dot{m}(h_i - h_o) \tag{3.1}$$

assuming that the control volume is at steady state, ignoring kinetic and potential energy effects, and ignoring heat transfer from the control volume. Here $\dot{m}$ is the mass flow rate and is given by (Moran and Shapiro 1999)

$$\dot{m} = \frac{AV_{ave}}{v} \tag{3.2}$$

where h_i and h_o are the enthalpies of the air at the inlet and outlet respectively. A is the cross sectional area of the pipe, V_{ave} is the average air velocity within the pipe, and v is the specific volume of the air in the mass flow rate equation. The specific volume of the air may be determined by considering the air to be an ideal gas at atmospheric pressure. The enthalpies were also found considering air to be an ideal gas.

Each convective thermocycler was run at steady state to determine the air velocity during heating within the thermocycler tube. For these tests, the heaters on both the single and double fan convective thermocycler were run at constant power (25% on time). The heating fan on both units were run at the same settings that were used in the thermal testing (reduced speed at 50 % power).

A test was run with both thermocyclers to determine the air velocity in cooling mode. The fan on the single fan convective unit was run at full power with the heater run at a 50 % duty cycle to determine the air velocity in cooling mode. The cooling fan of the double fan convective thermocycler was also run at a full power during cooling. This

cooling fan did not have a heater obstructing its path, so the air velocity was determined with the manufacturing specifications. The manufacturing specifications indicate that the fan is capable of driving 235 cfm of air at 0 static pressure (Rotron 2005). This value was used by considering an analysis of the flow in the vent tube. The pressure drop in the vent tube may be found using the Moody friction factor equation (Incropera and DeWitt 1996). The equation is

$$f = \frac{-(dP/dx)D}{\rho V_{ave}^2/2} \tag{3.3}$$

Where P is the pressure, x is the distance along the vent tube, D is the diameter of the tube, ρ is the density of air taken at ambient, V_{ave} is the average air velocity, and f is the friction factor. The friction factor may be obtained from the Moody diagram and is dependent on the Reynolds number. Some assumptions were made to get an idea of the pressure drop in the tube. For an air velocity of 4 m/s, which is an overestimate considering the specifications and the fan diameter, the Reynold's number is 25,000. This leads to a value for the pressure drop of 2.19 Pa using equation 3.3 and knowing the diameter and length of the vent tube. The airflow is near the maximum value for the fan considering the manufacturers static pressure versus airflow curve (Rotron 2005). Therefore, the air velocity was found from the maximum volumetric flow rate by dividing by the area of the fan.

The temperature at the outlet of the heating tube during steady state was recorded in order to determine the enthalpy of the air at the exit during all air velocity determinations except for the double fan convective thermocycler cooling fan. The inlet temperature of the air was room temperature. This allowed the enthalpy to be set at the inlet and the outlet. The control volume heat transfer was simply the power supplied to

the heater. The only unknown variable in Equation 3.1 was the air velocity. The results of the air velocity analysis are shown in Table 3.1

Table 3.1 Results of air velocity analysis for single and double fan convective thermocyclers

	Single fan heater	Single fan cooler	Double fan heater	Double fan cooler
Air velocity (m/s)	0.5	0.7	1.2	3.4
Fan input power (W)	32.4	64.8	16.5	32.9

The air velocities in Table 3.1 are also given with the fan input power in order to demonstrate the relationship between the two. The fan input power was found by multiplying the input voltage, current, and duty cycle of the fan. The air velocity of the single fan cooler is lower than the double fan heater air velocity. The single fan cooler fan was run at full speed while the double fan heater was run at 50 % duty cycle. The flow path in the single fan convective thermocycler was more obstructed by the heater than the double fan convective thermocycler because of the method of attachment. The double fan heater also used 4 times less power than the single fan cooler. This demonstrates that it is important to avoid obstructing the heating fan too much with the heating coil. The double fan cooler supplied an air velocity that was nearly three times greater than the double fan heater using only twice as much power. This was because the double fan cooler had no obstruction in its path.

The next variable found to characterize the convection thermocycler system was the Nusselt number. The reaction vessels that were placed inside the convection thermocycler were cylindrical or cylinder like, therefore a cylindrical Nusselt correlation was used. The correlation was (Incropera and DeWitt 1996)

$$\overline{Nu}_D = C\,\mathrm{Re}_D^m\,\mathrm{Pr}^n\left(\frac{\mathrm{Pr}}{\mathrm{Pr}_s}\right)^{1/4} \tag{3.4}$$

where $\overline{Nu}_D$ is the average Nusselt number over the surface of the cylindrical reaction vessel, Pr is the Prandtl number, Pr_s is the Prandtl number evaluated at the surface temperature of the vessel, and C, m, and n are constants based on Re_D and Pr. The temperature of the surface of the reaction vessel was unknown. This fact does not play heavily in the analysis, however. The only parameter evaluated at the surface temperature in Equation 3.4 is Pr_S. The largest temperature difference that could possibly be encountered in this analysis is 40 K, the difference between the denaturation temperature of 94 °C and the annealing temperature of 54 °C. The Prandtl number varies by only 0.006 between these temperatures, therefore the surface temperature of the vessel was assumed to be the setpoint temperature prior to the one being analyzed. For example, if the air temperature within the tube was at the 72 °C setpoint, then the surface temperature of the vessel was assumed to be 54 °C. All of the other parameters in the equation were evaluated at the air temperature within the vent tube. The diameter of the reaction tube in this case was taken to be 2.6 mm, which is the average diameter of the bottom 2.5 mm of a 200 µL polypropylene PCR tube. The bottom of the tube was measured only because this was the area that was filled when 10 µL of water were inserted into it as shown in Figure 3.10.

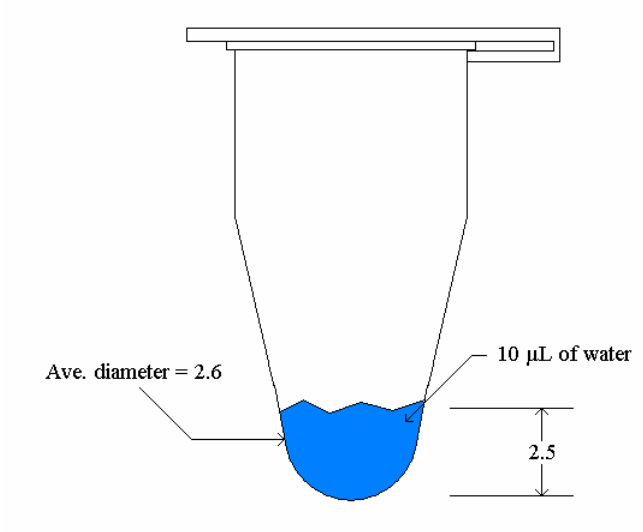

Figure 3.10 200 µL PCR tube with 10 µL of water used in convective analysis. All dimensions in mm

The Nusselt number and the average convection coefficient were found for the air velocities shown in Table 3.1. The results are summarized in Table 3.2.

Table 3.2 Nusselt number and convection coefficients for single and double fan convective thermocycler

Tinf (°C)	54				72				94			
Air velociy (m/s)	0.52	1.2	0.74	3.4	0.52	1.2	0.74	3.4	0.52	1.2	0.74	3.4
Average Nusselt number	4.4	6.6	5.2	11	4.2	6.3	5.0	10	4.0	5.9	4.7	9.6
Average convection coefficient (W/m^2 K)	48	71	57	120	48	71	56	120	48	71	57	120

3.2.3 System response with a test sample

The lumped capacitance method was used to derive an expression for the time constant of a contained water sample in the convective thermocycler that is useful for discussing the system dynamics. The lumped capacitance approximation is valid if the Biot number is less than 0.1 (Incropera and DeWitt 1996). In this case, the Biot number

was evaluated for a cylindrical reaction vessel with an average diameter of the bottom 2.5 mm of a 200 µL polypropylene PCR tube. The polypropylene tube is 0.3 mm thick. The thermal conductivity of this system was lumped together based on the volumetric percentage of water and polypropylene. This gives a thermal conductivity of 0.47 W/m K, considering that the thermal conductivity of water is 0.60 W/m K and polypropylene is 0.17 W/m K. Evaluating the Biot number with these constraints gives a value of 0.17 with an average convection coefficient of 120 W/m^{2}K and 0.1 with an average convection coefficient of 71 W/m^{2}K. These results indicate that the lumped capacitance model may be a poor choice for the cooling case in the double fan convective thermocycler, but may be a good fit for the other situations. Applying an energy balance on the reaction tube and sample, the following equations can be derived (Incropera and DeWitt 1996)

$$\frac{T - T_\infty}{T_i - T_\infty} = \exp\left[-\left(\frac{hA_s}{\rho V c} \right) t \right] \tag{3.5}$$

where T is the temperature at time t, T_i is the initial temperature of the system, T_∞ is the air temperature within the vent pipe, h is the convection coefficient, ρ is the density of the reaction vessel, V is the volume of the reaction vessel, c is the specific heat of the reaction vessel, and A_s is the surface area of the reaction vessel. This expression gives rise to an expression for the time constant of the reaction vessel

$$\tau_t = R_t C_t \tag{3.6}$$

The equation states that the time constant of the system is equal to the resistance to convection multiplied by the total thermal capacitance of the system. The analysis that follows will be performed first on a 200 µL polypropylene PCR tube with 10 µL of water

inside of it modeled as a cylinder of diameter 2.6 mm and height 2.5 mm. The time constant in this case is given by

$$\tau_t = \frac{V(\rho_w c_{pw} f_w + \rho_p c_{pp} f_p)}{\overline{h} A_s} \tag{3.6}$$

where V is volume of the reaction tube, ρ_w and ρ_p are the densities of the water and polypropylene, c_{pw} and c_{pp} are the specific heats of the water and polypropylene, A_s is the surface area of the cylinder, and f_w and f_p are the fraction volume of water and polypropylene in the reaction volume. A lumped thermal conductivity was found using the volumetric fraction of water and polypropylene that was used to determine the average heat transfer coefficient from $\overline{Nu_D}$.

$$k = k_w f_w + k_p f_p \tag{3.7}$$

Time constants were found for the system using the average convection coefficients found in Table 3.2. The results are shown in Table 3.3.

Table 3.3 Calculated time constants (τ) for the air velocities within the single and double fan convective thermocycler for a modeled 200 µL polypropylene tube with 10 µL of water

Air velocity (m/s)	0.52	1.2	0.74	3.4
Tau (s)	34	23	29	14

The time constant is the time that it takes the reaction volume to reach within 63.2 % of the difference between the initial temperature of the solution and the setpoint temperature. If the setpoint was 72 °C, the initial temperature was 52 °C, and the time constant was 34 seconds, the reaction should be at 64.6 °C after 34 seconds, for example.

A 200 µL polypropylene PCR tube filled with 10 µL of water was modeled using a 2-D heat transfer finite element program. A schematic of the model used is shown in Figure 3.11.

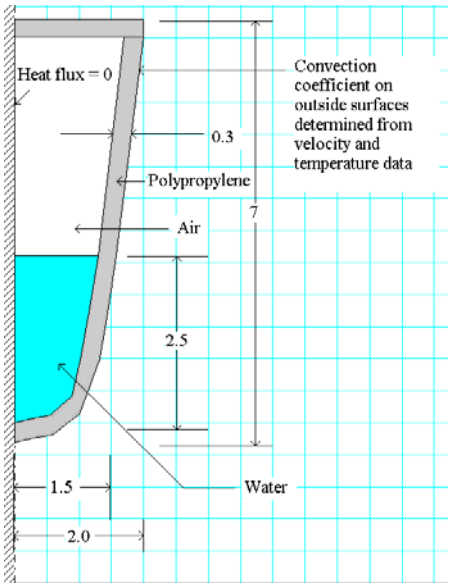

Figure 3.11 2-D model used for convective analysis of 200 µL polypropylene tube filled with 10 µL of water, dimensions in mm

The temperature profiles of the convective thermocyclers obtained in the results section were input into the 2-D model shown in Figure 3.11 along with the time average heat transfer coefficients, calculated with the velocity and temperature information from experiment. The experimental results were then compared with the 2-D model results to determine the validity of this method. The properties of polypropylene used in the model are shown in Table 3.4 (Goodfellow 2005).

Table 3.4 Polypropylene properties

	Density (kg/m^3)	**Thermal conductivity (W/m K)**	**Specific heat (J/K kg)**
Polypropylene	900	0.17	1800

Heating from 52 to 94 °C was modeled with the 2-D finite element program for the single fan convective thermocycler. The experiment with a 200 µL tube with 10 µL of fluid in the single fan convective thermocycler indicated that the initial temperature of the fluid before the heating began was 53.3 °C as shown in Figure 3.12.

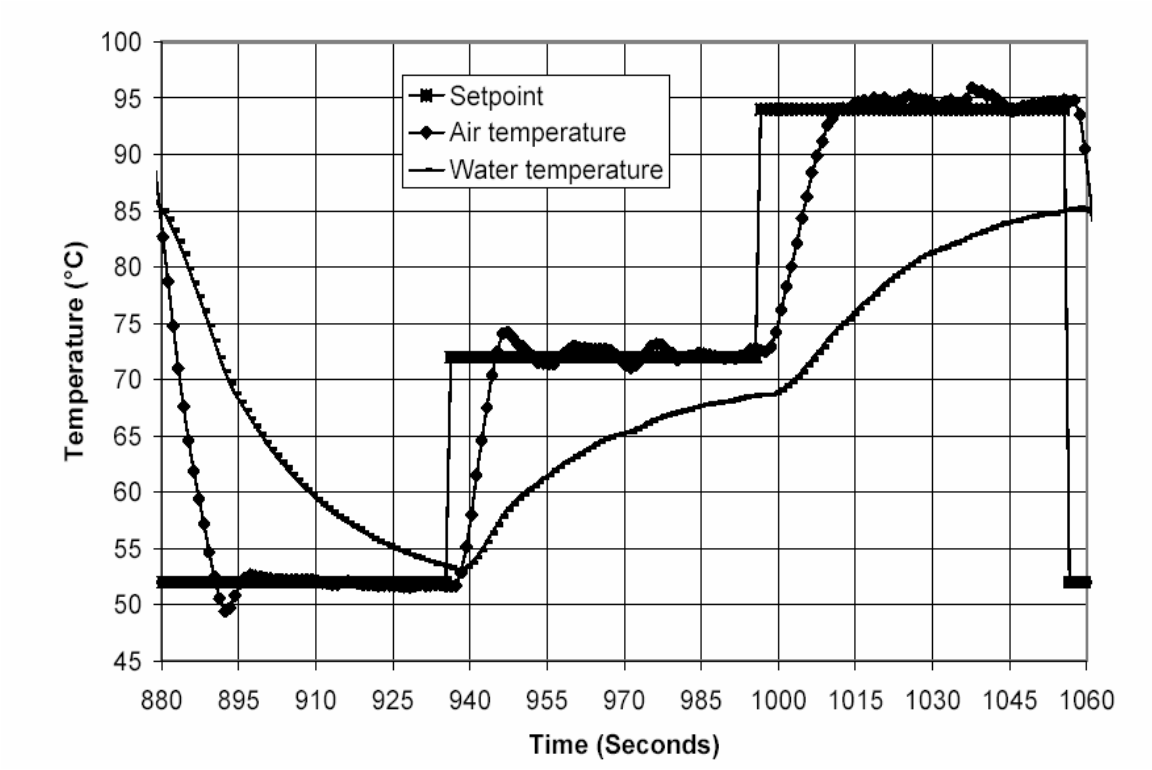

Figure 3.12 Experimental results for single fan convective thermocycler with 200 µL tube filled with 10 µL of water placed inside vent pipe

The temperature of the fluid inside the tube was measured with a thermocouple placed inside the tube, immersed in the fluid. Analysis showed that the average convection coefficient over the surface of the cylinder remained relatively constant during heating from 52 to 94 °C, varying by only 0.06 %. A constant value of $\overline{h}$, average convection coefficient, was used for this reason and was taken to be 48.0 W/m^{2}K.

The 2-D model produced the results shown in Figure 3.13.

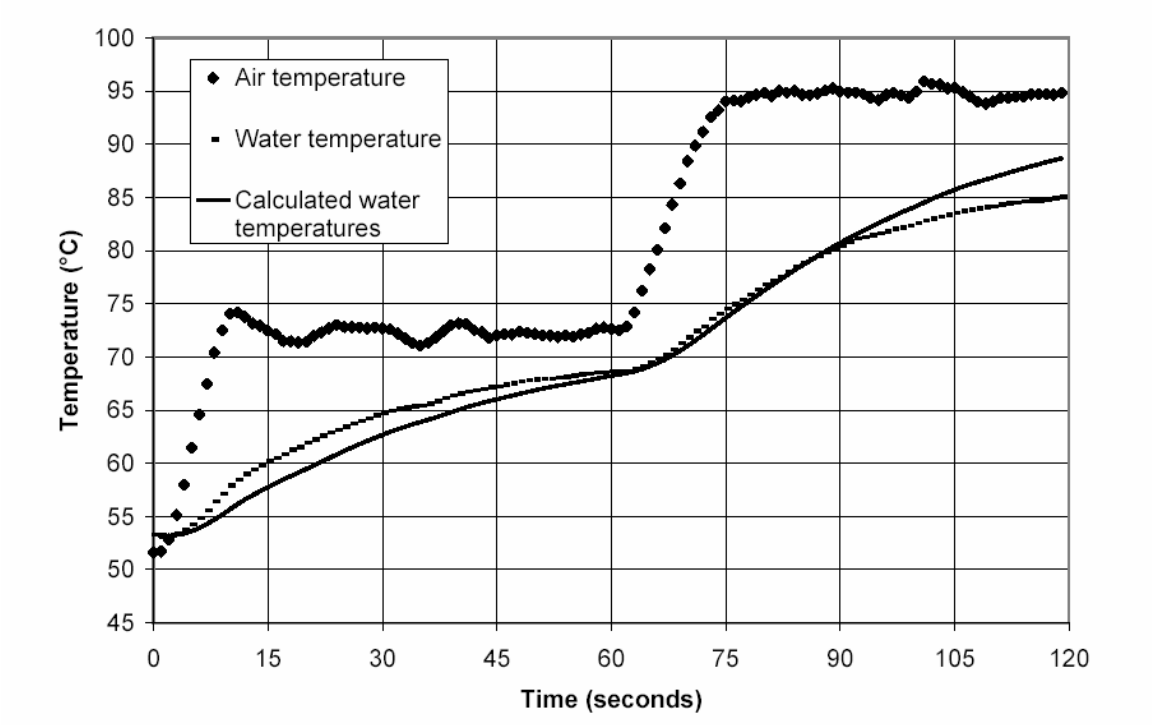

Figure 3.13 2-D model correlation with experimental results for single fan convective thermocycler with 200 µL PCR tube containing 10 µL of water during heating from 52 – 94 °C

The maximum error between the experimental value and the modeled value was 3.6 K. The calculated time constant for the system was 34 seconds using the lumped capacitance model. This means that the temperature at 34 seconds should be 64.6 °C for the heating case between 52 and 72 °C. The actual water temperature was 65.2 °C at this point while the 2-D finite element model predicted a temperature of 65.7 °C. The significant time lag of the reaction mixture in comparison with the air temperature is shown in Figure 3.13. The air temperature reached the setpoint of 72 °C within 8 seconds while the reaction mixture failed to reach the setpoint temperature within the 60 second time frame.

The single fan convective thermocycler with 200 µL PCR tube filled with 10 µL of water during cooling from 86 to 52 °C was modeled with the 2-D finite element

modeling package. The initial temperature of the solution at the beginning of the temperature decrease was 86.2 °C. The convection coefficients used were 57 W/m^{2}K for the first fifteen seconds of the cool down, corresponding to the time when the fan was on at full power, and 48 W/m^{2}K for the period after 15 seconds when the fan was pulsed. The results of the analysis are shown in Figure 3.14.

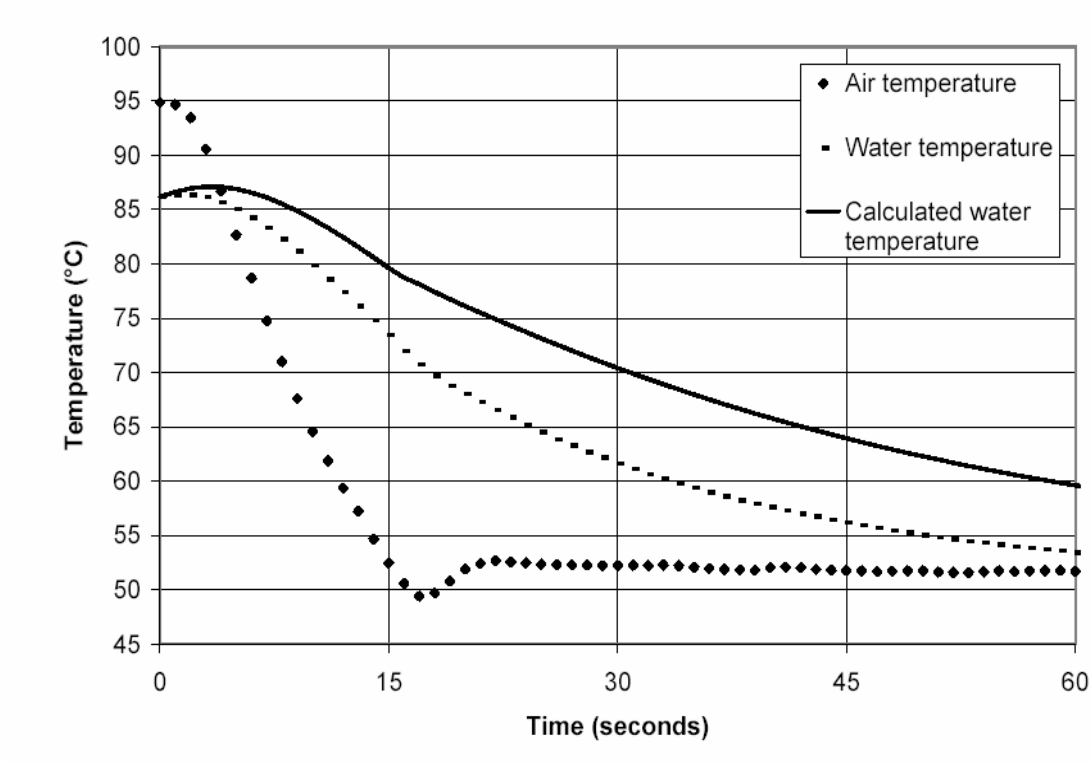

Figure 3.14 2-D model correlation with experimental results for single fan convective thermocycler with 200 µL PCR tube during cooling from 86 – 52 °C

The calculated time constant for this reaction volume during cooling was 29 seconds, indicating that the solution temperature should be at 64.5 °C after one time constant. The temperature of the solution was actually at 62.1 °C at this time. The 2-D modeled temperature was at 71 °C after 29 seconds. The maximum error between the model and the actual temperatures was 8.8 K, indicating poor agreement between the

model and experimental data. This result indicates that the actual air velocity in the tube may be higher than calculated using the control volume approach.

The double fan convective thermocycler reaction volume was modeled with the lumped capacitance method in order to validate this method for future work. The performance of the double fan convective thermocycler with a 200 µL polypropylene tube filled with 10 µL of water is shown in Figure 3.15.

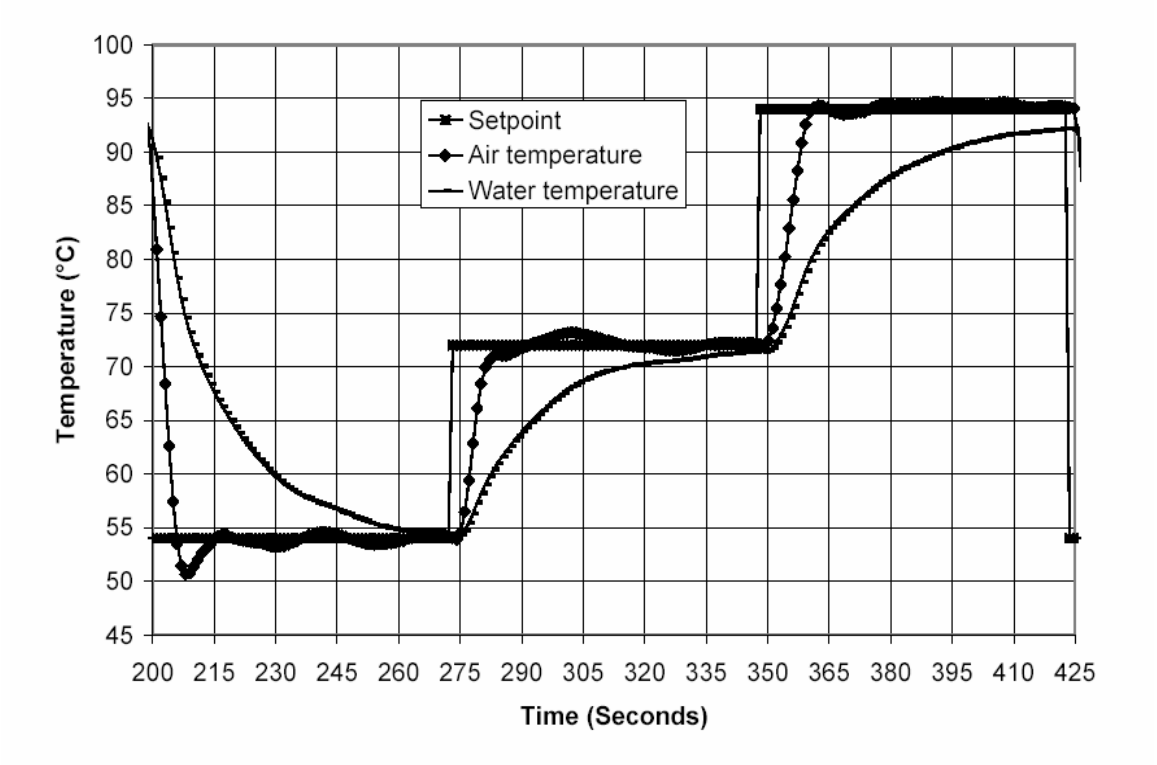

Figure 3.15 Experimental results for double fan convective thermocycler with 200 µL polypropylene tube filled with 10 µL of water placed inside vent pipe

Recall that the polypropylene tube was modeled as a cylinder with a diameter equal to the average 2.5 mm of the reaction tube and a wall thickness of 0.3 mm. The time constant for the air in the vent tube was 8 seconds for the heating modes and 6 seconds for the cooling mode. The calculated time constants for the fluid in the reaction tube are 23

seconds for the heating mode and 14 seconds for the cooling mode when the fan is on at full power as shown in Table 3.3.

The temperature at time *t* is dependent on T_∞, the temperature of the air stream, as shown in Equation 3.5. The temperature of the air stream is transient during the initial part of the heating phase. This gives two views on how to model this problem. The first view is to model the problem with the transient air temperature of the air, substituting the appropriate value of T_∞ (t). The second view is to model the problem using constant value representing the setpoint for T_∞ since the time constant of the reaction volume is 3 times greater than the time constant of the air within the vent tube during heating. These two approaches were used for the heating modes of the double fan convective thermocycler. The results of the modeling are shown in Figure 3.16.

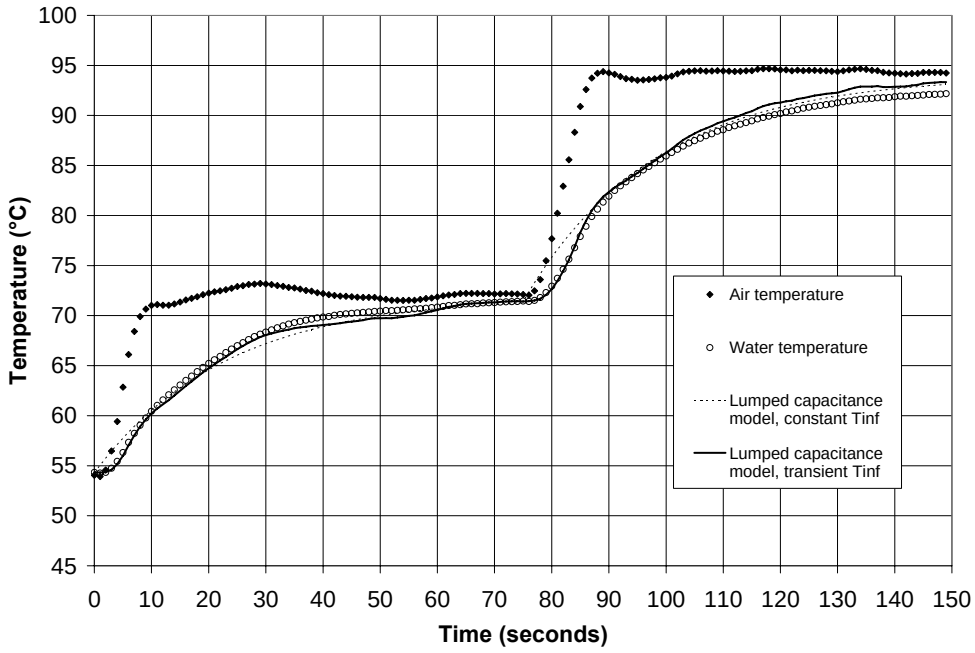

Figure 3.16 Lumped capacitance model with experimental results for double fan convective thermocycler with 200 µL PCR tube during heating from 54–94 °C

The correlation between experimental data and the lumped capacitance models is strong. The lumped capacitance model with constant T_∞ has more error associated with it then the model with transient T_∞ during the first eight seconds of the test, and again during the first eight seconds of heating from 72 to 94 °C. The average error over the first 8 seconds of heating from 54 to 72 °C for the constant T_∞ case was 1.0 °C while the average error associated with the transient T_∞ case was 0.4 °C. The average error over the first 8 seconds of heating from 72 to 94 °C for the constant T_∞ case was 2.0 °C while the average error for the transient T_∞ case was 0.5 °C. The average error for the remainder of the time period was also calculated. The average error for the transient T_∞ case turned out to be 0.5 °C while the average error for the constant T_∞ case turned out to be 0.6 °C. The time constant of the reaction volume for heating between 54 and 72 °C was 20 seconds. The time constant of the reaction volume for heating between 72 and 94 °C was 25 seconds. The calculated time constant was 23 seconds for these temperature intervals. These results indicate that accurate results can be obtained by ignoring the transient heating of the air in modeling the solution temperature with the lumped capacitance method as long as the time frame being analyzed is outside the time constant of the air, in this case 8 seconds, and the time constant of the reaction volume is 3 times larger than the time constant of the air.

The lumped capacitance model was used to model cooling of the reaction volume consisting of a 200 µL PCR tube containing 10 µL of water within the double fan convective thermocycler. The same approach was used as was used for the heating modes of the double fan convective thermocycler. The first situation was when T_∞ was

held constant at the setpoint temperature. The second situation was when T_∞ was allowed to vary with the air stream temperature. The cooling phase consisted of two different values of $\bar{h}$. The first value was the one associated with the fan at full power and was taken to be 120 W/m^2 K. Recall that during cooling, the cooling fan is turned on at full power and the heater fan is turned off. The second value of $\bar{h}$ was associated with the condition when the cooling fan was turned off and the thermocycler returned to its normal operating state, the heating fan pulsed with the heater on. The second value of $\bar{h}$ was taken to be 71 W/m^{2}K. The cooling fan was on at full power during the test for seven seconds. The results of the modeling using the lumped capacitance method are shown in Figure 3.17.

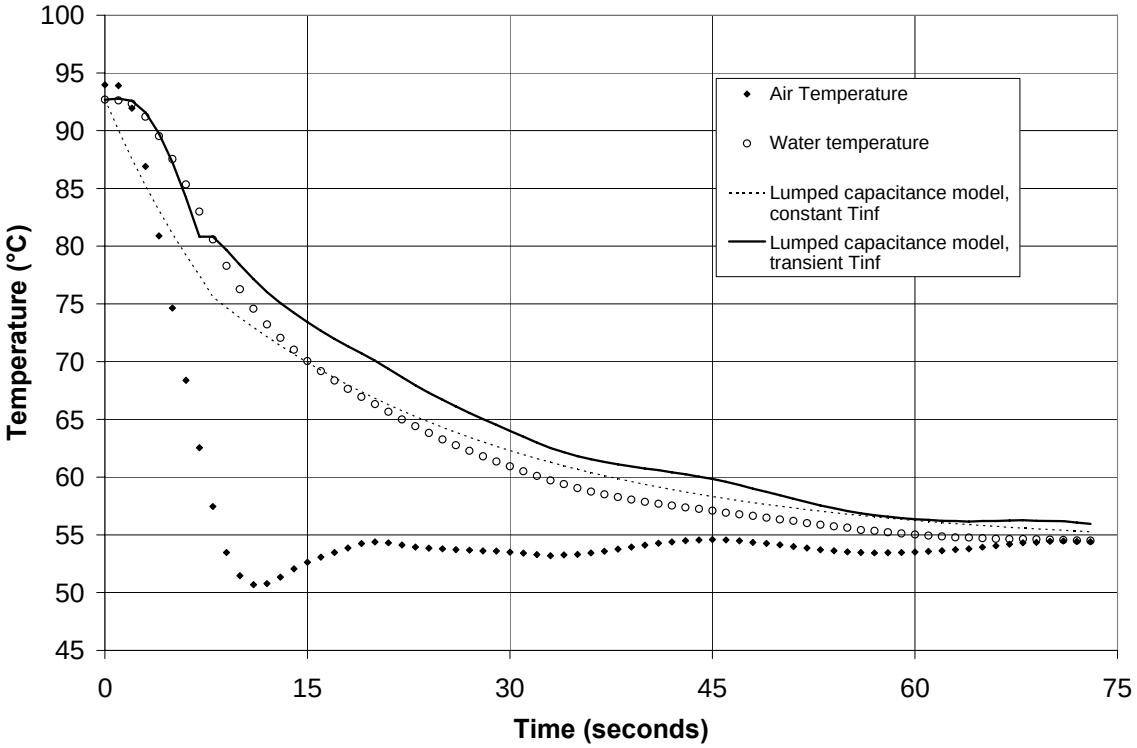

Figure 3.17 Lumped capacitance model with experimental results for double fan convective thermocycler with 200 µL PCR tube during cooling from 94–54 °C

The time constant for the cooling air was 6 seconds because it took the air temperature that long to reach 69 °C. The time constant for the reaction volume was 17 seconds. The calculated time constants for the fan at full power and the heating fan at 0.5 duty cycle were 14 and 23 seconds, or an average of 18 seconds, which corresponds well with the experimental results. It is clear by looking at Figure 3.17 that the error associated with the constant T_∞ case was much greater than the error associated with the transient T_∞ case over the six second time constant of the air temperature. The average error for the time period minus the initial six seconds for the transient T_∞ case was 2.4 °C while the average error for the constant T_∞ case was 1.4 °C. This indicates, as does the heating case, that the transient cooling of the air may be ignored when modeling the reaction volume using the lumped capacitance method for times much greater than the time constant of the air. If the reaction volume temperature is desired during a time less than the time constant of the air, than the transient T_∞ lumped capacitance model should be used. Both lumped capacitance models in Figure 3.17 have a small area where the curve is not smooth at t = 8 s. This is because this is the point where the heat transfer coefficient was changed, corresponding to the time when the cooling fan was turned off, and the heating fan was turned on, pulsed at 0.5 duty cycle.

3.3 Convective thermocycler options to enhance performance

Increasing the heating rate of the air within the vent tube is one way to enhance the performance of the thermocycler. Considering the heater itself, a heater with greater surface area could be designed to allow for more efficient heat transfer from the heater to

the air. More power could also be supplied to the heater to add more energy to the system.

High air velocity and high heating rate of the air is a challenge because the heater can only supply so much energy to the air as it flows by it. Two important parameters for high reaction volume heating rate are velocity and air temperature heating rate. The velocity of the air may only be increased by so much before the heater will not be able to heat the air to the setpoint temperature.

An increase in air velocity within the convective thermocyclers would increase the Reynolds number and would therefore increase the convection coefficient between the tube and the air. The time constant of the reaction was determined for a variety of different air velocities assuming a glass cylinder with wall thickness of 240 μm and outside diameter of 890 μm corresponding to the diameter of a commonly found glass capillary, an air stream temperature of 94 °C, a surface temperature of 72 °C, and a length of 2.6 mm. The capillary was filled with water. The plot of the time constant versus air velocity is shown in Figure 3.18.

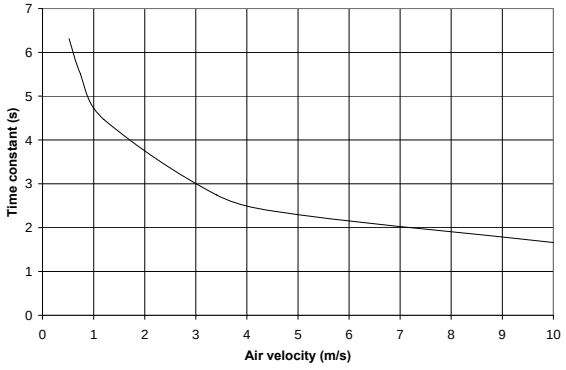

Figure 3.18 Plot of time constant versus air velocity for cylindrical configuration with constant diameter, length, wall thickness, surface temperature, and air temperature

All of the time constants, except one, graphed above are lower than the heating time constant of the convective thermocycler which was 8 seconds. The cooling time constant of the double fan convective thermocycler as tested was 6 seconds. All of the graphed time constants are less than this also, except for the 0.5 m/s case. The change in time constant for this reaction vessel versus air velocity levels out somewhat after 4 m/s. The benefit of increasing the air velocity after this point results in reduced return, compared with the benefit obtained before the 4 m/s point.

The reaction volume may be manipulated to enhance the heat transfer. One way to do this for a cylindrical reaction vessel is to decrease the diameter of the reaction vessel. It was shown above that a cylindrical glass tube with an outside diameter of 890 μm has a shorter time constant compared with the 2.6 mm diameter polypropylene tube. A plot of time constant versus cylinder diameter was made assuming a constant air velocity of 1.2 m/s, a wall thickness of 244 μm, a polypropylene tube, and a length of 2.6 mm is shown in Figure 3.19.

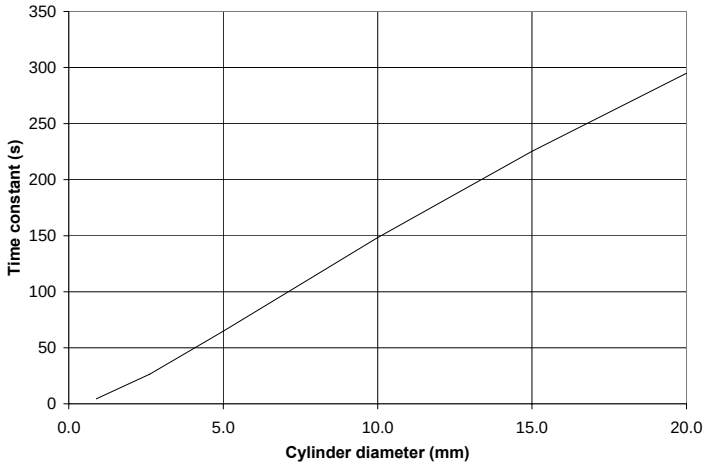

Figure 3.19 Plot of time constant versus diameter for cylindrical polypropylene configuration

This plot shows that the time constant with a cylinder of this diameter would be 5 seconds which is less than the double fan convection air temperature time constant of eight seconds. The cylindrical tube studied in Secion 3.2.3 is the point with diameter = 2.62 mm corresponding to a time constant of 23 seconds. This analysis shows the dramatic effect that changing the diameter of the reaction vessel can have on the time constant of the system. The cost of decreasing the diameter of the reaction vessel is that one can get less solution into it per unit length.

The lumped capacitance method was used to model the behavior of a glass capillary in the double fan convective thermocycler. The inside diameter of a commonly available glass capillary is 0.4 mm so it would be necessary to have a capillary 39.8 mm long to have 5 μL of PCR solution in it. For a reaction volume of this geometry with this amount of water in it, a wall thickness of 244 μm, and an air velocity of 1.2 m/s the lumped capacitance method yields a time constant for the system of 4.8 seconds, a value of 3.6 for the average Nusselt number, and 126 W/m^2K for the average convection coefficient. This time constant was used to model the behavior of the reaction volume in the double fan convective thermocycler as tested previously. The results of the analysis are shown in Figure 3.20.

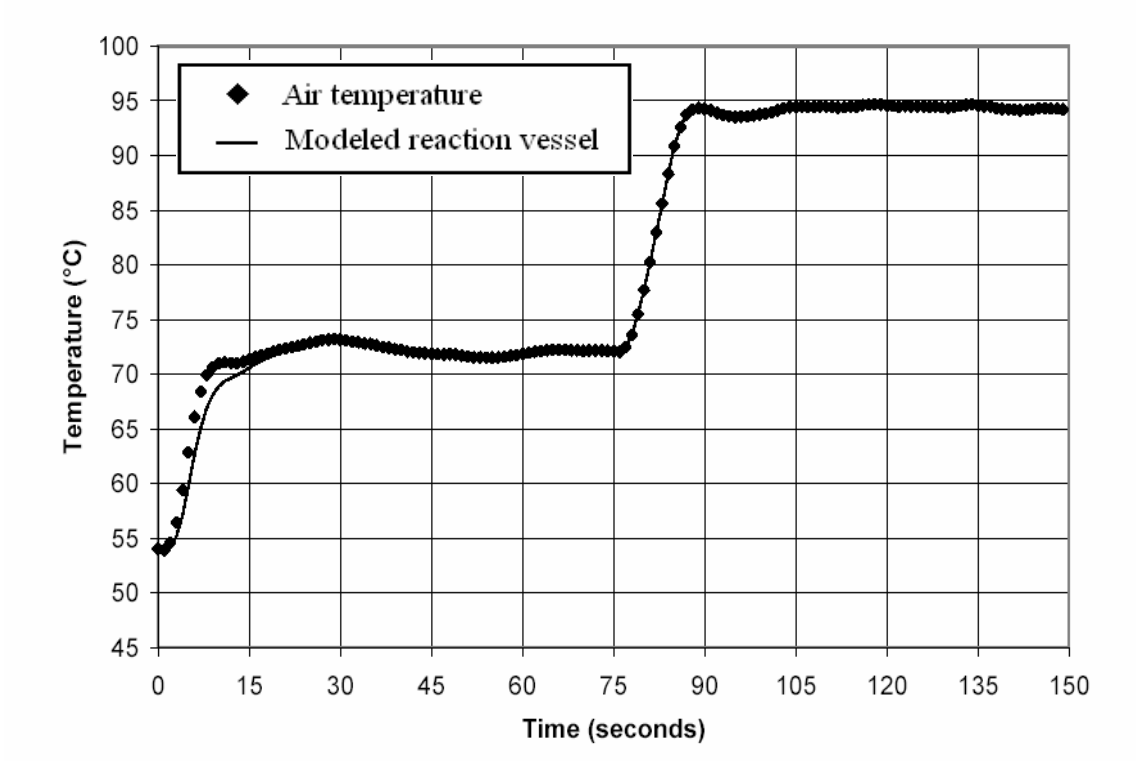

Figure 3.20 Lumped capacitance model of reaction volume temperature for glass capillary of 890 μm outside diameter with 5 μL of water inside

These results indicate that the solution temperature is nearly identical to the air temperature for the case with the glass capillary in the double fan convection thermocycler. This indicates that the limiting factor in PCR speed is the ability of the thermocycler to heat the air since the time constant of the reaction mixture is less than that of the air temperature within the thermocycler.

The reaction mixture may also be placed into a reaction vessel of different shape. One reaction vessel that is of interest is a sphere. A sphere of inside diameter 2.12 mm is needed to have a reaction volume of 5 μL. the average Nusselt number is given by (Incropera and DeWitt 1996)

$$\overline{Nu_D} = 2 + (0.4\,\mathrm{Re}_D^{1/2} + 0.06\,\mathrm{Re}_D^{2/3})\,\mathrm{Pr}^{0.4}\left(\frac{\mu}{\mu_s}\right)^{1/4} \tag{3.8}$$

The lumped thermal conductivity was used in the calculation of the average heat transfer coefficient as in Equation 3.7. A glass sphere with this inside diameter and wall thickness of 244 μm, an air velocity of 1.2 m/s, a surface temperature of 72 °C, an air stream temperature of 94 °C, and the lumped capacitance method, a time constant of 16.1 seconds is obtained with an average Nusselt number of 7.2, and an average value of the convection coefficient of 90 W/m^{2}K. The time constant for the spherical geometry is greater than the 890 μm outside diameter cylinder with the same reaction volume because the diameter of the cylinder is much less than the sphere. For the geometries used in this analysis, the surface area to volume ratio of the cylinder is almost twice as great as the sphere. Even though the average Nusselt number is twice as great for the sphere, the convection coefficient convection is smaller because of the smaller surface area to volume ratio of the sphere. The time constant of the spherical system versus diameter for a 1.2 m/s air velocity, glass wall thickness of 244 μm, surface temperature of 72 °C, and air stream temperature of 94 °C is plotted in Figure 3.21.

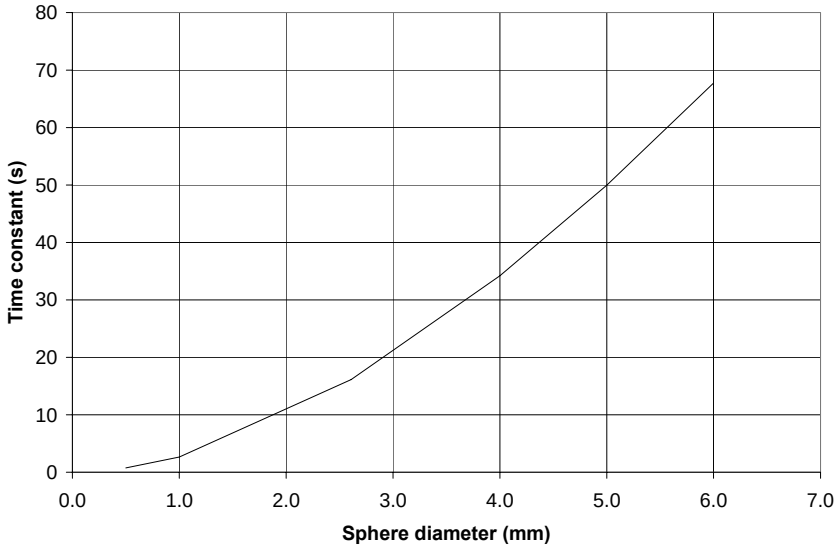

Figure 3.21 Plot of time constant versus diameter for spherical configuration with constant air velocity, and wall thickness

The materials and dimensions of materials needed to optimize the reaction vessel were found. The lumped capacitance model was used to determine all of the time constants above. It is clear that the lumped capacitance model is an accurate model of what is occurring as was seen in its comparison with actual experimental data. The lumped capacitance model is an idealization that ignores conduction within the reaction volume. This is the best case scenario because if the reaction volume was large enough such that the lumped capacitance model was not valid, then the reaction dynamics would be slowed by conduction within the volume. The lumped capacitance model is valid under the following condition (Incropera and DeWitt 1996)

$$Bi = \frac{hL_c}{k} < 0.1 \tag{3.9}$$

where L_c is the characteristic length and is given by the volume to surface area ratio of the reaction volume. The variable k is taken to be the lumped thermal conductivity of the reaction volume as in Equation 3.7.

The Biot number may be used to determine what reaction tube materials would allow for quick heating. Assuming a convection coefficient of 126 W/m^{2}K, which corresponds to the convection coefficient for the double fan convective thermocycler during heating for a cylindrical reaction vessel with 244 μm thick walls and an outside diameter of 890 μm, gives a value of 0.20 W/m K as the minimum thermal conductivity to satisfy the Biot number. Common materials used to build reaction vessels have thermal conductivities at or above this value. The thermal conductivities of several materials that could be used to make a reaction vessel are shown in Table 3.5 (Incropera and DeWitt 1996; Efunda 2005).

Table 3.5 Thermal conductivities of candidate materials for PCR reaction vessels

Material	Thermal Conductivity (W/mK)
Polypropylene	0.17
Polycarbonate	0.20
Silicon	148
Glass (soda lime)	1.4

The thermal conductivities of the materials listed in Table 3.5 are all greater or very close to 0.2 W/m K so any one of them could be used in the cylindrical configuration mentioned above without causing large spatial temperature gradients within the reaction vessel.

The diameter of the reaction vessel may also be varied. It is of interest to know the largest diameter possible of the cylindrical reaction vessel such that spatial variation in temperature does not play into the analysis. This calculation was run assuming that the velocity of the air was 1.2 m/s, the cylinder was 39.8 mm long, the cylinder was being heated from 72 to 94 °C, and the material was polypropylene with a wall thickness of 244 μm. The results of this analysis are shown in Table 3.6.

Table 3.6 Biot number for varying polypropylene cylindrical diameters

Cylinder Diameter (mm)	Average convection coefficient (W/m^2K)	k (W/mK)	Bi
0.89	126.	0.26	0.11
1.0	118	0.28	0.10
2.0	82	0.42	0.10
3.0	66	0.47	0.11
4.0	56	0.50	0.12
5.0	50	0.52	0.12
6.0	45	0.54	0.13
7.0	42	0.55	0.13

The results indicate that the Biot number for the cylinders is right around 0.1. The Biot number varies little for the diameters input above because as the convection coefficient decreases, the value of k increases because of the greater percentage of water, and the characteristic length increases, the net result is little change in the Biot number. These results indicate that varying the diameter of the cylinder up to 7 mm under these conditions has little effect on the Biot number, indicating that spatial temperature

gradients should be small. The problem with increasing the diameter of the tube is the decreased convection coefficient.

The Biot number becomes larger than 0.1 if the wall thickness of the capillary is increased. A polypropylene capillary with an air velocity of 1.2 m/s flowing past it during heating from 72 to 94 °C, and a length of 40.0 mm was analyzed by varying the tube wall thickness. The results of the analysis are shown in Figure 3.22.

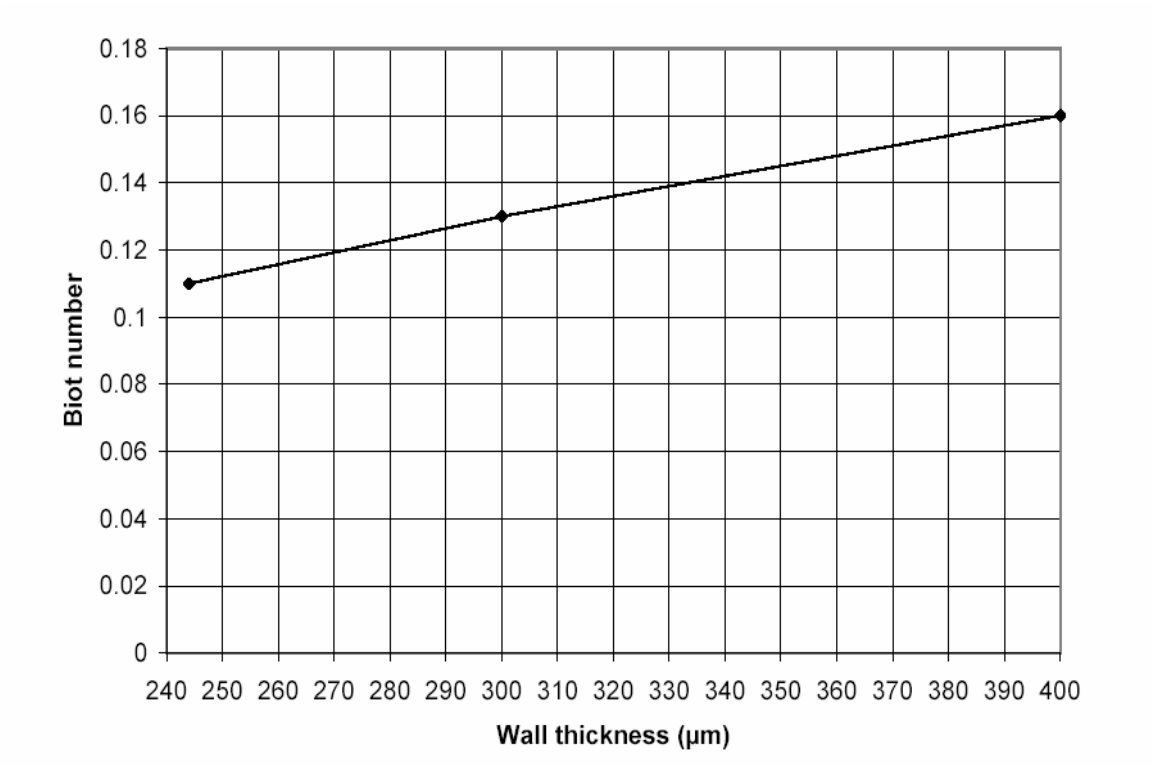

Figure 3.22 Biot number versus wall thickness for a poly propylene capillary of outside diameter 890 µm

Increasing the wall thickness of a polypropylene capillary under these conditions can cause an increase in the Biot number, which is an indicator of the temperature gradient that will be present within the reaction vessel. The reason for this is that the low thermal conductivity of polypropylene begins to dominate the reaction dynamics because of its thickness in relation to the water. If the capillary material is glass, which has a greater

thermal conductivity than water, than the Biot number decreases with increasing wall thickness as shown in Figure 3.23.

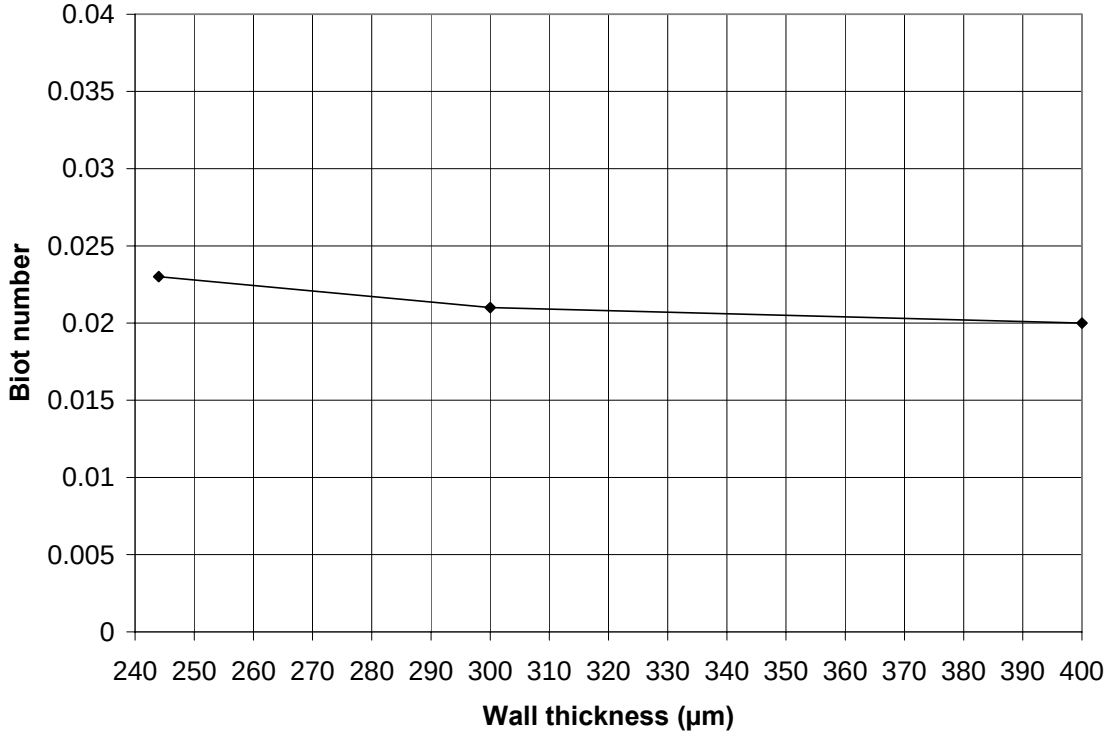

Figure 3.23 Biot number versus wall thickness for a glass capillary of outside diameter 890 μm

The decreasing Biot number means that the temperature of the reaction volume will be nearly uniform during the thermocycling process. Using materials with a higher thermal conductivity than water can be beneficial in making the reaction vessel more isothermal.

4. ANALYSIS OF MICROHEATERS FOR PCR

Another option for heating reaction volumes for PCR is the use of microheaters (Selvaganapathy, Carlen et al. 2003; Lee, Ho Park et al. 2004). Microheaters are heaters that have features that can be measured on the micron scale. Microsystems take advantage of reaction volumes on the μL or in some cases nL scale to enhance the speed of PCR (Matsubara, Kerman et al. 2004; Gulliksen, Solli et al. 2005). Reaction volumes that have low thermal capacitance allow rapid PCR by minimizing energy storage within the vessel. The microheater is typically tightly coupled to the reaction volume (Yoon, Lee et al. 2002), allowing heat transfer to occur rapidly, unlike Peltier devices which are typically covered with a ceramic layer, and in some cases have metal blocks mounted on top of them.

The work of other groups in this area was studied and a survey of that work is described in Section 4.1. Microheaters were designed and fabricated using standard MEMS techniques, as discussed in Section 4.2 . A control system, discussed in Section 4.3, for temperature cycling with the microheater was built and tested.

4.1 Synopsis of work done on microheaters by other groups

SU-8 is one option for creating microchambers on top of microheaters. It has been used as a mold for PDMS microchambers (Zhao, Cui et al. 2002). El-Ali and others have recently incorporated a thin film platinum heater with an SU-8 reaction volume to achieve heating and cooling rates five times faster than the fastest macroscale device and power consumption 126 times less (El-Ali, Perch-Nielsen et al. 2004). The device created by this group consists of an SU-8 based PCR chamber that is affixed to a 1 mm

thick glass substrate with a thin film platinum heater deposited on it. There are 83 individual heater elements, each element is 20 μm wide and 8.3 mm long with spacing between heater elements of 100 μm. The heaters extend beyond the boundaries of the reaction chamber to minimize cold wall effects. The glass also has an independent thermometer separate from the heater itself. The resistance of the platinum thermometer changes linearly with temperature making it possible to determine the temperature by measuring the resistance. The reaction chamber is 7 x 7 x 0.4 mm, giving a total reaction volume of 20 μL. Atop the reaction chamber a 0.5 mm glass piece is bonded with SU-8 utilizing SU-8 to SU-8 bonding. The lid has two small openings in it, through which the reaction chamber may be filled. It was not mentioned how these holes were sealed during cycling. The chip is cooled via natural convection and through a heat sink connected to the lower surface. A Labview PID controller was used to control the heating and cooling of the chip. A schematic of the device is shown in Figure 4.1 (El-Ali, Perch-Nielsen et al. 2004).

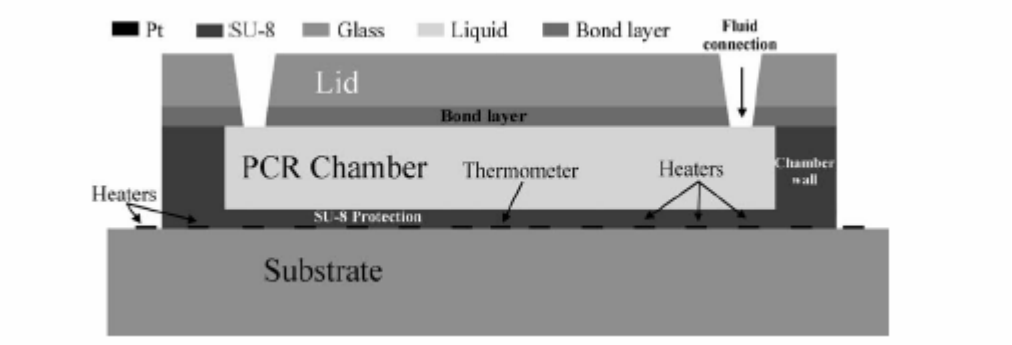

Figure 4.1 Heater with integrated well as designed by El-Ali et al.

El-Ali et al. used standard MEMS techniques to fabricate the device shown above. The heater electrodes and the thermometer were patterned with lift-off on the glass substrate. The platinum was deposited via e-beam evaporation using a 100 Å titanium layer for adhesion. A 5 μm SU-8 layer was spun onto the wafer. The pattern was soft baked and patterned with photolithography. The purpose of this layer was to protect the electrodes from the PCR solution. The 400 μm deep reaction vessel was defined with two spins of 200 μm each. A soft bake step was used in between each spin. The glass lid was next bonded to the SU-8 reaction vessel using SU-8 to SU-8 bonding by first applying a thin coat of SU-8 to the glass lid, soft baking the lid with SU-8 on it, positioning the lid on top of the SU-8 section, soft baking, exposing with UV light, and finally another bake. It was necessary for the researchers to treat the SU-8 surfaces of the reaction chamber with the silanizing agent dichlorodimethylsilane to make it PCR compatible. The dichlorodimethylsilane makes the surface PCR compatible by inhibiting adsorption of DNA and polymerase to the surface of the chamber (Kopp, de Mello et al. 1998). The final step in the production of the chip was drilling two holes in the glass lid for filling of the reaction vessel (El-Ali, Perch-Nielsen et al. 2004).

Silicon has also been tested as a material for microchambers (Daniel, Iqbal et al. 1998; Nagai, Murakami et al. 2001; Matsubara, Kerman et al. 2004). Zhao et al. designed a PCR microchip with an integrated heater utilizing silicon as the material for the reaction vessel (Zhao, Cui et al. 2003). The device developed by this group was an 8 x 4 mm chip. The reaction vessel is 4 x 2 x 0.27 mm, giving a total reaction volume of 2 μL. The reaction vessel was manufactured on one side of the chip while the thin film platinum heater was deposited on the opposite side of the chip. The heater was separated

from the reaction volume by a distance of only 2 μm. Two channels were etched on opposite sides of the reaction vessel to provide a method for filling the vessel with PCR reagents. The chip was anodically bonded with a 0.2 mm thick piece of borosilicate glass. Two holes were drilled in the glass and were aligned with the chip to allow filling. A schematic of the setup is shown in Figure 4.2. The device consists of a heating power supply circuit, temperature controller, keypad, and display. The heater was controlled with a microcontroller and a PID scheme. The heater power was controlled with pulse width modulation at a frequency of 19.5 kHz (Zhao, Cui et al. 2003).

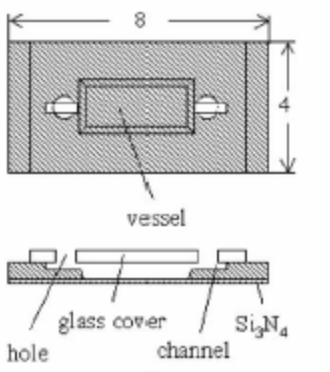

Figure 4.2 PCR reaction vessel designed by Zhao et al. (Zhao, Cui et al. 2003).

The device was fabricated using a 270 μm double-side polished silicon wafer. Prior to etching, silicon nitride was deposited on each side of the wafer to a thickness of 2 μm. The reaction vessel was wet etched with KOH utilizing the silicon nitride as a stop layer. A 100 nm oxide layer was deposited after the wet etch to provide a suitable surface for the PCR reaction. Two 1 mm length channels were etched on each side of the reaction vessel to allow filling. The platinum heater and temperature sensor were patterned on the backside of the wafer using standard photolithography and lift off. The chip was next mounted on a PCB board with patterned electrodes to connect to the heater (Zhao, Cui et al. 2003).

Researchers have turned to plastic microchambers for use with microheaters (Giordano, Ferrance et al. 2001; Liu, Rauch et al. 2002). Zou et al. have taken this approach to designing a PCR microchip with integrated heater. The device consists of

multiple silicon blocks with a thickness of 680 μm bonded to a 500 μm PCB substrate with a heat sink attached to the bottom. Heaters and temperature sensors are fabricated on the underside of the silicon blocks. The reaction chambers were thermally molded in plastic with a silicon plate etched with KOH. The type of plastic used was not specified. The 4 x 4 array of reaction chambers are affixed to the top of the heaters with thermal grease and mechanical means. The reaction chambers are 400 μm deep, are approximately 5 mm square, and have a wall thickness of 100 μm yielding a reaction volume of 20 μL. A schematic of the device is shown in Figure 4.3 (Zou, Miao et al. 2002).

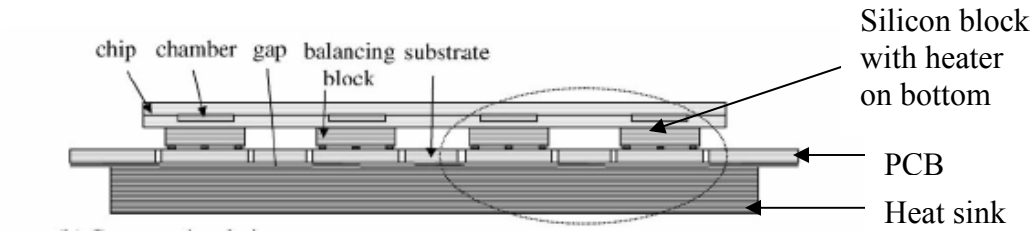

Figure 4.3 Microheaters with integrated reaction vessels as designed by Zou et al.

The heater array manufactured by Zou used standard MEMS techniques. The process began with a thermal oxide deposition on the top of the wafer. The heaters and temperature sensors were manufactured by depositing the aluminum to a thickness of 2.4 μm and then patterning. Plasma enhanced chemical vapor deposition was next used to deposit a silicon nitride layer on top of the heater elements. This layer was patterned to allow connections with some of the underlying metal components of the heater with the PCB board. The next step for the designers was to deposit and pattern the under bump metal (UBM) layers. This consisted of a Ti/Ni/Au multilayer. Soldering balls were next printed onto the UBM surfaces. The PCB was produced with electrical connections for

the heaters and temperature sensor. The silicon blocks were placed on top of the PCB and soldered using temperature and pressure in a flip chip bonding technique. The PCB was next mounted to a heat sink with electrically non-conductive epoxy. The researchers used polypropylene tape or bonded a thin sheet of plastic to the top of the reaction vessels with epoxy or with solvent bonding. A schematic of the process sequence is shown in Figure 4.4 (Zou, Miao et al. 2002).

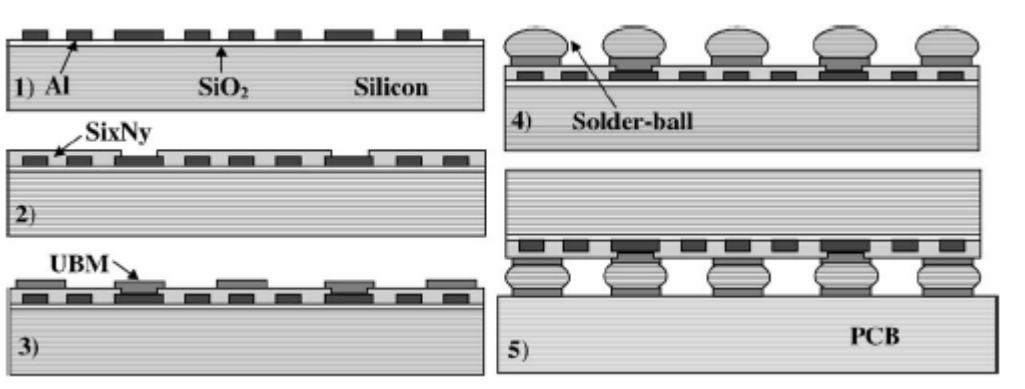

Figure 4.4 Flip chip design process used by Zou et al. for fabrication of PCR microheaters

4.1.1 Comparison of designs

The aim of a microscale device is to complete the PCR reaction as quickly as possible with little power consumption. Table 4.1 at the end of this section summarizes the operating parameters of the heaters designed by the researchers discussed above. The maximum heating rate of the device manufactured by El-Ali was approximately 50 °C/s, with a cooling rate of about 12 °C/s at a location on the heater surface. The power consumption of the heating device was 6.3 W at 94 °C (El-Ali, Perch-Nielsen et al. 2004). The device manufactured by Zhao achieved heating rates of 15 °C/s and cooling

rates of 10 °C/s at a location on the heater. This device was shown to be able to successfully complete a PCR reaction in 15 minutes (Zhao, Cui et al. 2003). Zou's group fabricated a device capable of a 42 °C/s heating rate and a 27 °C/s cooling rate with a 15 μL sample loaded in the reaction volume measured at the surface of the heater. Zou's device used, on average, only about 0.9 W per chamber . Zou's device was capable of successfully completing a PCR reaction with a 320 bp piece of plasmid DNA in a time of 15 minutes (Zou, Miao et al. 2002).

The manufacturing approach taken by El-Ali et al utilized SU-8 as the reaction volume. SU-8 is a polymer. El-Ali found that the reaction volume needed to be silanized in order to be PCR compatible. It was also necessary for Zhao's group to add an oxide layer to the silicon to make it PCR friendly. The reaction chamber used by Zou's group was made of an unspecified form of plastic and was formed with thermal molding. Zou was the only researcher who did not report the need to passivate the surface of the reaction volume.

Zou chose aluminum as the metal for his heater. The choice of aluminum is an interesting one. The other two researchers presented chose platinum as the metal for the heaters. Zou reported that he was using aluminum thicknesses upward of 2.5 μm. Zou did not report how this was done

Zou's device was the most ready for mass production. Zou incorporated an array of heaters in his design and had a thermal molding process for producing reaction chambers. Thermal molding is faster than building reaction vessels out of SU-8 or etching them out of silicon, processes used by El-Ali and Zhao. Zou also utilized flip chip bonding, which enabled him to quickly attach his heater assembly to the PCB board.

Zou's device was the only one to utilize separate reaction chambers from the heaters. El-Ali had his reaction volume attached to the heater and Zhao had his heater manufactured on the same wafer as the reaction volume. This strategy by El-Ali and Zhao was a poor one. Their heating and cooling rates were no greater than Zou's. Zou's heater may be reused, however, by simply throwing away the reaction volumes and reusing the heaters. Metal deposition is an expensive and time consuming process. Platinum prices are approximately $40/gram so it is not a good idea to throw heaters made of platinum away. Zou had a good strategy when considering the reuse of his mechanism.

A summary of the designs is shown in Table 4.1. The two conventional choices for PCR, the Peltier device, Techne Techgene studied earlier, and the LightCycler, a convection device, use large amounts of power and have heating and cooling rates slower than microheater systems. Neither of the traditional devices require surface treatments. Two of the microheater devices required surface treatments due to the higher surface area to volume ratio of these devices.

Table 4.1 Comparison of thermocycling devices (Zou, Miao et al. 2002; Zhao, Cui et al. 2003; El-Ali, Perch-Nielsen et al. 2004; LightCycler 2005)

	Power Consumption (W)	Heating Rate (°C/s)	Cooling Rate (°C/s)	Number of Reaction Chambers	Reaction Volume (µL)	Surface Treatment Necessary for Biocompatibility?	Time to Complete PCR Reaction (minutes)
Traditional Peltier Device	264 (max)	3.6 (max heating block)	2 (max heating block)	20	20	No	150
Traditional Convective Device	800 (max)	5.5 (average in capillary)	5 (average in capillary)	20	10	No	30
El-Ali's Device	6.4 (@ 94 °C)	50 (max on heater)	30 (max on heater)	1	20	Yes	N/A
Zhao's Device	N/A	15 (max on heater)	10 (max on heater)	1	2	Yes	15
Zou's Device	0.9 (Average)	42 (max on heater)	27 (max on heater)	1	20	No	15

4.2 Microheater design

There are several key aspects in designing a microheater for PCR. The first items to be kept in mind are what will the power source be, how much current will the control system be able to handle, how big should the heaters be, what material should the heaters be made of, on what substrate will the heaters be fabricated on, and what heat flux is desired.

The power required by the heater in our case was an important question. The heater that we decided to design was to have platinum heating elements along with a platinum temperature sensor. The heater needed to be powerful enough to increase the sample temperature by greater than 6 K/s in order for it to heat faster than commercially available devices such as the LightCycler which is capable of heating the reaction volume at 6 K/s (LightCycler 2005). A 2-D finite element heat transfer package was used to understand the power requirements needed by a microheater. A 20 W/cm^2 heater was desired, so this power requirement was examined using the 2-D package. The material that looked promising for a reaction vessel was polycarbonate. Polycarbonate can be easily machined, molded, and bonded (Martin, Matson et al. 1998; Klintberg, Svedberg et al. 2003). The first case modeled was a polycarbonate well machined into a 2 mm thick substrate. The well was 3.2 mm in diameter and 1.5 mm deep. The model was arranged such that 10 μL of water was in the well. This meant that the height of the water in the well was 1.2 mm. The model was axisymmetric and was done with a cylindrical coordinate scheme. The heat flux across the centerline was considered to be zero. A schematic of the model is shown in Figure 4.5.

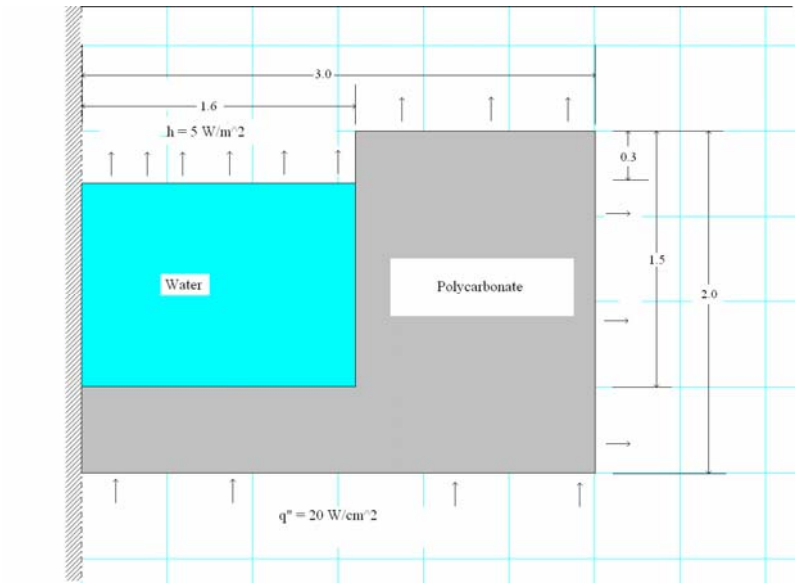

Figure 4.5 Schematic of 2-D model used in analysis of heating power

The model was run to determine the heating characteristics of the fluid in the chamber assuming that the water in the chamber is stationary. The results of that analysis are shown in Figure 4.6.

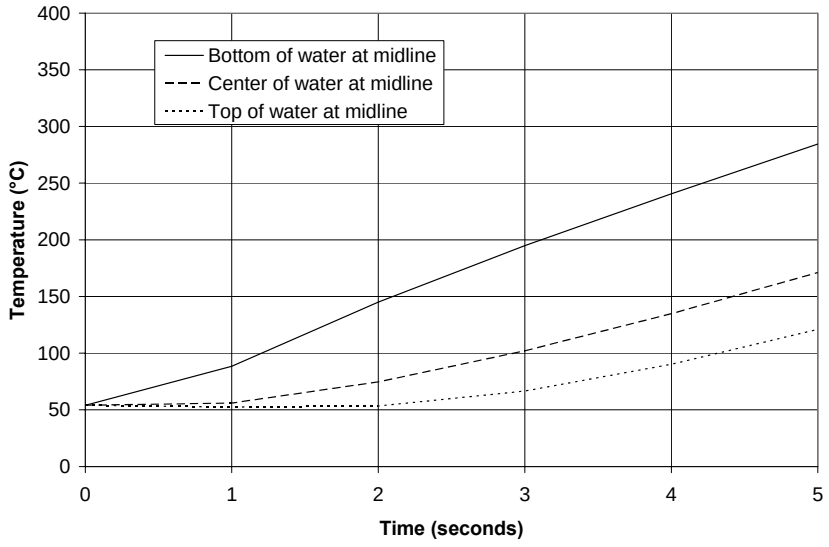

Figure 4.6 Response of 3.2 mm diameter polycarbonate chamber of thickness 2 mm with 10 µL of water in it and a heat flux of 20 W/cm^2

The three curves in Figure 4.6 are for three different positions in the reaction vessel. Figure 4.5 shows the reaction vessel with the midline at the center. The three lines in Figure 4.6 represent three positions along that axis in the water. The portion of the chamber in contact with the water heats up rapidly while the heating rate decreases as the distance from the heat flux increases. The heat flux of 20 W/cm^2 heats the bottom portion of the chamber to 88 °C in one second. This is satisfactory, but it is desired to heat the water in the reaction vessel rapidly also. This model has a polycarbonate thickness of 500 μm between the heat flux and the water with a water thickness of 1500 μm on top of it.

A polycarbonate chamber fashioned out of 2.0 mm section with a 1.5 mm deep hole and a diameter of 5.0 mm was analyzed with the 2-D finite element package to compare the performance with the previous example. This geometry allowed 10 μL of water to occupy the reaction chamber at a height of 500 μm as opposed to 1500 μm in the previous case. A schematic of the model is very similar to Figure 4.5 except that the dimensions are slightly different. The results of the analysis are shown in Figure 4.7.

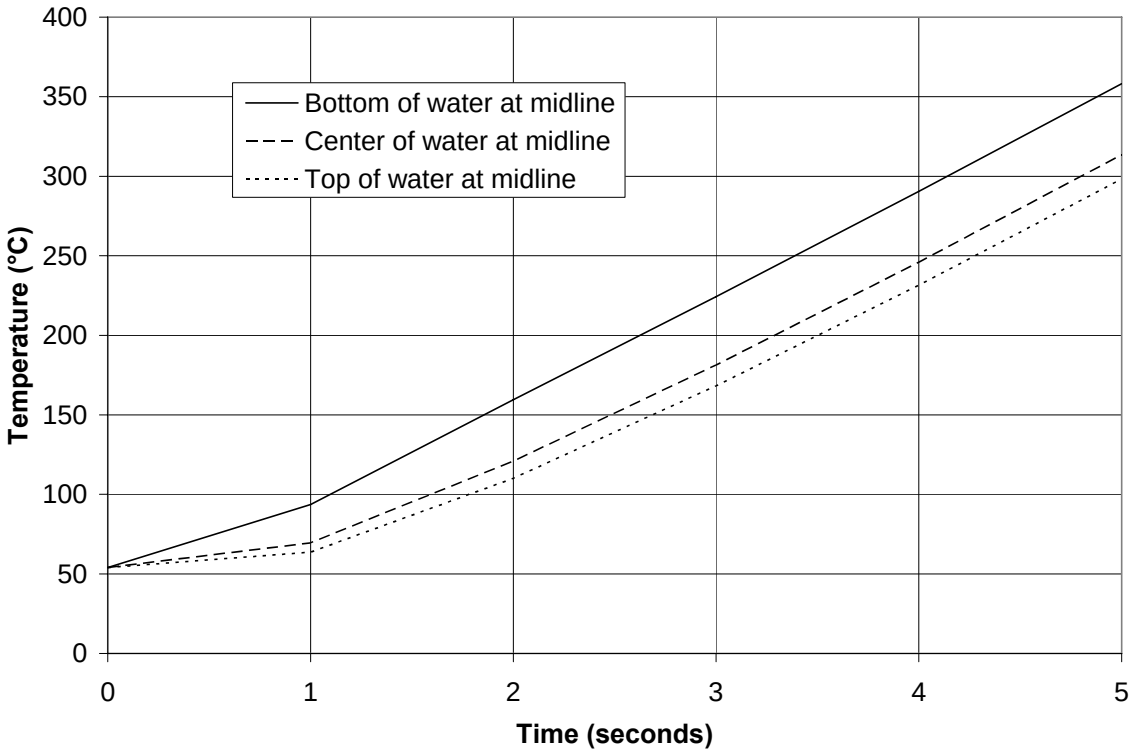

Figure 4.7 Response of 5 mm diameter polycarbonate chamber of depth 2 mm with a 10 μL sample of water in it and a heat flux of 20 W/cm^2

The average heating rate for the water at the top of the water sample for the first second is 10 °C/s and increases to 28.0 °C/s over a two second duration. These heating rates for the sample were considered acceptable and are comparable to those achieved by the researchers in section 4.1. It is clear that the bottom of the reaction chamber reached over 150 °C within two seconds of heating with this heat flux. This excessive heat is a problem that will be handled by the control system. A short burst of high heat flux could be supplied by the heater and after this the heater power could be reduced. As a result of this modeling, a heater flux of 20 W/cm^2 was chosen.

The heater flux may be related to the size of the heater and the resistance of the heater. The power output by electricity flowing through a resistor is given by

$$P = IV \tag{4.1}$$

The current is given by Ohm's Law

$$I = \frac{V}{R} \tag{4.2}$$

Substituting Equation 4.2 into Equation 4.1 gives an expression relating the heater resistance, the applied voltage, and the power.

$$P = \frac{V^2}{R} \tag{4.3}$$

Now the desired resistance of the heater may be found, knowing the desired power and the voltage. The desired input voltage was 10 V based on safety and practical considerations of available power supplies. Two square heaters were desired, a 5 mm and a 2.5 mm heater. The power dissipated by these two heaters considering that a 20 W/cm^2 heating flux was desired was 5 and 1.25 W respectively. This gives values of 80 Ω for the 2.5 mm square heater and a resistance of 20 Ω for the 5 mm square heater.

The next step in the design of a platinum resistance heater is to determine the heating element orientation such that the heating elements fit well within the allotted space and the resistance requirement is satisfied. In order to design the heater elements, the resistivity of deposited platinum must be known. The resistance of a conductor is given by the following formula

$$R = \frac{\rho L}{wt} \tag{4.4}$$

where ρ is the resistivity of the material (typical units are Ω-m), L is the length of the wire, and w and t are the width and thickness of the wire respectively, corresponding to the wire cross section. It was a given that e-beam evaporation followed by lift-off would be used for the process sequence since there was uncertainty about obtaining a platinum

target for sputtering. Platinum heaters were initially manufactured using a resistivity value for platinum of 1 x 10^{-7} Ω-m (Winter 2005). This resistivity is a bulk value for platinum. It was discovered that platinum deposited on top of a thin chrome adhesion layer had a higher resistivity than that listed above after experimentation. The actual resistivity of a platinum wire of thickness 0.1 μm, a width of 50 μm and a length of 4.7 mm on a chrome adhesion layer of 150 Å was 4.4 x 10^{-7} Ω-m as measured with a multimeter without any heat treatment of the film. This value of resistivity was therefore used in subsequent design calculations. Researchers have reported that this effect is due to a large number of open and closed voids in the platinum film causing the density of the platinum to decrease with a consequent increase in resistivity (Lourenco, Serra et al. 1998; Giani, Mailly et al. 2002).

The information for the resistivity and power requirements of the heater was used to design two square heaters of size 2.5 and 5 mm. It was decided that the platinum thickness would be 0.1 μm since thicker platinum layers have higher stress in them that may cause them to crack (Rottmayer and Hoffman 1971). The 5 mm heater was designed with 39 individual 5 mm long heater elements in parallel. The elements had a cross section of 0.1 x 30 μm. This gave an element resistance of 725 Ω and a heater resistance of 18.6 Ω (725 Ω/39). Masks were designed for fabrication of the heaters. Schematics of the 5 mm heater are shown in Figures 4.8 and 4.9.

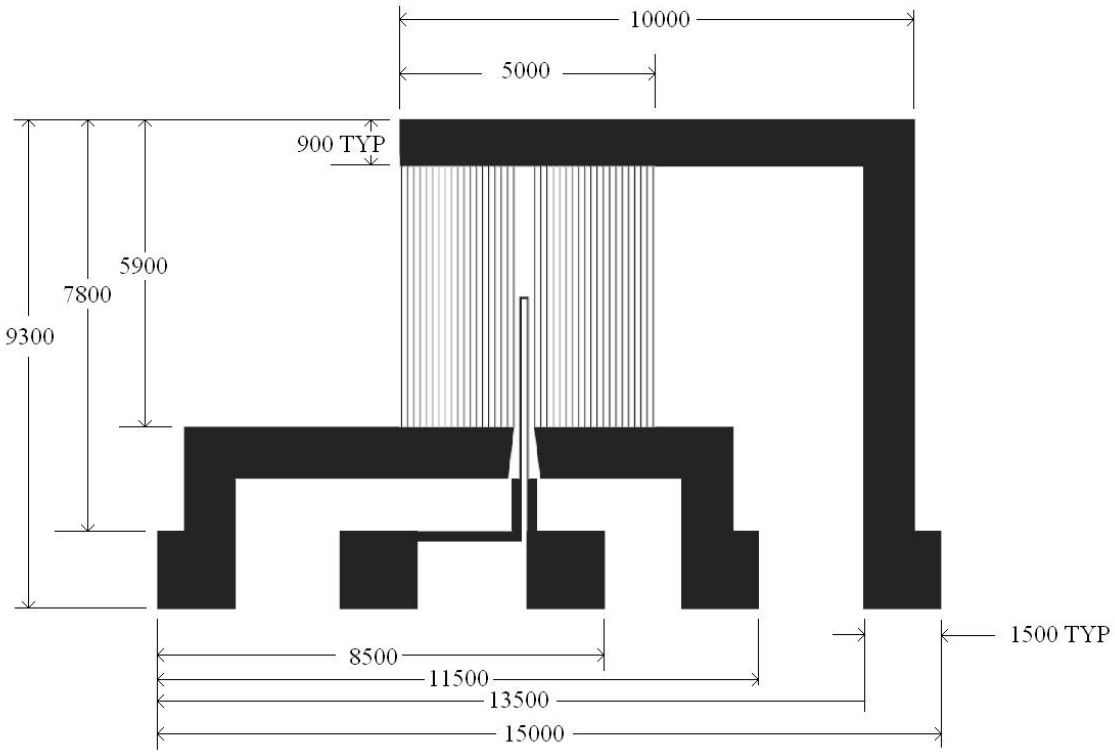

Figure 4.8 Schematic of 5 mm heater. All dimensions in μm.

The 39 parallel heater elements are visible in Figure 4.8. A platinum temperature sensor is located in the center of the device. The intent of the design was to deposit a 150 Å chrome adhesion layer followed by 1000 Å of platinum. The large connectors at each end of the heater have a chrome adhesion layer deposited on top of them followed by a layer of gold. Gold was chosen as the material for the leads because of its low resistivity of 0.22×10^{-7} Ω-m. Low resistivity and large cross sections were designed to keep power dissipation in this area to a minimum. The leads for the 5 mm heater were 900 μm wide as shown in Figure 4.8. The resistance of the lead at the top of the heater was 4.5 Ω considering that it is 9.4 mm long, 900 μm wide, and has a thickness of 0.1 μm. The temperature sensor is clearly visible in Figure 4.9. The temperature sensor was designed with a resistance of 617 Ω.

The 2.5 mm heater was designed with a heater resistance of 80.6 Ω. There were 9 heater elements each with a resistance of 725.4 Ω considering a resistivity for platinum of 4.4 X10^{-7} Ω-m, a line width of 30 μm, and a deposition thickness of 0.1 μm. Schematics of the 2.5 mm heater are shown in Figures 4.10 and 4.11.

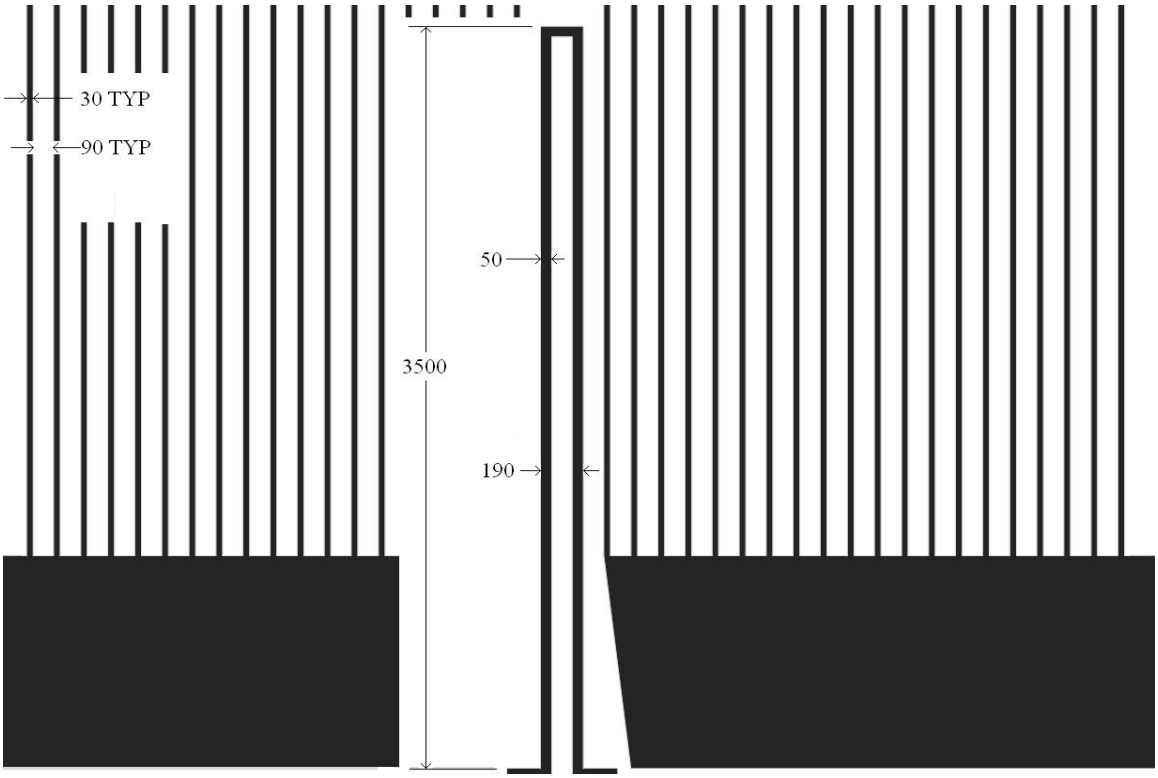

Figure 4.9 Exploded view of 5 mm heater with some elements deleted for clarity. Center portion is the temperature sensor. All dimensions in μm.

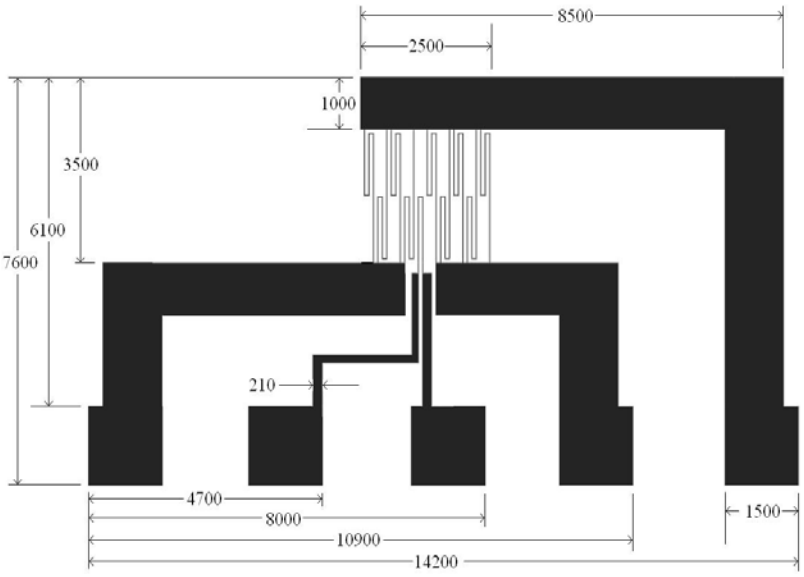

Figure 4.10 Schematic of 2.5 mm heater. All dimensions in μm.

The 2.5 mm heater was similar to the 5 mm heater in that the design intent was to deposit a 150 Å layer of chrome followed by 0.1 μm of platinum. The gold leads would then be formed by putting a chrome gold layer on top of the platinum in the lead areas. In this design, the heater elements are not single lines, in this case. The elements double back on themselves, thereby increasing the resistance. An exploded view of the heater elements and temperature sensor are shown in Figure 4.11.

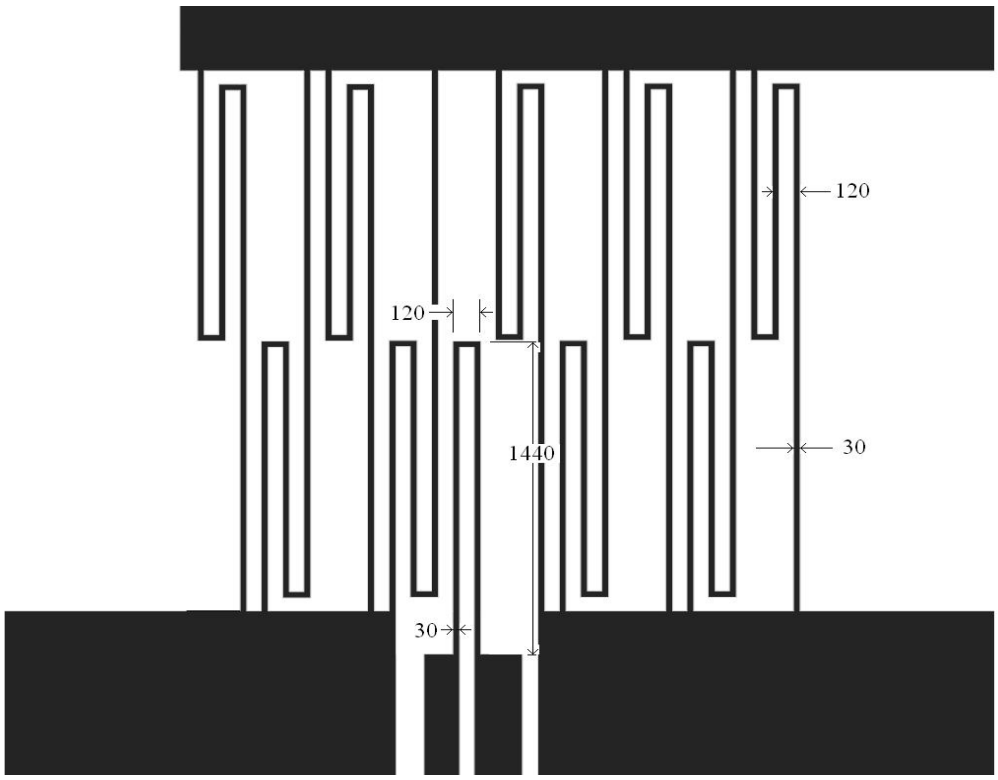

Figure 4.11 Exploded view of 2.5 mm heater. Center portion is the temperature sensor. All dimensions in μm.

The temperature sensor in this case was designed with a resistance of 435 Ω. The heater elements were staggered with the part of the heater that wraps back on itself on alternating sides of the heater. The purpose of this was to give more uniform heating.

Masks were also created for the second step of photolithography which was the deposition of the gold leads. These masks are shown in Figures 4.12 and Figures 4.13. All of the masks shown are actually inverted from the actual masks. The actual masks had the black area transparent and the surrounding area opaque.

Figure 4.12 Gold lead mask for 5 mm heater

Figure 4.13 Gold lead mask for 2.5 mm heater

4.2.1 Electronic control system design

The temperature of the heaters needed to be controlled in order to run the PCR reaction. The options that were considered were PWM and a continuous controller that utilized a Wheatstone bridge. The continuous controller configuration was chosen because it made use of the heater element as the temperature sensor for the control system. A Wheatstone bridge is a configuration of resistors that is commonly used to measure strain gages. This configuration has been used by other researchers for

temperature control and is documented in the literature (Benammar and Maskell 1989). A diagram of the circuit used to control the microheaters is shown in Figure 4.14.

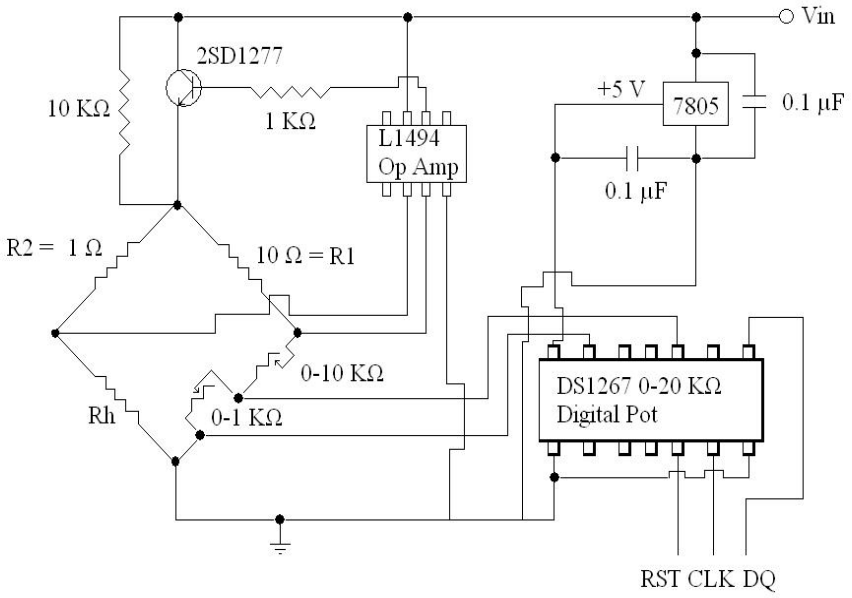

Figure 4.14 Circuit schematic for microheater control

The main function of the control system is to feed current to the heater (R_h) causing its temperature to be controlled at a fixed value for a given set of values of the variable resistors and the digital potentiometer. The circuit works by amplifying the imbalance in the bridge and supplying more current when the error is larger. The fact that the heater element resistance follows a known function of temperature allows the heater element to act as the sensing element as well as the final control element. The DS1267 is a digital potentiometer that is controlled by a computer via a three wire serial interface. The purpose of the digital potentiometer is to provide a setpoint to the control circuit. The 7805 is a power regulator. It takes the input voltage and regulates it to 5 V in order to power the digital pot. The purpose of the L1494 operational amplifier is to amplify the

differential input in order to open or close the transistor. The purpose of the 10 kΩ resistor around the transistor is to allow a small amount of current to flow through the bridge at startup to initiate the control process.

The control system can be calibrated to control the temperature of the heater. The resistance of the platinum heater increases with temperature. This fact can be used to control the circuit. When the temperature of the heater has reached the proper temperature, the voltage difference across the bridge should be zero. The voltage difference across the bridge can be read at the input to the operational amplifier. This information can be used to set the 0-10 kΩ resistor and the 0-1 kΩ resistor for a particular heater. At bridge equilibrium the following expressions hold (Alciatore and Histand 2003)

$$\frac{R_1}{R_1 + R_{4B}} - \frac{R_2}{R_2 + R_{hB}} = 0 \tag{4.5}$$

$$\frac{R_1}{R_1 + R_{4E}} - \frac{R_2}{R_2 + R_{hE}} = 0 \tag{4.6}$$

where R_1 and R_2 are the resistances as shown in Figure 4.14. R_{hB} refers to the resistance of the platinum heater at the top of the PCR operating range, in this case 100 °C. R_{hE} refers to the resistance of the platinum heater at ambient temperature, 21 °C. R_{4B} refers to the resistance of the leg of the bridge containing the digital potentiometer when the heater was at its upper setpoint of 100 °C, while R_{4E} refers to the resistance of that leg at ambient temperature. The potentiometer was set at 20 kΩ for operation of the heater at its upper setpoint and 0 kΩ for operation at ambient temperature. R_4 is given by the following equations

$$R_{4B} = R_S + \frac{1}{\frac{1}{20000} + \frac{1}{R_p}} \tag{4.7}$$

$$R_{4E} = R_S + \frac{1}{\frac{1}{1000} + \frac{1}{R_p}} \tag{4.8}$$

where R_s is the resistance of the manual potentiometer in series with the parallel combination of the digital potentiometer and R_p, the resistance in parallel with the digital potentiometer. These equations may be solved simultaneously to obtain the values of the manual potentiometers.

The onboard temperature sensor was used as a redundant method to determine the temperature of the heater. The temperature sensor contact pads were hooked up to a simple circuit that used a 500 Ω resistor and a voltage measurement, as shown in Figure 4.15, to determine the resistance of the sensor (R_t), and then the temperature could be inferred from the calibration of resistance versus temperature.

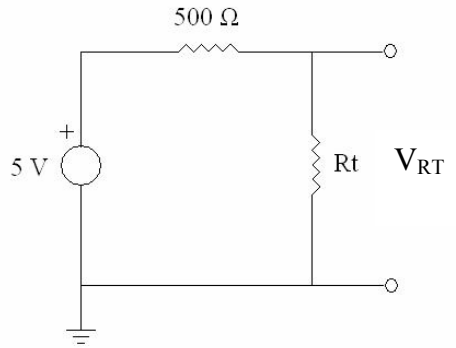

Figure 4.15 Schematic of circuit used to measure temperature of platinum temperature sensor

The voltage was measured across the platinum thermometer, R_t, as shown in Figure 4.15. The current through the circuit could be found with the following equation

$$I = \frac{5V - V_{RT}}{R_{500}} \tag{4.9}$$

where V_{RT} is the voltage across the platinum thermometer. The resistance of the platinum thermometer could be found from Ohm's Law knowing the current.

$$R_t = \frac{V_{RT}}{I} \tag{4.10}$$

4.3 Microheater fabrication

The microheaters were fabricated using standard photolithographic methods. Photolithography was performed using positive photoresist. After exposure, a chlorobenzene soak and drive in period was used to form an outer layer on the surface of the photoresist that would develop slower(Halverson, MacIntyre et al. 1982). E-beam evaporation was used to deposit the chrome and then platinum (chrome adhesion layer) after photolithography. Lift-off was used to form the heater pattern.

4.3.1 Microheater fabrication equipment and techniques

The masks for the heaters were designed in AutoCad and then converted to Adobe Illustrator. The masks were designed as negatives, meaning that areas that were black in the original would be clear in the final product and vice versa. The masks were printed by RGM Graphics, Inc., of Bethesda Maryland. They were printed on a 100 μm thick mylar sheet. The masks were setup to be printed on a standard sheet with dimensions 215.9 X 279.4 mm. A 3000 dpi printer was used to print the masks.

The wafers used in the fabrication process were 700 μm thick, 3 inch diameter soda lime glass wafers obtained from Valley Design Corp. An optically clear substrate was desired because some detection schemes involve shining light on the reaction volume from one side and detecting fluorescent response on the other side. The wafers were first rinsed with acetone, methanol, isopropanol, and finally with deionized water. Hot plates were used to dehydrate the wafers and to harden the photoresist. The hot plates used were Thermolyne type 1900 with Taylor 9940 temperature controllers.

The photoresist application, exposure and development required several items. S1813 photoresist from Rohm and Haas was spun onto the wafers using a Headway Research Inc. spinner at 4000 RPM for 40 seconds. Exposure was performed using the masks from RGM Graphics and the Karl Suss MJB3 type 100DU030 photolithography machine. The wafers were exposed with a UV light intensity of 8 mW/cm^2 at 365 nm for 25 seconds. Chlorobenzene was obtained from JT Baker, product number 9179 and was used to profile the photoresist. An oven was used to drive in the chlorobenzene. The oven used was from Blue M, model OV-8A. Development of the photoresist took place in a 3:1 solution of AZ400K:water. The AZ400K photoresist developer was obtained from Microposit.

Several components were necessary for the metal deposition. A buffered oxide etch (BOE) was necessary to prepare the surface of the glass. The buffered oxide etch (BOE) used was BOE Improved supplied by Transene Company, Inc. The BOE was carried out in a plastic container using plastic wafer holders. The chrome used was stock chrome while the gold and platinum were obtained from Kurt J. Lesker Company. The gold and platinum were 99.99% pure and came in 6.35 mm diameter 6.35 mm long

cylinders. The thermal evaporator used to deposit the gold was from Metra Inc., model TEBC-22-26. The e-beam evaporation unit was a Temescal, model 1800. Profiles of metallized features were taken with a Tencor Alphastep profilometer.

4.3.2 Microheater fabrication sequence

A simplified process sequence is shown in Figure 4.16.

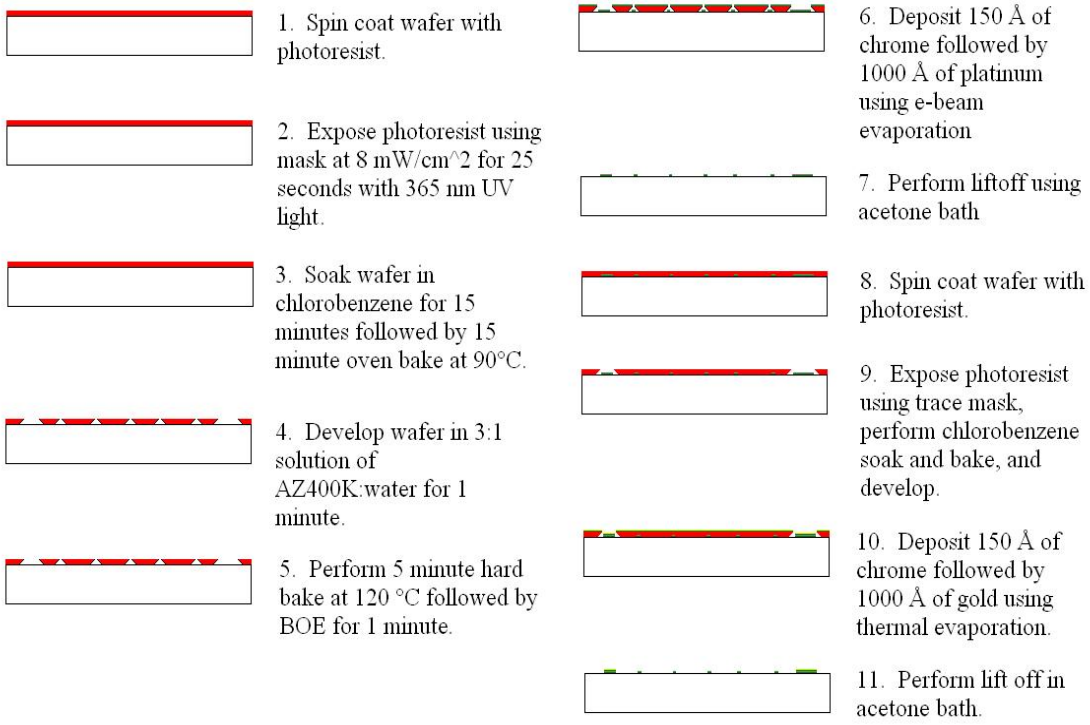

Figure 4.16 Simplified fabrication sequence for microheaters

The wafers were cleaned with acetone, methanol, isopropanol, and DI water. The wafers were next placed on a hot plate at 120 °C for two minutes to dehydrate the wafer to prepare it for photoresist application, shown in step 1 in Figure 4.16. A 2 minute soft bake was done at 120 °C after the application of the photoresist to prepare it for exposure. The wafer was then exposed and soaked in chlorobenzene for 15 minutes, corresponding to steps 2 and 3 above. The purpose of the chlorobenzene is to form an undercut

structure in the photoresist. The chlorobenzene penetrates into the photoresist to a depth determined by the length of exposure to it. It removes residual solvent and low molecular weight resins. This causes the affected region to develop more slowly then the region underneath it (Halverson, MacIntyre et al. 1982). This aids in lift off by forming a discontinuous metal structure that can be easily lifted off. A blown up picture of chlorobenzene treated photoresist profile after development corresponding to step 4 is shown in Figure 4.17.

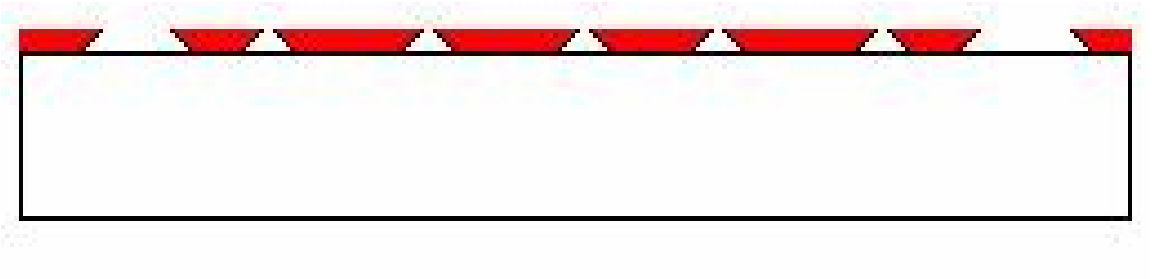

Figure 4.17 Effect of chlorobenzene on photoresist development

The chlorobenzene soaked wafer was taken out of the solution, blow dried with N_2, and inserted into the oven at 90 °C for 15 minutes to drive the chlorobenzene into the photoresist. The wafer was then developed in the AZ400K solution and optically inspected under the microscope to ensure that complete development had taken place.

The wafer was metallized with chrome and platinum. The wafer was hard baked at 120 °C for 5 minutes to strengthen the resist matrix prior to metallization. A 1 minute BOE was performed to roughen up the exposed glass surface, allowing the chrome to adhere better to the surface, corresponding to step 5 in Figure 4.16. The wafer was placed into the e-beam evaporation chamber and 150 Å of chrome was deposited followed by 1000 Å of platinum. The platinum and chrome deposition rates were kept below 5 Å/s. The wafer was removed from the e-beam evaporator and placed in an

acetone bath to lift off the unwanted metal and photoresist. The wafer was soaked for approximately 1 hour. The wafer was then removed, rinsed with DI water, blow dried with N_2, and optically inspected corresponding to step 7 in Figure 4.16.

The gold leads were then deposited on the heaters. The wafer was cleaned, blow dried, dehydrated, and had photoresist applied to the metallized surface. A 2 minute soft bake was done at 120 °C as in the previous step. The trace mask was then aligned to the metallized area using the features as guides. Exposure was carried out on the wafer and the chlorobenzene soak and drive in step were carried out. Development proceeded as described above. The wafer was then hard baked at 120 °C for 5 minutes. The wafer was placed in the thermal evaporator and 150 Å of chrome was deposited followed by 1000 Å of gold. The wafer was removed from the thermal evaporator and soaked in an acetone bath for 1 hour followed by rinsing with DI water. The wafer was then blow dried with N_2 and optically inspected under the microscope.

4.3.3 Microheater fabrication results

The microheaters suffered from some delamination problems after liftoff in the acetone solution. Two 2.5 mm square heaters and two 5 mm square heaters were manufactured on a wafer. The 2.5 mm heaters did not turn out at all due to a mask problem that made it impossible to align both the 2.5 and the 5 mm heaters. 5 mm heaters were the only ones produced for this reason. Typical delamination of heater elements is shown in Figure 4.18.

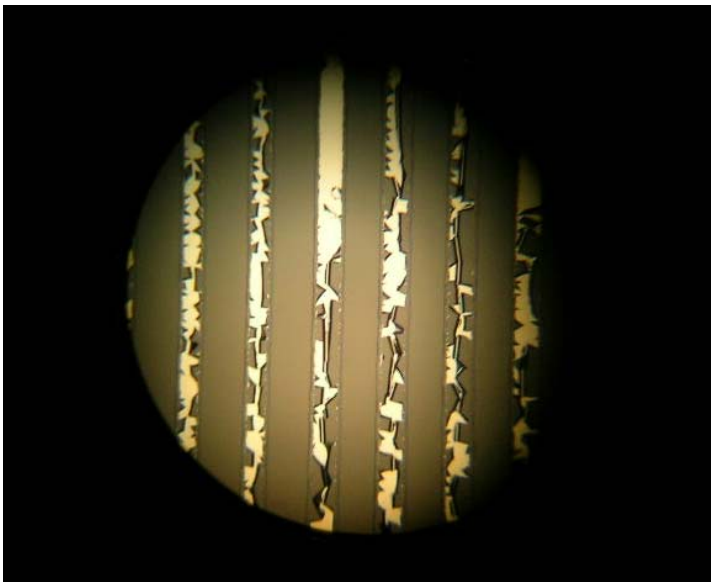

Figure 4.18 Delamination of heater elements from soda lime glass substrate

The delamination shown in Figure 4.18 is for a heater with a 150 Å titanium adhesion layer with 1000 Å of platinum deposited on top of it. This type of delamination was common for the case where a chrome adhesion layer was used also. It was typical that only one heater would turn out with no discontinuities in the heater elements due to delamination out of four heaters manufactured. A discontinuity in a heater element refers to a heater element with a section missing due to delamination or photolithography problems. Even heaters that did not suffer from discontinuities in any heater elements had imperfections as shown in Figure 4.19.

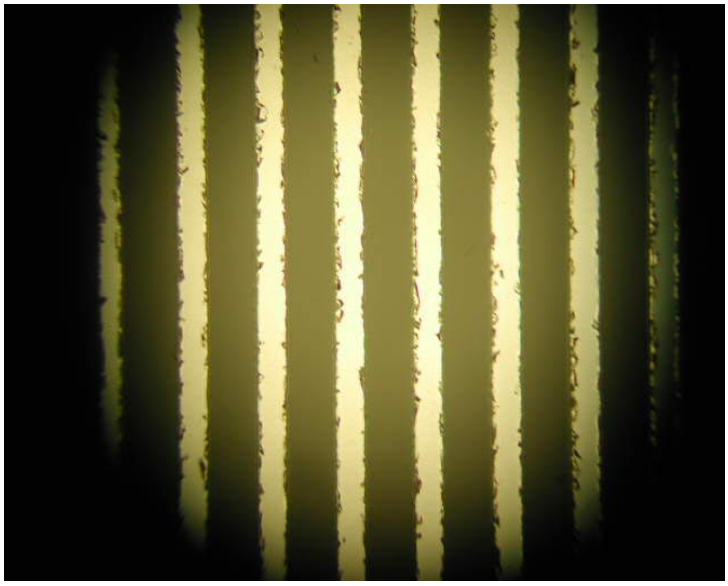

Figure 4.19 Heater elements from a heater with no discontinuities

The image shown in Figure 4.19 is from a heater with no discontinuities in any of the heating elements. It is clear that the heater elements have pits, particularly at the edges of the elements. The feature size of the heater elements was 30 µm. Elements with feature sizes greater than 30 µm had fewer defects. The comparison of 50 µm wide temperature sensor elements with 30 µm wide heater elements is shown in Figure 4.20.

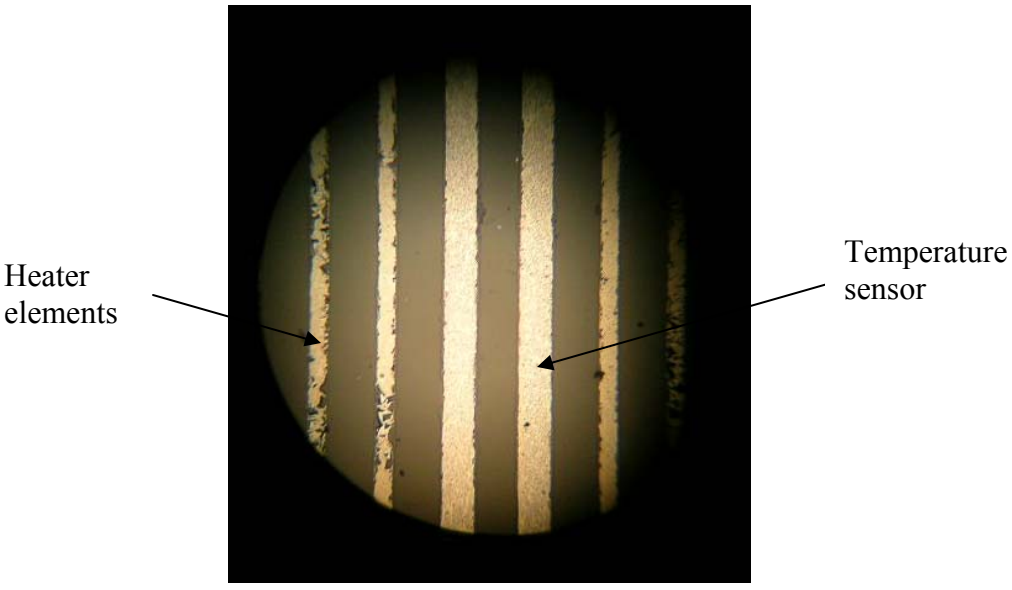

Figure 4.20 Comparison of 30 µm heater elements with 50 µm temperature sensor

The 50 μm wide heater element clearly has fewer defects than the heater elements. The result of this problem could be found in measuring the resistance of the temperature sensor and the heater and comparing it with the design resistance. The design resistance of the 5 mm platinum heater was 20 Ω while the design resistance of the temperature sensor was 617 Ω. The actual resistance of the heater immediately after fabrication was 18.2 Ω and the temperature sensor resistance was 470 Ω. The design resistance was calculated considering that the resistivity of platinum was 4.4×10^{-7} Ω-m with a deposition thickness of 1000 Å. The actual heaters produced had a platinum deposition thickness of 817 Å with a chrome adhesion layer underneath of it. Profilometry revealed that this was indeed the case. Observation under a microscope indicated that the width of the elements matched the design intent. The effective resistivity of the platinum considering these factors was 3.6×10^{-7} Ω-m for the heater itself and 2.7×10^{-7} Ω-m for the temperature sensor. The fact that temperature sensor resistivity was much lower than the heater resistivity was attributed to the imperfections in the heater elements which impede current flow through the device.

4.4 Microheater heat treatment and calibration

It was found that the resistance of the heaters and temperature sensors were changing with time making it very difficult to control the heaters and making temperature measurements with the platinum thermometer problematic. A study was done to determine the effect of heat treatment on the heaters in an effort to stabilize the heater and temperature sensor resistance. The resistance of four 5 mm heaters was tracked during this study. The test consisted of baking the heaters in an oven at temperatures ranging

from 200 to 265 °C. The resistances of the heaters and temperature sensors were measured using a multimeter. The resistances were measured at the points indicated in Figure 4.21.

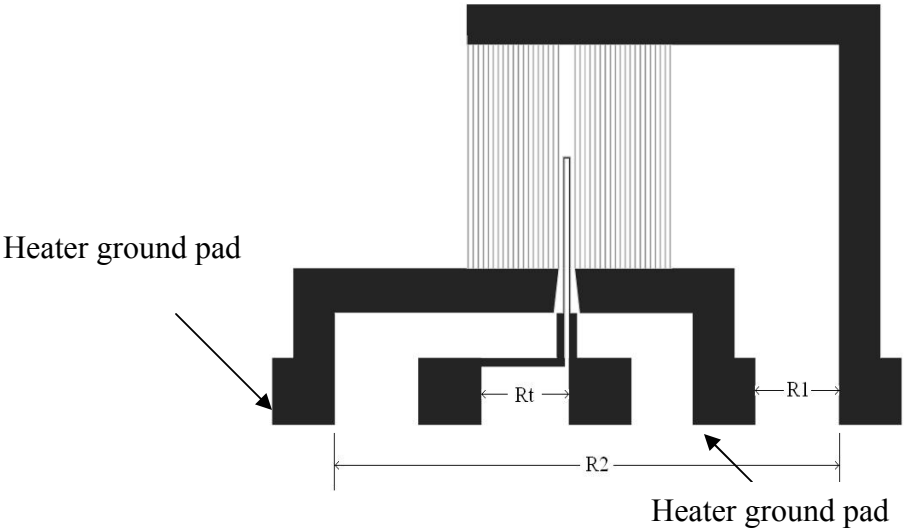

Figure 4.21 Points of resistance measurement for 5 mm microheater

The resistance of the thermometer was measured between the thermometer contact pads. The heater consists of two heater sections in parallel if the heater ground pads are linked together. R1 was measured between the bottom right contact pads while R2 was measured between the bottom right contact pad and the left most contact pad. The resistance of the heater is the parallel combination of R1 and R2 and is given as Rh. The results for one of the heaters are summarized in the following table.

Table 4.2 Result of heat treatment on heater and temperature probe

Temperature (°C)	Time	Total elapsed time (h)	R1 (Ω)	R2 (Ω)	Rh (Ω)	Rt (Ω)
21	0.0	0.0	N/A	N/A	18.2	470
200	1.5	1.5	N/A	N/A	16.7	387
225	1.5	3.0	32.0	35.3	16.8	380
225	0.8	3.8	31.9	35.4	16.8	376
225	1.5	5.3	32.0	35.6	16.8	375
265	1.0	6.3	32.2	35.6	16.9	371
265	1.0	7.3	32.4	35.6	17.0	370
265	1.0	8.3	32.6	36.0	17.1	369
265	1.0	9.3	32.5	36.0	17.1	367
225	1.5	10.8	32.4	36.5	17.2	366
205	3.0	13.8	32.4	35.8	17.0	366

The results of the heat treatment on the 5 mm heater indicate that the resistance of the temperature probe decreased by 22 % and the resistance of the heater decreased by 7 %. Over the last 5.5 hours of heat treatment the resistance of the heater changed by only 0.1 Ω and the resistance of the thermometer change by only 1 Ω indicating that the resistances had stabilized for heat treatment at these temperatures. The effective resistivity of the heater after heat treatment was 3.2 x 10^{-7} Ω-m while the effective resistivity for the temperature sensor was 2.1 x 10^{-7} Ω-m. It has been reported that after heat treatment up to a temperature of 1000 °C the resistivity of a 110 μm thick platinum film on a titanium adhesion layer reached 1.4 x 10^{-7} Ω-m (Lourenco, Serra et al. 1998).

The resistance of the heater was measured at ambient and at 100 °C in an oven in order to calibrate the electronic control system. The heater used for this test was another one of the heaters that had been heat treated but is not the same one listed in Table 4.2. These temperatures define the limits of operation for the device. The temperature versus resistance data was plotted for the heater and is shown in Figure 4.22.

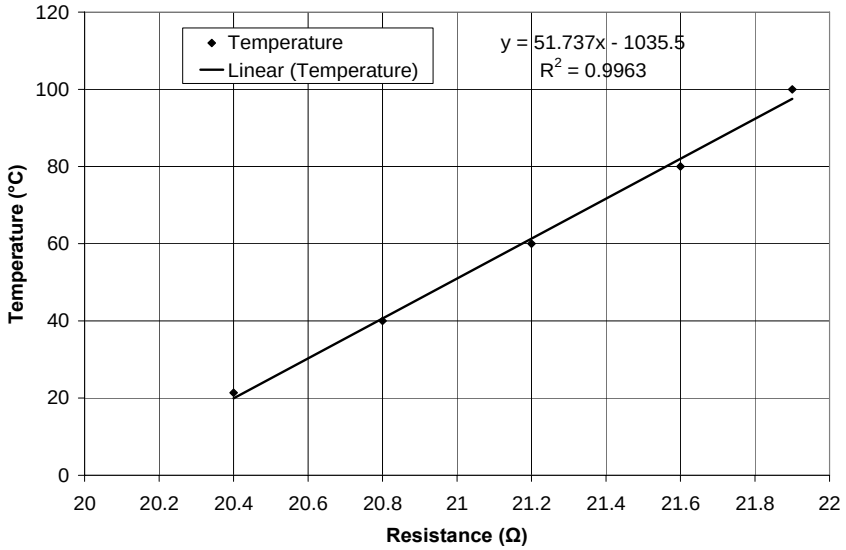

Figure 4.22 Temperature versus resistance with linear fit for microheater

The resistance of the heater increased from 20.4 Ω at ambient temperature to 21.9 Ω at 100 °C, a difference of 1.5 Ω or an increase in 7.4% from its ambient value. The calibration plot for the platinum thermometer is shown in Figure 4.23.

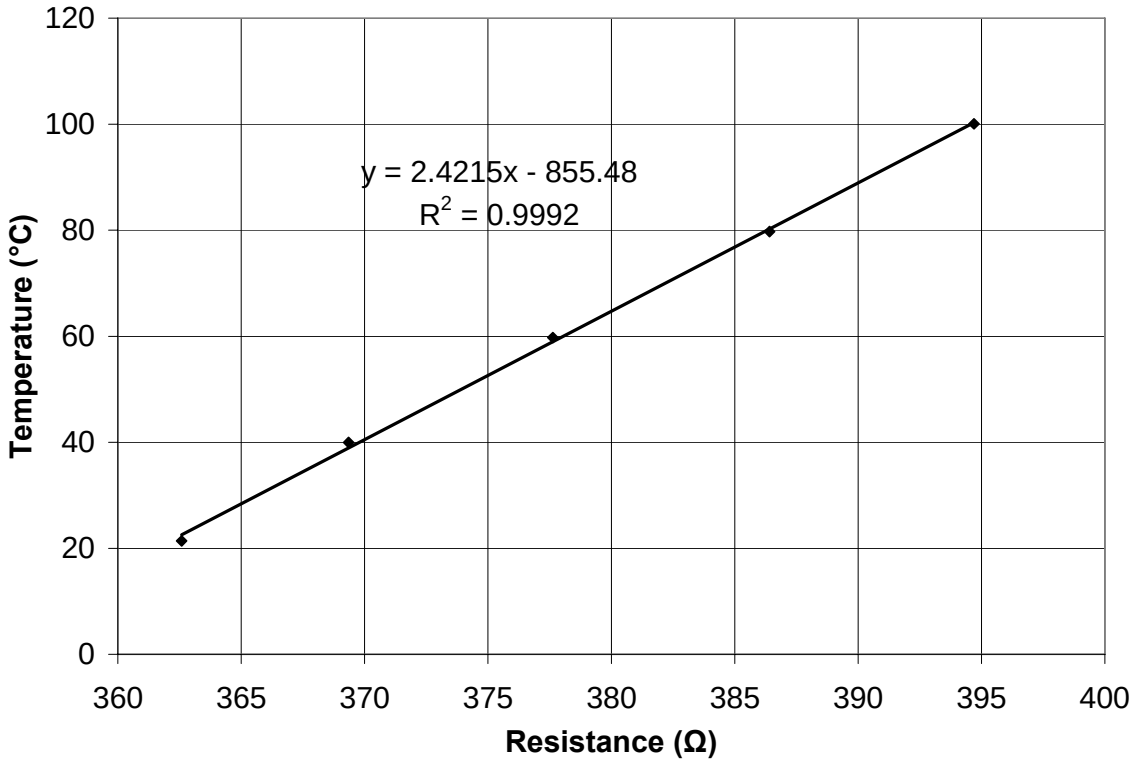

Figure 4.23 Temperature versus resistance graph with linear fit for microheater temperature sensor

The resistance of the temperature sensor increases from 362.6 Ω at ambient temperature to 394.7 Ω at 100 °C. This is a difference of 32.1 Ω or a percent increase of 8.9 %. The slope of the calibration curve for the heater is much steeper than the slope of the curve in Figure 4.23. The percent change in resistance for each case is nearly identical but the resistance range over which it happens for the heater is much smaller than that for the temperature sensor.

Heater recalibration was redone in the oven after 1 week of use to determine if the resistance of the temperature sensor was remaining constant. The result of that test is shown in Figure 4.24.

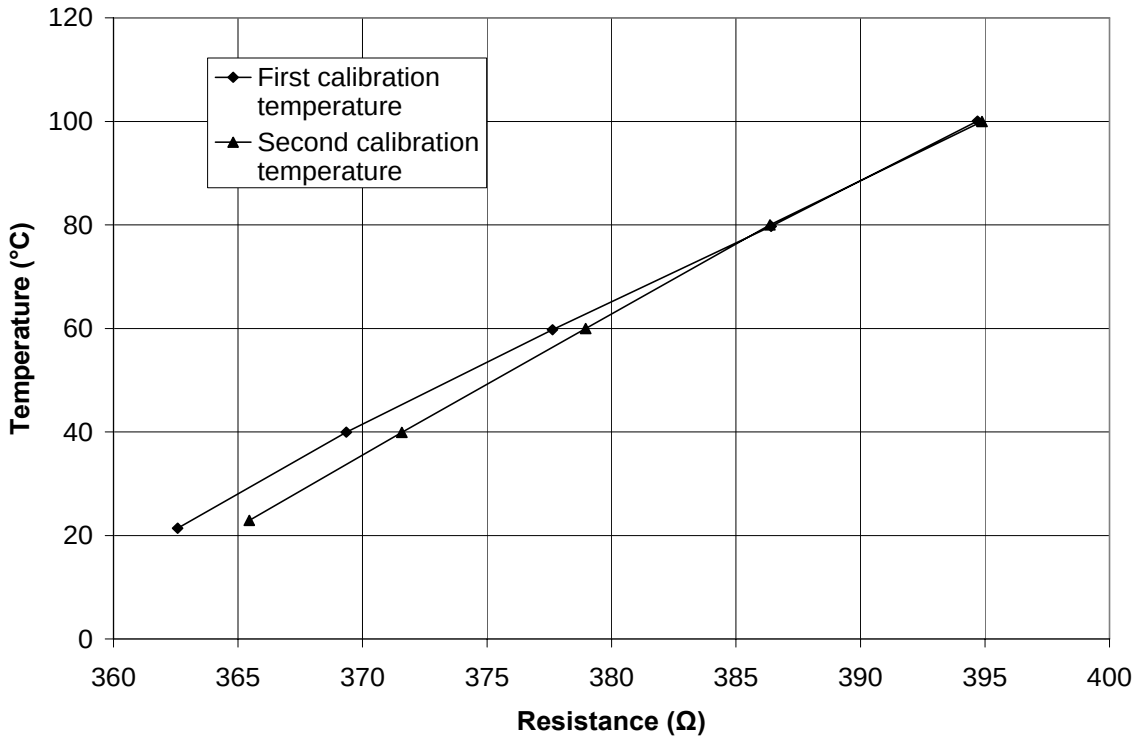

Figure 4.24 Comparison of initial calibration of temperature sensor and after 1 week of use

The results show that the temperature sensor was slightly out of calibration after 1 week of use, especially at lower temperatures. At temperatures higher than 60 °C there was agreement between the first and second calibrations.

4.5 Microheater testing

The microheaters were tested for heating rate, cooling rate, and power consumption under two conditions. The first condition was with fan cooling. The fan was turned on during cooling from 94 to 54 °C, but was otherwise off. The second

condition was with the cooling fan and a heat sink placed underneath the heater to speed cooling.

The heater circuit was powered with a Mastech HY1803D power supply. The cooling fan mounted on top of the test fixture was a RadioShack brushless, 12 VDC blower fan, part number 273-199 as shown in Figure 4.25.

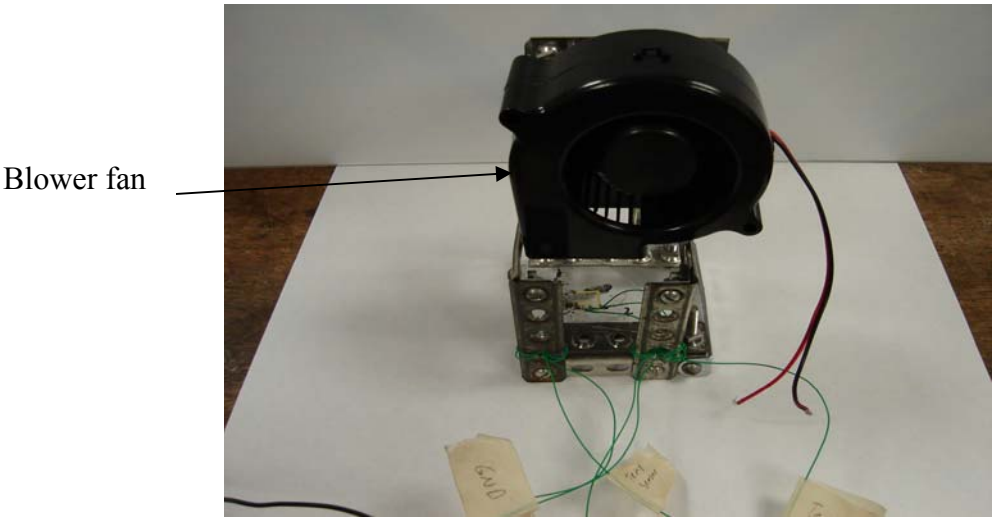

Figure 4.25 Microheater test fixture

The circuit that was used to measure the temperature of the heater, and the blower fan were powered by an ATC power supply, model ATC-230U. The fan was supplied with 12 V, while the temperature sensing circuit was supplied with 5 V. The variable resistor was controlled with the Instrunet 100 data acquisition system. The temperature of the heater, heater voltage, period, and three other thermocouple temperatures were recorded once every second by the Instrunet 100.

The second configuration of the microheater tested was with a heat sink, obtained from RadioShack, part number 276-1368, underneath the microheater. The purpose of the heat sink was to determine if it would help in cooling the device from 94 to 54 °C. The microheater test fixture with heat sink is shown in Figure 4.26.

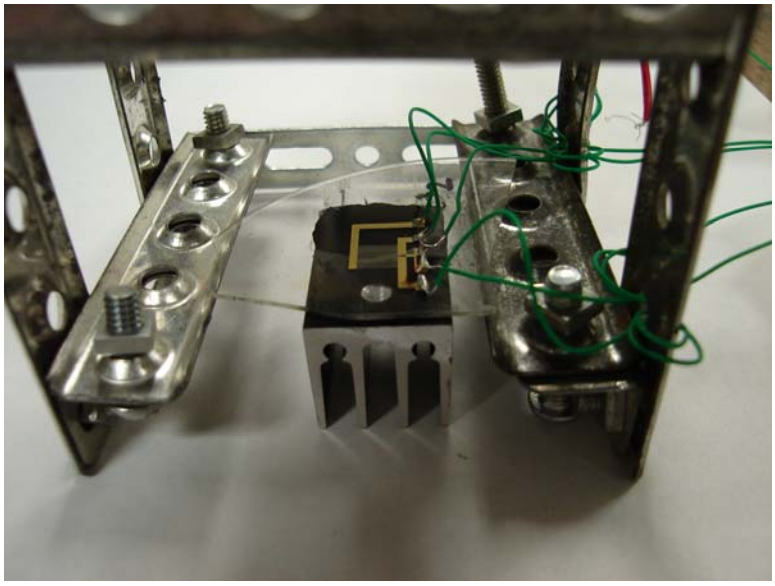

Figure 4.26 Microheater test fixture with microheater mounted on heat sink

The power calculations were made by measuring the voltage across the heater using an inverting operational amplifier that would multiply the input voltage by -0.22 and then output that voltage to the data acquisition unit. The resistance of the heater could be determined by knowing the calibration curve for the heater and the temperature of the heater. The temperature of the heater was determined by the platinum thermometer. The power supplied to the fan was significant in comparison with the power supplied to the heater. The power consumed by the fan was 2.4 W while the power consumption of the heater was on the order of 0.5 W. The power consumed by the fan was included in the average and maximum power calculations for this reason.

4.5.1 Microheater testing results

The first case examined was for the heating and cooling rates of the microheater system with the cooling fan and no heat sink. The cooling fan was only turned on during cooling from 94 to 54 °C. The microheater was suspended in air for this test. There was

no test section on the heater. The purpose of this test was to determine the performance of the heater and control system only. The results of the test are shown in Figure 4.27.

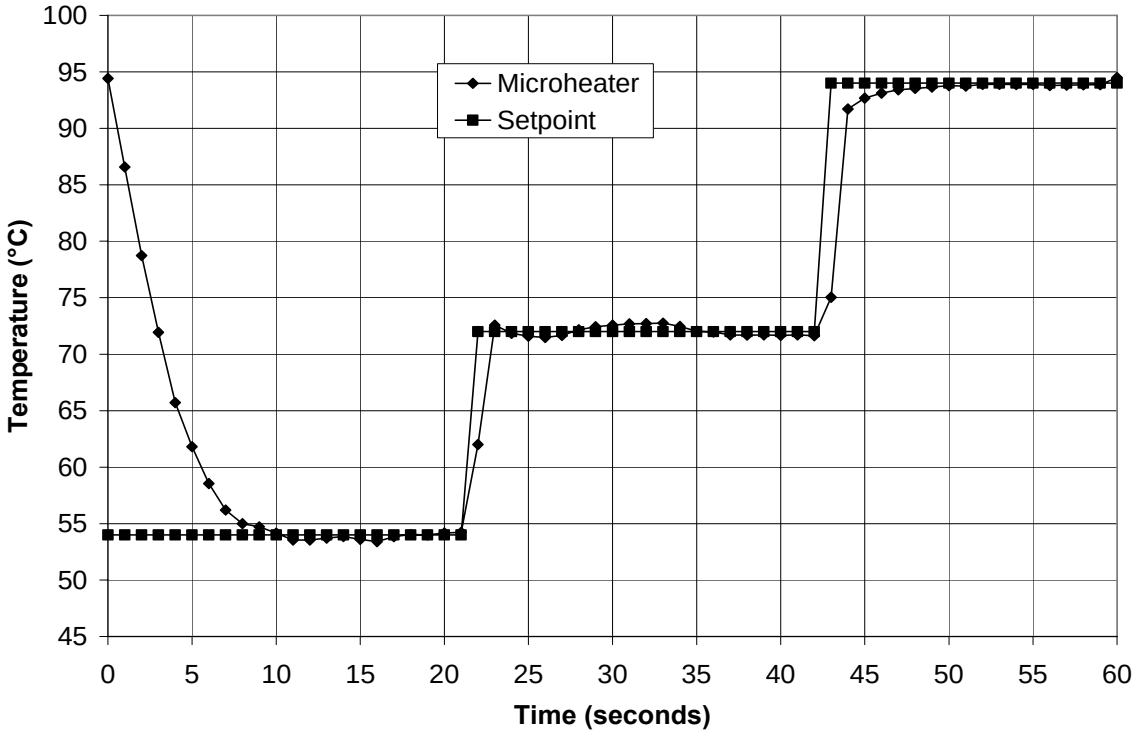

Figure 4.27 Heating and cooling characteristics of microheater with cooling fan, no heat sink, 12 V input

The maximum heating rate for this configuration was 16.7 K/s while the maximum cooling rate was 7.8 K/s. The average cooling rate was 4.0 K/s. The average heating rates were 9.2 K/s and 3.6 K/s for the intervals between 54 and 72 °C and between 72 and 94 °C respectively. The average heating rate between 72 and 94 °C was low considering that the maximum heating rate during this interval was 16.7 K/s. This can be attributed to poor control of the microheater during this interval and is not a property of the heater.

The case with the cooling fan and the microheater mounted on top of an aluminum heat sink was examined. The configuration of the setup is shown in Figures

4.25 and 4.26. The cooling fan was turned on only during cooling. The results of that testing are shown in Figure 4.28.

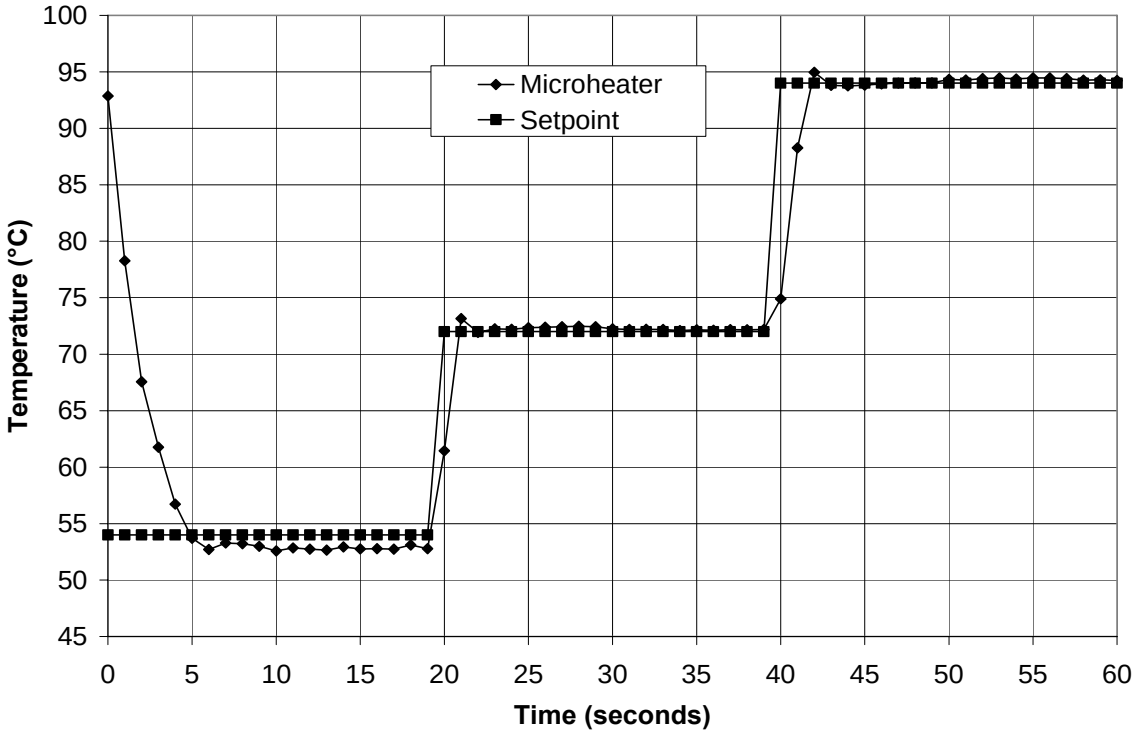

Figure 4.28 Heating and cooling characteristics of microheater with cooling fan, heat sink, 12 V input

The maximum cooling rate for this scenario was 14.6 K/s while the maximum heating rate was 13.4 K/s. The average cooling rate between 94 and 54 °C was 8 K/s. The average heating rate between 54 and 72 °C was 9 K/s while the average heating rate between 72 and 94 °C was 11 K/s.

The power requirements of the microheater and fan were recorded. A summary of the results along with the heating characteristics of the microheater are shown in Table 4.3. The maximum power required by the microheater system with and without the heat sink was 2.4 W which is the power required to run the fan during cooling. During cooling the heater is not on. The average power over a cycle for the microheater without

heat sink was 0.5 W. The average power over a cycle for the case with the heat sink was 1.0 W.

Table 4.3 Comparison of microheater operation with and without heat sink

	Max Heating rate (K/s)	Max Average heating rate (K/s)	Max Cooling rate (K/s)	Average cooling rate (K/s)	Max Power consumption (W)	Average power consumption over a cycle (W)
Microheater without heat sink	16.7	9.2	7.8	4.0	2.4	0.5
Microheater with heat sink	13.4	11.0	14.6	8.0	2.4	1.0

The purpose of the heat sink was to increase the cooling rate of the microheater. The addition of the heat sink doubled the average cooling rate and increased the maximum cooling rate by 7.8 K/s. The heat sink reduced the maximum heating rate, however, because some of the heat energy was traveling to the heat sink. The average heating rate actually increased with the heat sink, however, because in the case without heat sink there was poor control at the 94 °C setpoint. The cost of using the heat sink can be seen in the average power consumption column, however. The microheater needed twice as much power on average to maintain the required temperatures.

5. MICROCHAMBERS FOR PCR

Silicon microchambers are one option for thermal cycling on a microheater or on another flat, heated surface. Daniel et al. designed a silicon microchamber for rapid thermal cycling. The researchers recognized that in order to perform rapid PCR the thermal mass of the system must be small. A schematic of the device that was fabricated is shown in Figure 5.1 (Daniel, Iqbal et al. 1998).

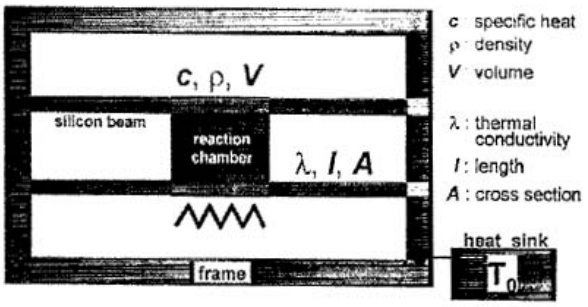

Figure 5.1 Silicon reaction chamber fabricated by Daniel et al.

The reaction chamber consists of a well fabricated from silicon that is suspended by four beams. The reaction volume was designed to hold 2 μL of PCR reaction mixture along with 1 μL of silicone oil, used to prevent evaporation.

A simplified process sequence for the device is shown in Figure 5.2 (Daniel, Iqbal et al. 1998). The reaction vessel was fabricated from a 400 μm thick silicon wafer with a silicon nitride layer on both sides. Reactive ion etching was next used to pattern the nitride layer on the top surface to define the areas that would be etched with KOH. The wafer was then etched in KOH forming the pits shown in Figure 5.2. The central pit is the reaction chamber while the pits on each side are to provide thermal isolation of the reaction volume. The two lateral pits have a web of silicon nitride above them. The purpose of the webbing was to prevent oil from the reaction from creeping into the thermal isolation pits. The idea behind this was that if the webbing was small enough, it would prevent liquid from flowing into it because of surface tension. Platinum heaters were patterned on the bottom of the reaction volume with a lift off technique using chrome as an adhesion layer. The reaction chamber was coated with a SiO_2 layer using plasma enhanced chemical vapor deposition. The reaction volume then had a bovine serum albumin treatment. It was found that this surface treatment was necessary to make the microchamber PCR friendly by blocking adsorption of PCR reactants to the chamber walls (Daniel, Iqbal et al. 1998).

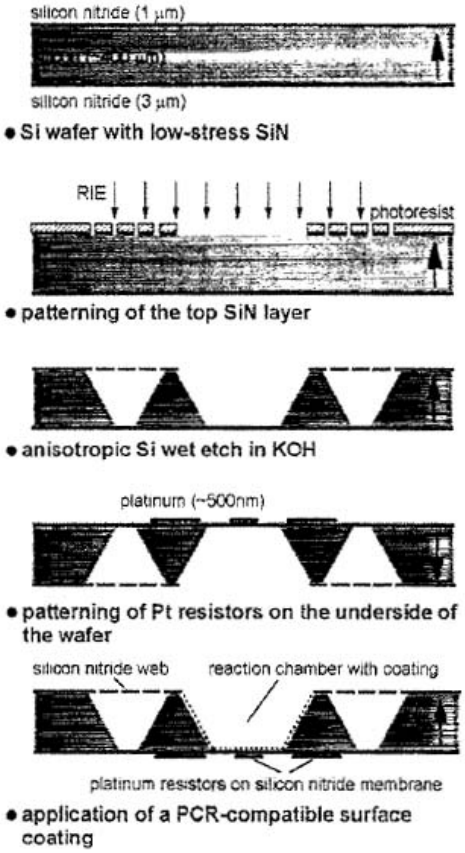

Figure 5.2 Simplified fabrication sequence used by Daniel et al.

This reaction volume was successfully used to amplify a 260 bp DNA segment. The protocol was 5 seconds at 94 °C, 7 seconds at 55 °C, and 5 seconds at 72 °C. The time constant for this system was 0.4 seconds (Daniel, Iqbal et al. 1998).

Shoffner et al. have also found it necessary to perform a surface treatment on silicon chambers in order to perform PCR. The researchers first tested the effect of treated powder silicon on PCR in standard polypropylene PCR tubes in commercially available thermal cyclers. This was accomplished by incubating the silicon powder at room temperature overnight in excess silanizing agent in a test tube. The excess silanizing agent was then removed and the powder was dried overnight in an oven at 70 °C. The powder was then rinsed with distilled, deionized water and dried overnight in the oven again. The powder was next separated into tubes and treated with 1 mL of 10 mg/mL polymer solution. The polymer solutions were prepared with 0.1 M Tris buffer. The following polymers were used: poly-α-alanine, poly-L-aspartic acid, polyglycine, poly-L-Leucine, poly-DL-phenylalanine, poly-DL-tryptophan, poly-L-lysine, polyvinylpyrrolidone, polyadenylic acid, polymaleimide or maleimide. The silicon powder was incubated at room temperature overnight at room temperature. The excess solution was removed and the powder was oven dried overnight at 45 °C. It was found that untreated silicon completely inhibited the reaction. Silicon powder treated with a silicone fluid consisting mainly of dichlorooctamethyltetrasiloxane followed by a coating of polyadenylic acid compared well with PCR run with no silicon powder (Shoffner, Cheng et al. 1996).

This information was used to test the efficacy of PCR in silicon microchambers (Shoffner, Cheng et al. 1996). The microchambers tested were 14 x 17 x 0.12 mm. The

reaction chambers had a Pyrex glass cover anodically bonded to them. The silicon chips were first treated with the silanizing agent for 15 minutes at room temperature and then removed. The chip was rinsed with distilled, deionized water and dried. The PCR chip was filled with one of the various polymer solutions listed above and allowed to sit for 1 hour at room temperature. The polymer solution was removed using a vacuum, and the chip was rinsed, and dried. SiO_2 and Si_3Ni_4 layers of thickness 1000 Å were also applied to some of the chips to determine the affect of these layers (Shoffner, Cheng et al. 1996).

The surface treatments enhanced PCR in the silicon microchambers compared with untreated silicon (Shoffner, Cheng et al. 1996). The untreated silicon microchambers showed some inhibition of the PCR reaction while those treated with the silanizing agent and polymer coating showed results comparable to those performed in a polypropylene tube in a commercially available thermocycler. The results from the silicon chips treated with the silanizing agent and the polymer coating were not repeatable, however, and this was attributed to a non-uniform surface treatment. Another explanation was the coating may degrade over the course of the PCR reaction. SiO_2 and Si_3N_4 surfaces were also tested. These surfaces had a more uniform coating. The bare silicon surface and silicon coated with Si_3N_4 showed inhibition of PCR. The SiO_2 coated chips showed the best performance as compared with the polypropylene tube in the commercial thermal cycler. The results from these chips were repeatable. (Shoffner, Cheng et al. 1996).

Silicon chambers have been shown to be PCR compatible when coated as discussed above. Silicon microchambers are time consuming to fabricate, however. KOH etching of silicon progresses at 1 μm/minute (Kovacs 1998). For a 500 μm wafer it

would take 7 hours to etch 400 μm of the material away. It has been shown above that these wafers need additional surface treatment in order to be PCR compatible. Researchers have focused their attention on building PCR reaction chambers out of materials such as polycarbonate and polypropylene for these reasons.

Yang et al. have successfully completed PCR in a polycarbonate reaction volume. The device fabricated consisted of three layers of polycarbonate thermally bonded. Each polycarbonate layer was 250 μm thick. The top and bottom of the chamber were made of clear polycarbonate while the middle section was made of black polycarbonate. The polycarbonate was cut using a $C0_2$ laser engraving system. The chamber itself was a serpentine channel, designed to decrease dead volume and bubble trapping. A picture of the chamber is shown in Figure 5.3 (Yang, Liu et al. 2002).

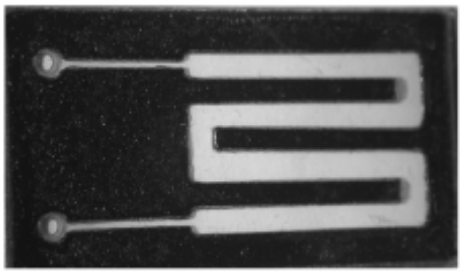

Figure 5.3 Polycarbonate chamber fabricated by Yang et al.

The channel is 1.5 mm wide, 0.25 mm high, and can hold 40 μL of PCR reaction fluid. The holes at the end of each channel were 0.7 mm in diameter. The chambers were bonded using a Carver Inc. thermal press with a platen temperature of 133 °C and a pressure of 1400 psi for 2 hours. The inlet and outlet holes were sealed with double sided adhesive tape after the PCR solution was loaded. A layer of paraffin was then put on top of the tape followed by a polycarbonate plate. A hand press was used to press down on

this assembly, causing the tape to be pressed down into the filling holes, creating a strong seal (Yang, Liu et al. 2002).

This reaction chamber was used to complete a rapid PCR reaction (Yang, Liu et al. 2002). The chamber was cycled using a dual Peltier chip setup. The chamber was sandwiched in between two thermoelectric coolers. PCR was completed using this setup with a total reaction time of 30 minutes. 15 seconds was spent at each temperature plateau in the PCR cycle. The PCR yield was comparable with that achieved with a conventional thermal cycler (Yang, Liu et al. 2002).

The PCR reaction mixture used by these researchers was modified in order to accommodate the large surface area to volume ratio of the chamber. Polyethylene glycol was added to the PCR reaction buffer to increase the yield. This approach has been shown to be effective for increasing the PCR yield in polyimide microchips (Giordano, Ferrance et al. 2001). The PCR yield was highest when using 0.75 % polyethylene glycol 8000. Different molecular weights of polyethylene glycol are available. The 8000 refers to the molecular weight. Bovine serum albumin was also added to the reaction volume at a concentration of 250 μg/mL to increase the yield. It was thought that the combination of these two treatments helped block adsorption of any of the PCR reactants to the chamber walls (Yang, Liu et al. 2002).

Other researchers have also produced polycarbonate reaction chambers. Chen et al. has designed a polycarbonate reaction vessel for electrokinetic flow. Three temperature zones were maintained and the fluid was moved from temperature zone to temperature zone as required (Chen, Musundi et al. 2005). The channel designed had a width of 100 μm, a depth of 70 μm, and was 7.9 cm long. The volume of the reaction

vessel was 0.55 μL. The chamber was fabricated using a brass molding die and hot embossing in polycarbonate. The brass mold insert was heated to 180 °C and pressed into the polycarbonate sheet at 1000 lbf for 4.5 minutes. The cover for the chamber was thermally bonded in an oven at 150 °C for 20 minutes. The PCR reaction was degassed in a vacuum after loading into the chamber to reduce the formation of air bubbles. 2 % ethylene glycol was also added into the PCR reaction mixture to increase the boiling point of the mixture and to reduce bubble formation in the device (Chen, Musundi et al. 2005).

Bubble formation in polycarbonate chambers can be a problem as noted by the efforts taken by Chen et al. to reduce bubble formation in the chamber. Zhao et al. also noticed problems caused by bubbles in a silicon microchamber. It was recommended that the reaction volume not be filled completely. A small bubble should be left in the reaction chamber to allow for expansion of the liquid upon heating. The researchers found that the bubble should be located at the edge of the reaction vessel. Bubbles that arose in the middle of the reaction vessel expanded upon heating and forced liquid to the edges of the reaction chamber. This caused a problem with temperature uniformity in the device because the temperature sensor was located directly below the heating chamber. If all of the fluid was pushed out into the filling capillaries, that reaction volume would not reach the required temperature (Zhao, Cui et al. 2003).

It was necessary to use a surface treatment or to add substances to the PCR reaction vessel to inhibit adsorption of protein to the chamber walls in the research described above that used polycarbonate and silicon. Surface treatments were done to silicon that made the surface hydrophilic. Polycarbonate can also be made hydrophilic.

An oxygen plasma etch on a polycarbonate sample of thickness 1.2 mm was shown to dramatically decrease the water contact angle (Larsson and Derand 2001). The researchers used a Plasma Science PSO500 reactor. A 100 standard cubic centimeters per minute (sccm) oxygen flow rate was used with the best results coming with an RF power of 300 W. The water contact angle after this 5 minute plasma treatment was 3 ° compared to contact angles around 70.1 ° for untreated polycarbonate. The samples were stored in aluminum foil to test the stability of the plasma treatment in dry storage. Samples still had contact angles around 20 ° after six months of storage wrapped in aluminum foil. This behavior was observed for polycarbonate treated with reactive ion etch (RIE) bias voltages of 480-600 V. Intense plasma treatments also produced changes in the Young's modulus of the material of up to 1 GPa (Larsson and Derand 2001).

Polycarbonate can also be treated with UV light to increase the surface hydrophilicity (Liu, Ganser et al. 2001). A 4 W manual UV lamp was used for the surface treatment of the polycarbonate. The polycarbonate that was treated was 1 mm thick. The polycarbonate was exposed to UV light for variable amounts of time ranging from 0 to 13 hr. As time increases the surface becomes increasingly hydrophilic until the contact angle levels off after 5 hours at 22 °. The polycarbonate was able to be thermally bonded after surface treatment and no detectable changes in mechanical properties were present (Liu, Ganser et al. 2001).

5.1 Microchamber design considerations

The purpose of the reaction chamber is to distribute the reaction volume in a thin layer and have a thin layer separating it from the microheater to ensure rapid heating. A 2-D finite element heat transfer package was used to develop a sense of what chambers might be acceptable. The first material to be examined was polycarbonate. Polycarbonate can be thermally bonded (Bilitewski, Genrich et al. 2003; Ye, Yin et al. 2005), is easy to cut, and can be commonly found in thin sheets of 250 µm. The microheater that was available was 5 mm square. A chamber 5 mm square or smaller was desired for this reason. A reaction volume 5 mm square with a depth of 250 µm would hold 6.25 µL of PCR solution. The 2-D model that was used to model this situation is shown in Figure 5.4. The water was assumed to be static in this calculation.

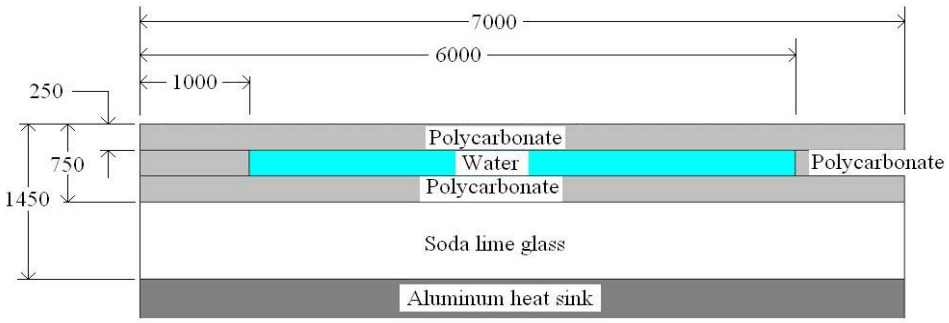

Figure 5.4 2-D heat transfer model for polycarbonate chamber. All dimensions in µm.

The boundary condition around the outside of the polycarbonate, glass, and heat sink was free convection with a value of 5 $W/m^2 K$. A temperature boundary condition was set on the 5 mm long border between the glass and the polycarbonate, directly beneath the water section, to simulate the surface of the microheater. The results of running the model with an initial system temperature of 72 °C are shown in Figure 5.5.

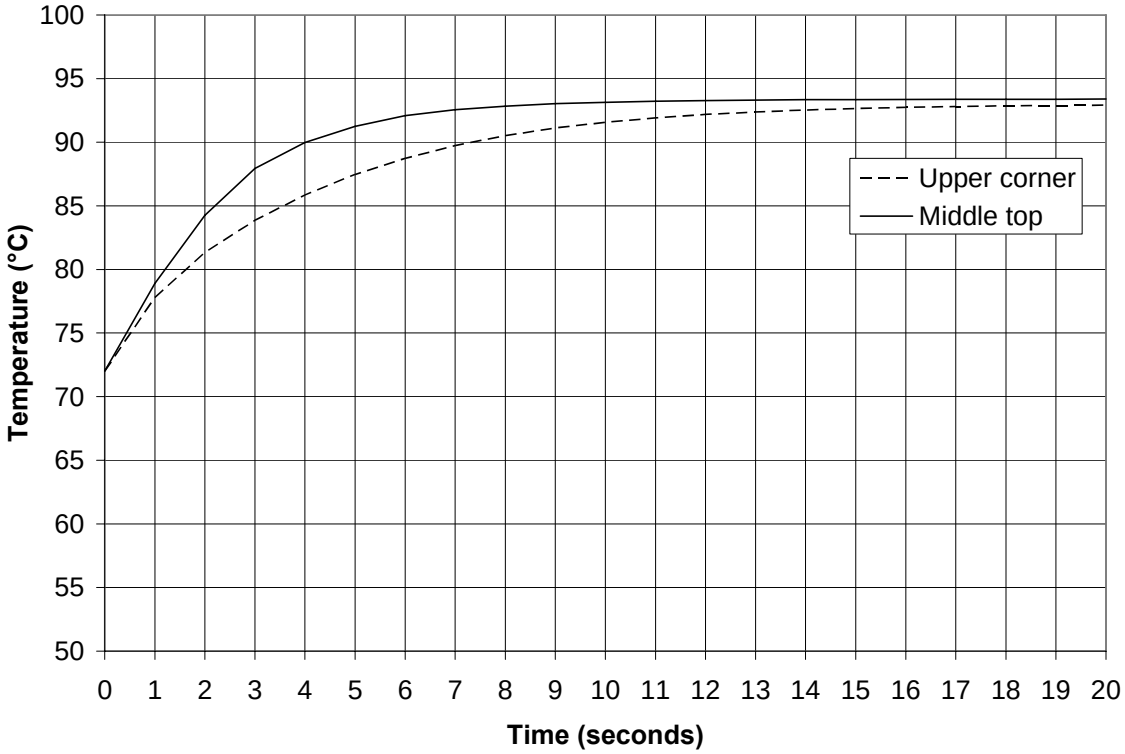

Figure 5.5 2-D conduction model of 5 mm square polycarbonate chamber on 5 mm square microheater

The lower trace is for a node in the upper left hand corner of the chamber while the upper trace is for a node in the top center of the chamber. Both of these nodes were in contact with the water. The time constant for the top middle node was 2.5 seconds while the time constant for the upper corner node was 4 seconds. Considering that it takes four time constants for the reaction volume to reach 98 % of its final value, this may not be an optimal design for rapid PCR.

The reaction volume for this setup was reduced to see the effect of a smaller reaction volume on heating between 72 and 94 °C. The reaction chamber in this second model was 3 mm square. The polycarbonate surrounding the reaction chamber had the same dimensions as shown in Figure 5.4. This meant that for the 5 mm square heater 1

mm of heater lay outside of the perimeter of the PCR solution on each side. The volume of this reaction chamber is 2.2 μL. The results of the FEA model are shown in Figure 5.6.

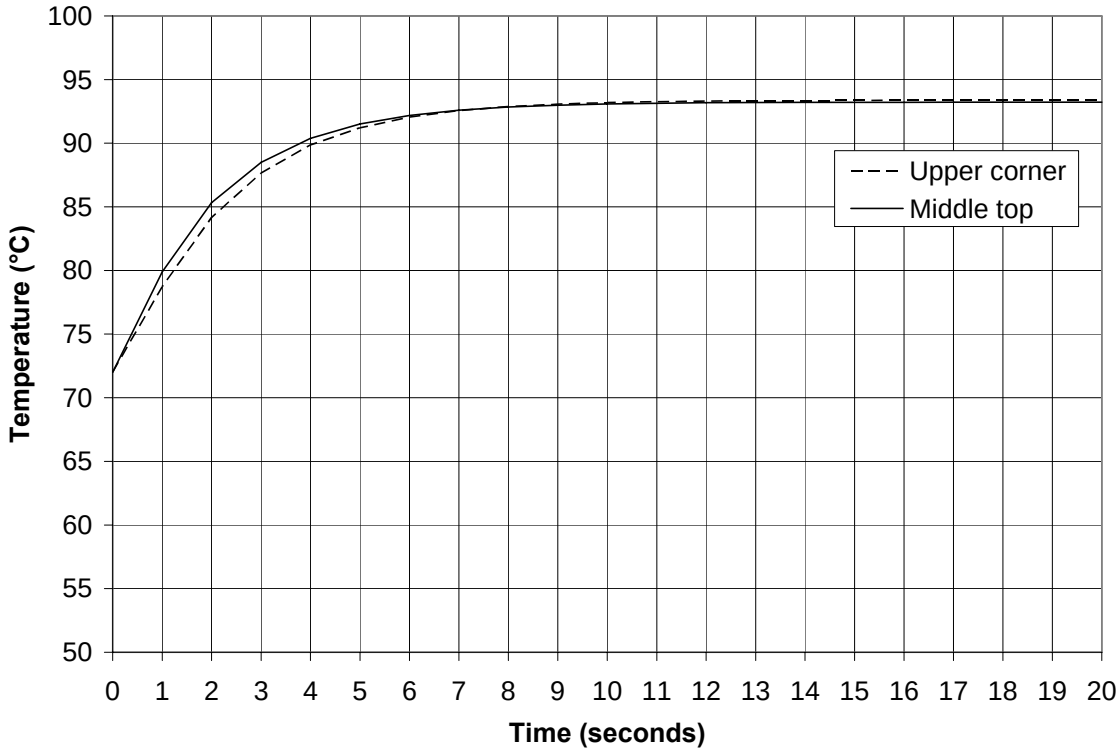

Figure 5.6 2-D conduction model of 3 mm square polycarbonate chamber on 5 mm square microheater

The upper corner trace corresponds to a node at the upper corner of the reaction vessel in contact with the PCR mixture, where the temperature was expected to increase slowest. The middle top trace represents a node at the top center of the PCR reaction vessel in contact with the solution. Nodes at the top surface of the liquid were of interest because these points would be the slowest to respond. The temperature uniformity in the reaction vessel is much better in this case than in the case with the 5 mm reaction chamber. The time constant for the upper corner node was 2.5 seconds while the time constant for the

middle top node was 2 seconds. The time constant for the top middle node remained the same while the time constant for the upper corner node was decreased by 2 seconds compared to the 5 mm reaction chamber. The upper corner node showed a decrease in time constant because of the overhang of the heater in this case.

A 3 mm square reaction chamber with the same thickness shown in Figure 5.4 made from silicon with a 5 mm square heater centered beneath it was also examined to see the effect of a different material on the time response of the chamber. Silicon has a thermal diffusivity of 89 x 10^{-6} m^2/s while the thermal diffusivity of polycarbonate is 138 x 10^{-9} m^2/s(Incropera and DeWitt 1996). The silicon chamber will heat up much faster than the polycarbonate one. The result of that calculation is shown in Figure 5.7.

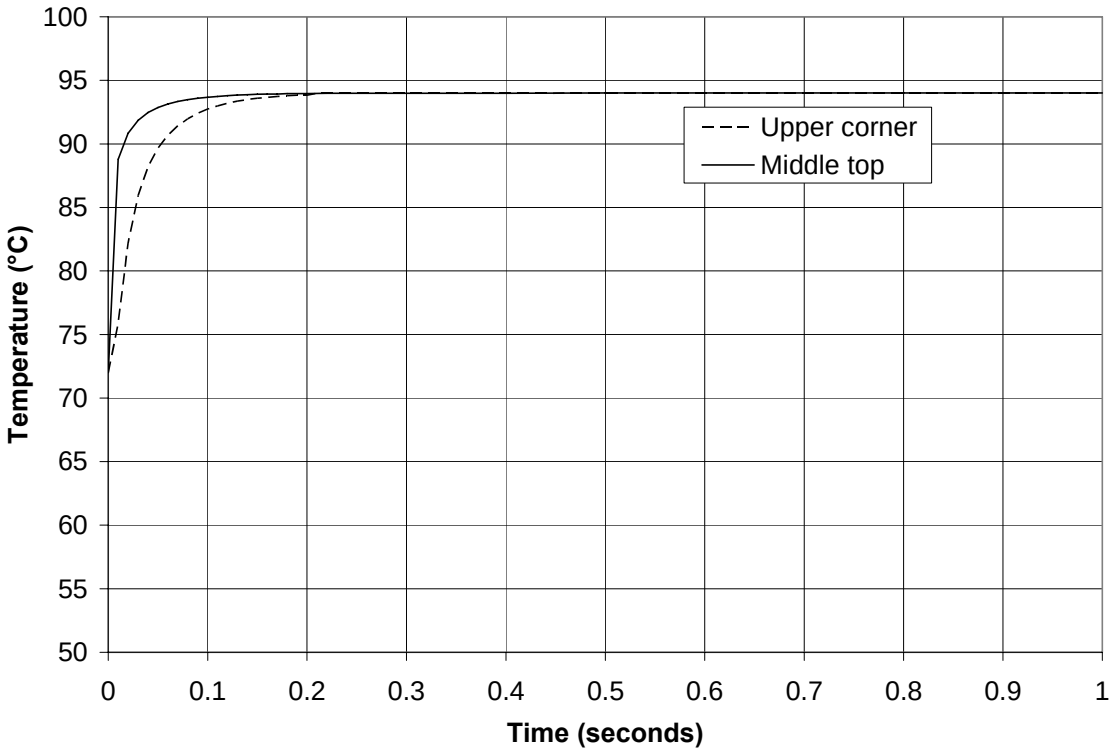

Figure 5.7 2-D conduction model of 3 mm square silicon chamber on 5 mm square microheater

Comparing Figures 5.6 and 5.7, it is clear the dramatic affect changing the reaction chamber vessel material has on the speed of heating. The time scale on Figure 5.7 is different because of the very rapid heating that the model predicts. The time constant for a node at the middle top of the reaction volume in contact with the liquid was 0.01 seconds while the node at the upper corner of the reaction mixture in contact with the liquid had a time constant of 0.03 seconds. This is very small compared to the 2 second time constant of the polycarbonate chamber of identical dimensions.

The same chamber was analyzed to determine the speed at which a glass microchamber could be heated on the 5 mm square microheater. The thermal diffusivity of glass is 328×10^{-9} m^2/s while the thermal diffusivity of polycarbonate is 138×10^{-9} m^2/s. This means that the glass will heat up faster than polycarbonate. The analysis indicated that the time constant for a node at the upper corner of the reaction chamber was 1.1 seconds while a node at the top middle of the reaction mixture had a time constant of 0.9 seconds indicating a uniform reaction chamber temperature.

Glass capillaries have been used for PCR in convection thermocyclers (Loeffler, Henke et al. 2000). Glass capillaries have also been coated with indium tin oxide which served as both a heater and a temperature sensor. PCR was performed in ten minutes using this device (Meldrum, Evensen et al. 2000). A heat transfer model was made of a glass capillary on the microheater to determine the time constant of the system. A schematic of the model is shown in Figure 5.8.

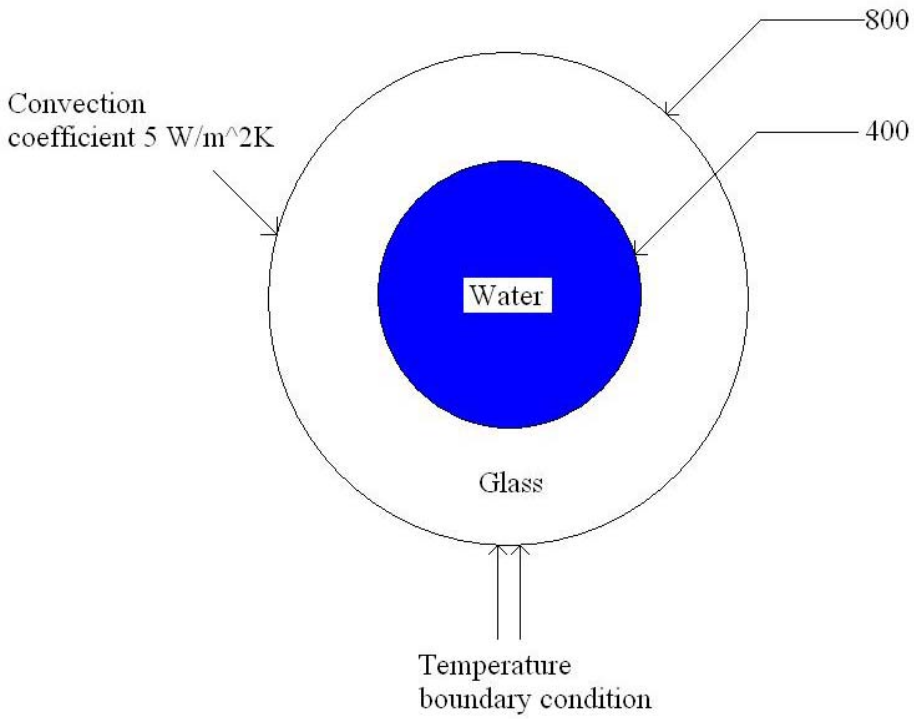

Figure 5.8 Schematic of 800 μm capillary on microheater

The capillary outer diameter was 800 μm with an inner diameter of 400 μm. The boundary condition around the outside of the capillary was assumed to be 5 W/m^2K except for at the bottom of the capillary where a 200 μm segment had a temperature boundary condition. The time constant for heating between 72 and 94 °C was 1.5 seconds for a node in the water area farthest from the heater. The time constant for this system lies in between the 3 mm square glass chamber and the polycarbonate chamber. The biggest difference between these chambers is in the cross section of the chamber. The glass capillary has a reaction chamber with a 0.13 mm^2 cross section area while the 3 mm square chamber has a cross sectional area of 0.75 mm^2. Even though the glass capillary reaction chamber has a smaller cross sectional area than the planar design, the time constants for both systems are comparable because planar design utilizes the heater surface better and minimizes thermal penetration depth.

The above analysis demonstrates that reaction volumes made of different materials with different sizes have different thermal time constants. The trend shows that smaller reaction volumes and smaller penetration depths aid in heating speed. Materials with higher thermal conductivities, such as silicon, perform much better than those with low thermal conductivity materials like polycarbonate and glass.

A complete PCR reaction consists of many thermal cycles with temperatures reaching as high as 94 °C. Liquid and air both expand, so it is necessary to know by how much they expand so the reaction volume may be filled appropriately and to understand how they should be sealed. PCR microchambers can be sealed with a drop of mineral or silicone oil or by bonding material over the top of the filling hole (Nagai, Murakami et al. 2000; Matsubara, Kerman et al. 2005). One possible polycarbonate reaction volume is shown in Figure 5.9.

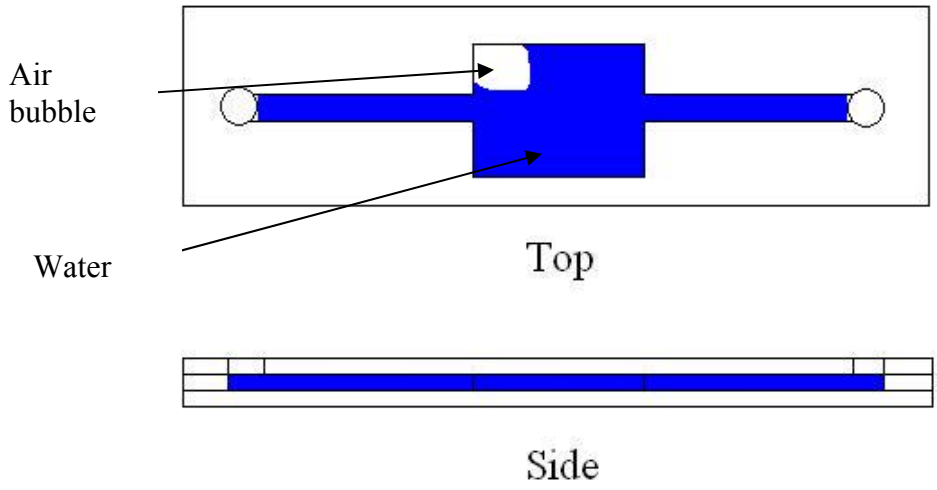

Figure 5.9 Polycarbonate reaction vessel thermally bonded from three 250 µm thick sheets

A reaction vessel of this type is made out of three layers of polycarbonate thermally bonded. The top layer has the filling holes, the middle layer contains the reaction vessel, and the bottom layer has no features and is meant to seal the reaction vessel. A reaction vessel of this type can be sealed with oil in the filling reservoirs or by bonding additional pieces of polycarbonate over the filling holes after filling. If the ends are sealed through polycarbonate bonding, the reaction vessel is closed and pressure may increase in the volume during heating.

The central reaction area of a polycarbonate chamber sealed at the ends of the type shown in Figure 5.9 was modeled. The model assumed that the system was closed and rigid, that the air in the reaction chamber is an ideal gas mixture of air saturated with water vapor, and that no new air bubbles arise in the reaction mixture. The governing equations of this model are given in Table 5.1 along with a description of the model.

Table 5.1 Model to predict pressure in sealed two-phase system

Physical Meaning	**Equation (written as EES code)**	**Equation Number**
Total volume sum of vapor and liquid	$V_{tot} = V_v + V_l$	5.1
Air component is ideal gas	$m_{air} = \frac{P_{air} V_v}{R_{air} T}$	5.2
Vapor pressure of water	$P_w = pressure(Water, T_{amb}, x = 1)$	5.3
Water vapor is ideal gas	$m_{wv} = \frac{P_{wv} V_v}{R_{water} T}$	5.4
Liquid volume	$m_{wl} = \frac{V_l}{volume(Water, T = T_{amb}, x = 0)}$	5.5
Mass of water	$m_w = m_{wv} + m_w$	5.6
Total pressure sum of partial pressures	$P = P_w + P_{air}$	5.7

where V refers to volume, P is pressure, R is the universal gas constant divided by the molecular weight of air or water as specified by the subscript, m is the mass, T is temperature, and x is vapor quality. The subscripts are defined as follows: w refers to water, wl refers to liquid water, wv is the water vapor, i is an initial value, air refers to the air-water vapor mixture in the chamber, and tot is a total amount. *Pressure* and *volume* are EES functions that return the pressure and specific volume of water at the indicated temperatures and qualities.

The model was run for temperatures between ambient and 100 °C. The volumes used correspond to a reaction vessel measuring 5 mm square with a height of 250 µm. The reaction vessel was filled with 4.2 µL of water with a 2 µL air bubble. The initial pressure inside the reaction vessel was 1 atm. Pressure increased in the reaction chamber as shown in Figure 5.10.

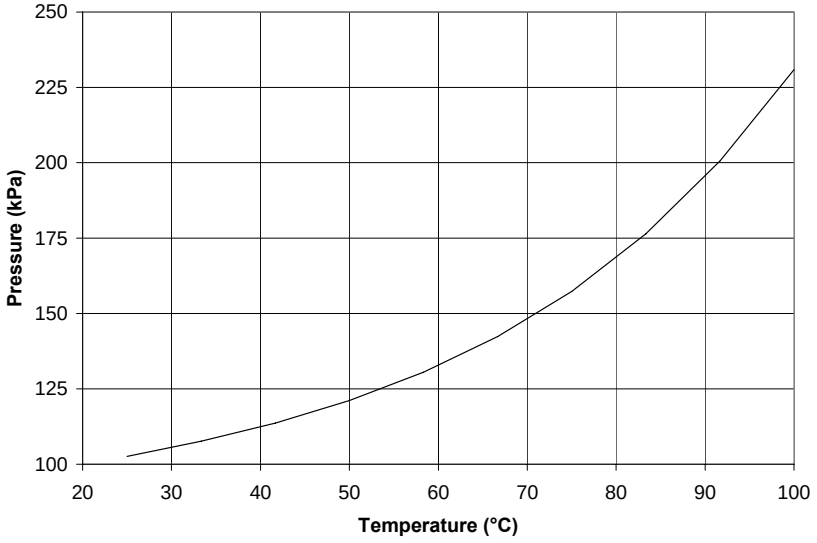

Figure 5.10 Predicted pressure rise inside closed reaction vessel with water and 33% of the volume filled with air

The predicted pressure at 95 °C is 210 kPa, or a gauge pressure of 110 kPa. A typical cyanoacrylate glue (often called super glue) has a polycarbonate bonding strength of 5000 kPa (Loctite 2000). A gauge pressure of 110 kPa would create a 2.2 N force on a circular filling hole of diameter 2 mm. Assuming that the cyanoacrylate is applied to an area of 9 mm^2, a pressure of 244 kPa would be present in the glued region. This value is well below the polycarbonate bonding strength for cyanoacrylate making it feasible to use cyanoacrylate to bond the cover when considering pressure only.

This model also shows that an air bubble present in the reaction vessel should also shrink as a result of the expanding water. A graph depicting this behavior is shown in Figure 5.11.

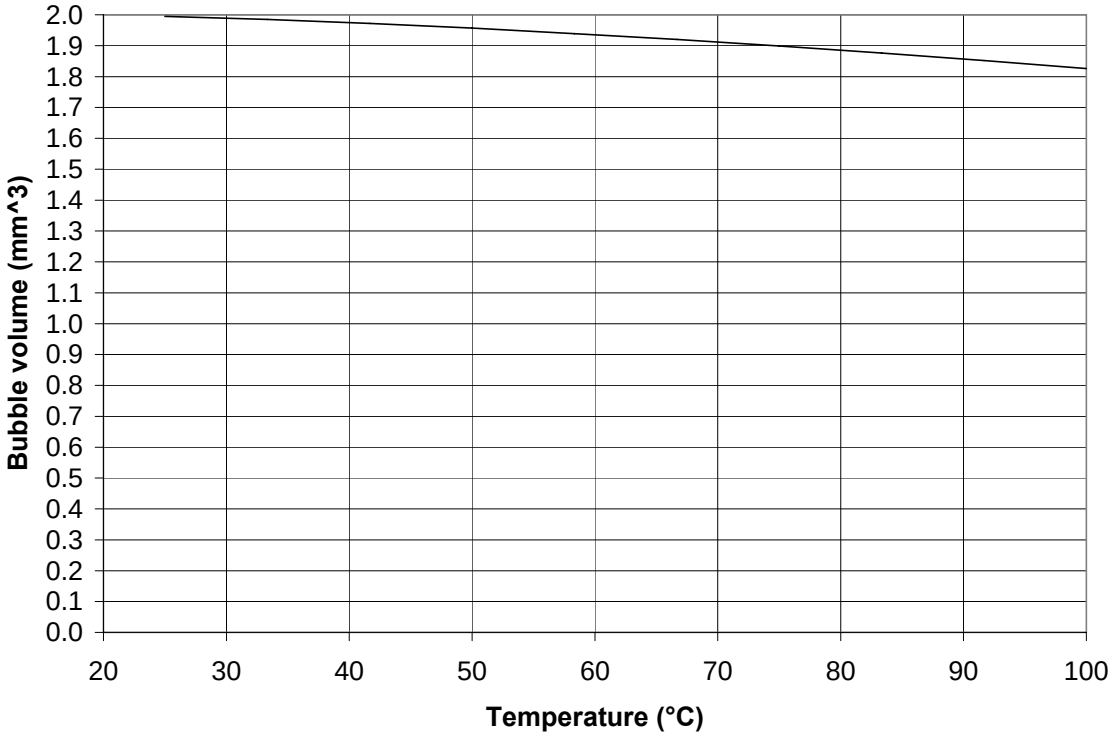

Figure 5.11 Predicted bubble volume inside closed reaction vessel with water and 33% of the volume filled with air

5.2 Microchamber fabrication equipment and techniques

Thermally bonded polycarbonate chambers of the type shown in Figure 5.12 were fabricated. 250 µm or 125 µm thick polycarbonate film was used. The chamber profiles were drawn in Corel Draw and then cut into the polycarbonate using a PII-30 vinyl cutter from a company called GCC. The cutter was unable to cut all the way through the polycarbonate so it was necessary to complete the cutting with a razor blade. The individual polycarbonate pieces were then rinsed with isopropanol and thermally bonded in an oven. The polycarbonate was sandwiched between two slabs of metal coated with Teflon. The assembly was clamped together using a spring loaded clip. The assembly was placed in the oven at 163 °C for 15 minutes and then removed. The chamber was removed from the clamp four minutes later. The chambers were sealed with acetone, methyl ethyl ketone, methylene chloride, or cyanoacrylate and polycarbonate.

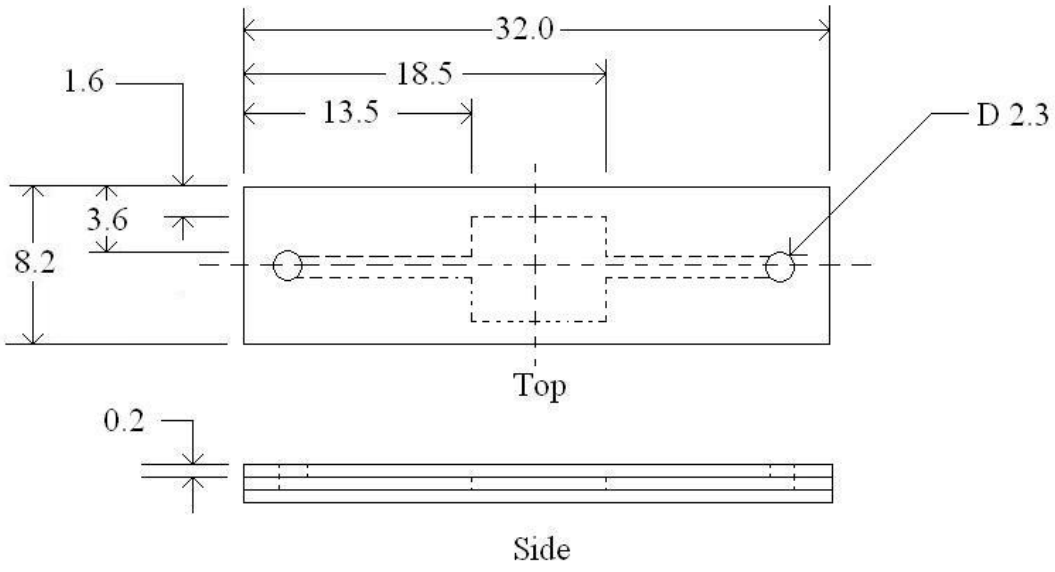

Figure 5.12 Polycarbonate chamber fabricated from three 250 µm thick sections. All dimension in mm

This particular chamber has a 5 mm square reaction chamber with 1 mm wide filling capillaries. The reaction volume of this chamber is 6.2 µL. Polycarbonate reaction vessels of this type were also fabricated with a 3 mm square reaction chamber. These chambers had a reaction volume of 2.2 µL.

Chambers with an alternative design were made by drilling into a 2 mm thick sheet of Hyzod polycarbonate from Sheffield Plastics, Inc. A Dremel Multipro model 395 was mounted in a Craftsman model 572.530320 drill press stand. A 3 mm diameter router bit was used to create the profiles. Some chambers were sealed by placing a drop of mineral oil on top of them. The mineral oil used was supplied by Biomerieux, part number 70100. A schematic of one of these chambers is shown in Figure 5.13.

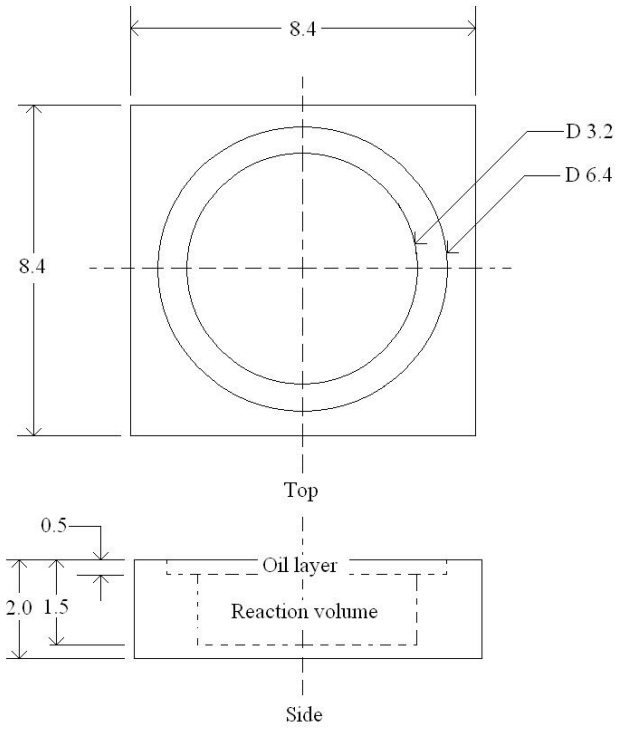

Figure 5.13 Countersunk polycarbonate chambers created with router bit

The polycarbonate chambers shown above were designed to put the PCR reaction volume in the lower section. The thin layer surrounding the reaction volume was intended as an oil layer. The purpose of the oil was to prevent solution evaporation.

Polycarbonate chambers of the type shown in Figure 5.13 were made hydrophilic using an oxygen plasma etch in a Trion Technology minilock reactive ion etcher. The polycarbonate was first rinsed with isopropanol and deionized water. The polycarbonate pieces were than placed on a Thermolyne type 1900 hot plate with Taylor temperature controller, model 9940 at 110 °C for ten minutes. The RIE was set to 125 W with a pressure of 250 mTorr and an oxygen flow rate of 100 sccm. The oil reservoir was made hydrophobic after RIE treatment by wiping it with isopropanol.

Polycarbonate was also made hydrophilic by using a portable UV light source. The light source was a Spectroline UV lamp, model UV-4BSW from Spectronics Corporation. The bulb used in this device emitted UV light at 254 nm.

Glass capillaries were also used as a reaction volume that had the potential for rapid thermal cycling. The glass capillaries had an outer diameter of 890 μm with an inside diameter of 400 μm. The capillaries were supplied by Drummond Scientific Co., Broomall PA.

5.3 Microchamber testing

Polycarbonate chambers were the main focus of chamber manufacture. Two types of polycarbonate chambers were tested. The first type was the countersunk chamber discussed earlier. The second type was the thermally bonded polycarbonate chamber. Different methods were used to attempt to seal the thermally bonded

polycarbonate. Glass capillaries were also studied to determine their effectiveness for rapid PCR thermocycling.

5.3.1 Countersunk polycarbonate chambers

Countersunk polycarbonate chambers were tested. The testing of these chambers was done on the thermoelectric cooler (TEC) with an oil layer on top of the water with blue food coloring. The testing involved a simulated PCR cycle consisting of an initial six minute heating period at 95 °C and 30 cycles of PCR with 60 seconds at each temperature and a final elongation step of 5 minutes at 72 °C. Untreated polycarbonate chambers were tested. The chambers were simply drilled and then tested. Untreated drilled polycarbonate wells exhibited total evaporation of the water. Large air bubbles formed within the liquid in the chambers and eventually, all of the reaction mixture would evaporate. A picture of these bubbles is shown in Figure 5.14.

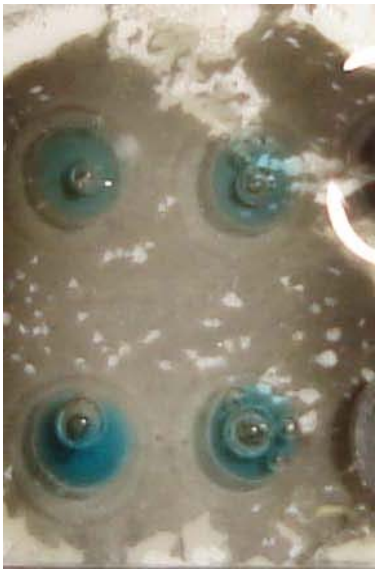

Figure 5.14 Bubble formation in untreated polycarbonate chambers covered with mineral oil

The bubbles would first start to form in independent locations and then coalesce into one large bubble. These bubbles seemed to displace the oil allowing the water to evaporate.

The bubbles were assumed to be from trapped air on the polycarbonate surface. It is noted that glass vessels were tested (larger geometry) similarly and no air bubbles were observed. One of the differences between glass and polycarbonate is that glass is hydrophilic while polycarbonate is hydrophobic. Attempts were made to make the polycarbonate chambers hydrophilic for this reason. The first attempts at making polycarbonate hydrophilic were with an O_2 plasma etch. Different reactive ion etch powers were used to determine the optimal power. A picture showing the results of these tests is shown in Figure 5.15.

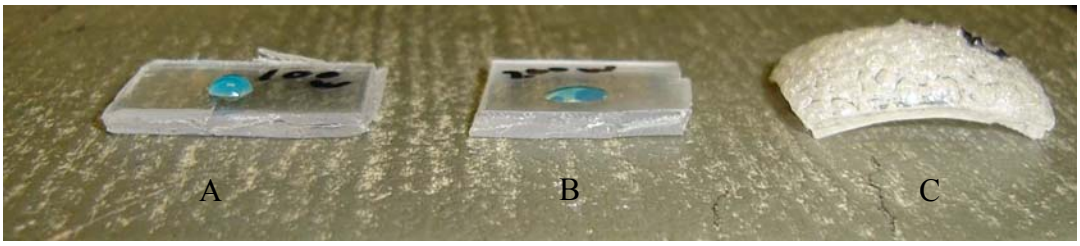

Figure 5.15 2 mm thick polycarbontate after O_2 plasma etch at A)100 W, B) 200 W, C) 250 W

The 100 W sample showed a decreased contact angle versus untreated polycarbonate with no deformation of the sample. The water on the surface of the 200 W sample was almost flat to the surface as shown in Figure 5.15. The 200 W case had slight deformation. The 250 W case showed significant deformation. Further testing showed that the optimal level for O_2 plasma treatment of a 2 mm thick polycarbonate sample using the RIE mentioned in the fabrication equipment section was 125 W based on physical distortion and water contact angle.

O_2 plasma etching was done on the countersunk polycarbonate chambers. After treatment the oil layer reservoir surface was wiped with isopropanol to remove the surface charge on that area. This led to a hydrophilic reaction volume and a hydrophobic oil reservoir. The purpose of this was to isolate the water in the bottom of the chamber. These chambers allowed a simulated PCR cycle to be run in the chambers without any observed evaporation. Bubbles still appeared in the solution, but they did not coalesce nor disturb the oil layer as they did in the untreated polycarbonate case.

5.3.2 Glass capillaries

Glass capillaries were used frequently for PCR in this effort because it was found that glass gave more consistent results than polycarbonate. Glass capillaries with a 400 μm inside diameter and an outside diameter of 890 μm proved to be very effective vessels for PCR. They could easily be filled with PCR solution and capped with oil through capillary action. There were never any problems with evaporation with these chambers when heating on the TEC or microheater. The time constant of glass capillaries filled with ethylene glycol was similar to those predicted by the heat transfer model described in Section 5.1. Ethylene glycol was used for this test because it has a boiling point of 197 °C. This allowed the capillary to be filled without having to seal the ends with oil. The thermal diffusivity of ethylene glycol is 93 x 10^{-9} m^2/s compared with 145 x 10^{-9} m^2/s for water. This means that ethylene glycol will respond to changes in temperature slower than water. Heat transfer analysis showed that capillaries filled with water and capillaries filled with ethylene glycol should perform similarly. A graph showing the performance of a glass capillary on the microheater is shown in Figure 5.16.

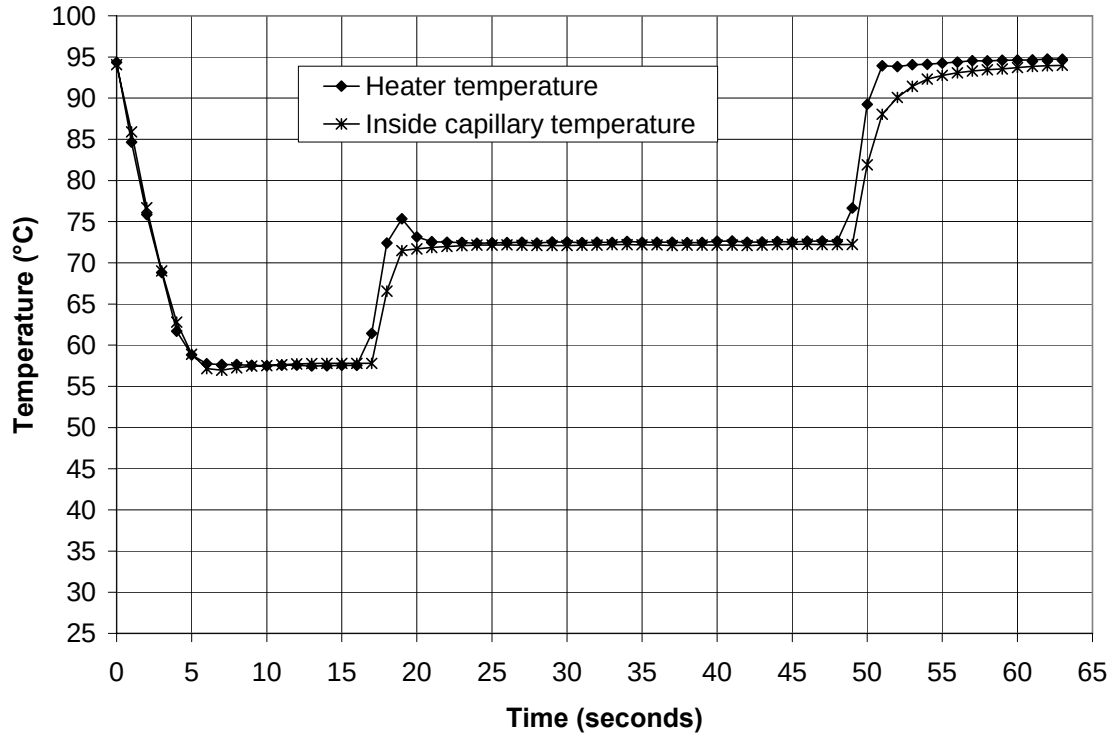

Figure 5.16 PCR cycle showing 5 mm square microfabricated heater and temperature inside a 400 μm inside diameter glass capillary filled with ethylene glycol

A thermocouple was inserted into the glass capillary filled with ethylene glycol to obtain the inside capillary temperature. The capillary temperature matches the heater temperature very closely during cooling. During heating from 72 to 95 °C the time constant of the heater is 1 second while the time constant for the capillary was 3 seconds. This is similar to the calculated time constant of 1.5 seconds obtained in the 2-D analysis which was obtained with a temperature step input.

5.3.3 Thermally bonded polycarbonate chambers

Thermally bonded polycarbonate chambers of the type shown in Figure 5.12 consisting of three 250 μm thick layers were tested on the microheater. The first

chamber tested was a chamber that had a 5 x 5 mm reaction chamber. The reaction chamber volume was 6.2 μL. The chamber was filled with ethylene glycol and the capillary channel was cut off at a point just before the square reaction chamber so a thermocouple could easily be inserted into the chamber. A clamp on the heater setup held the test section securely in place. The clamp was made of polycarbonate and was off of the heated portion of the chamber. Grease was placed in between the heater and the polycarbonate surface to enhance heat transfer. The results of that test are shown in Figure 5.17.

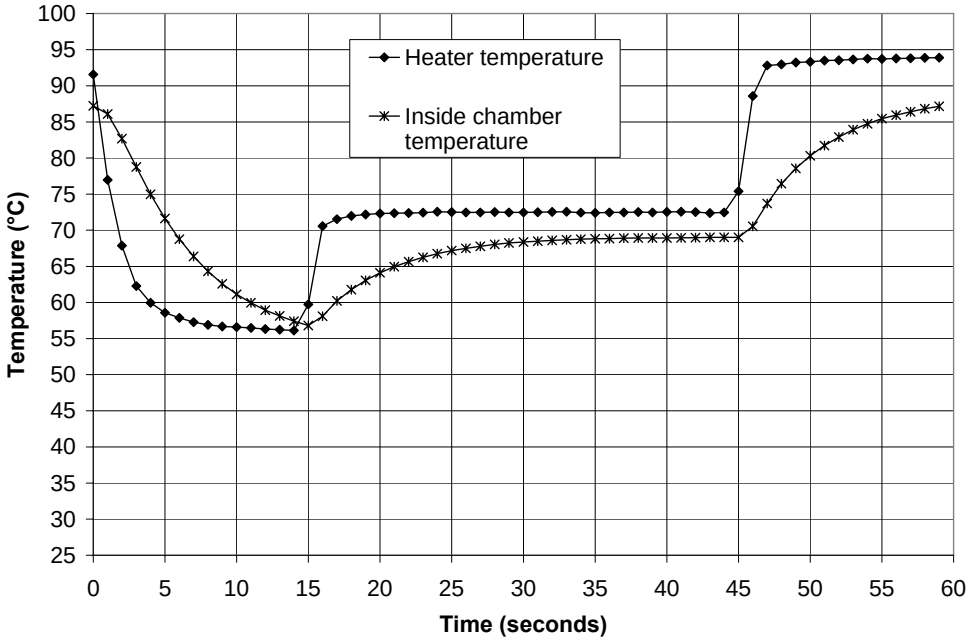

Figure 5.17 PCR cycle showing 5 mm square microfabricated heater and temperature inside a 5 mm square polycarbonate reaction volume filled with ethylene glycol

When the heater temperature was at 72 °C, the temperature inside the chamber stabilized at 68 °C as shown in Figure 5.17. This is indicative of a thermal resistance between the heater and the thermocouple. The time constant for heating between the 72 and 94 °C setpoint for the reaction chamber was ten seconds, which is much larger than the 2.5 – 4

seconds calculated with the FEA model. This poor performance is attributed to poor thermal contact between the chamber surface and the heater.

A chamber was tested that was made by thermally bonding three 250 μm thick pieces of polycarbonate. This chamber only had a central reaction chamber of 3 x 3 mm, however. The volume of the central reaction chamber was 2.2 μL. This chamber was placed onto the microheater in the exact same way as the 5 x 5 mm chamber. The temperature inside the chamber was recorded and is shown in Figure 5.18.

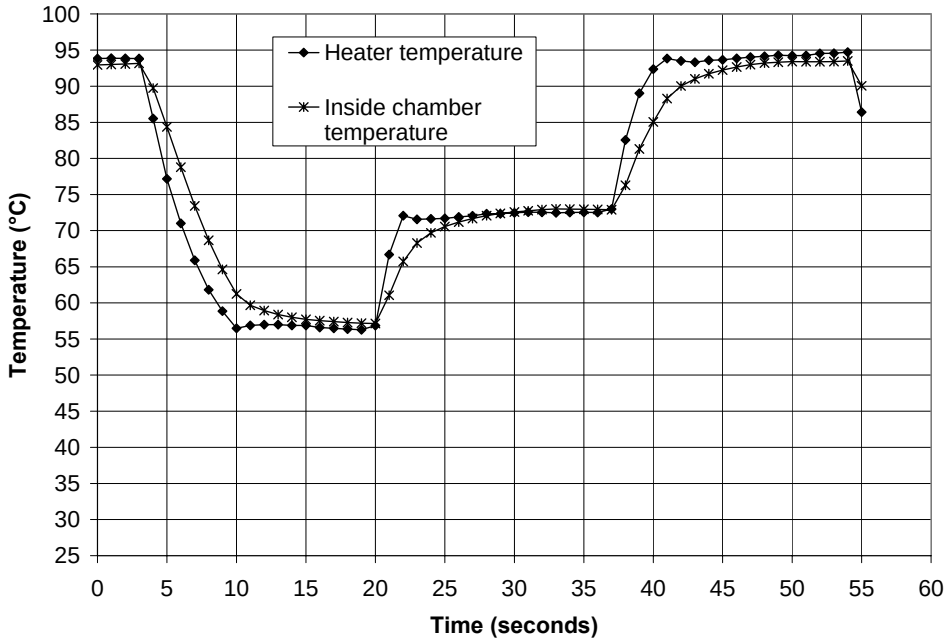

Figure 5.18 Simulated PCR cycle showing 5 mm square microfabricated heater and temperature inside a 3 mm square polycarbonate reaction volume filled with ethylene glycol

The 3 x 3 mm polycarbonate chamber followed the heater temperature closer than the 5 x 5 mm chamber. The time constant for heating between 72 and 94 °C for the 3 x 3 mm chamber was 3 seconds. The time constant of the heater itself was 1.5 seconds as shown

in Figure 5.18. This value is comparable with the 2 second time constant calculated with the conduction analysis done with a step temperature input.

A thermally bonded microchamber was tested that had reaction chamber 3 mm square with a 125 μm thick polycarbonate section bonded to the top and bottom of the 250 μm thick middle section. The 125 μm thick sections were in place of the 250 μm thick sections that were bonded to the top and bottom in prior experiments. The purpose of the experiment was to see if having a thinner polycarbonate section on the bottom of the chamber would increase the heat transfer to the chamber. The chamber was once again filled with ethylene glycol and a thermocouple was inserted into the reaction chamber. The chamber was clamped to the microheater. The results of this test are shown in Figure 5.19. The time constant for the chamber during heating from 72 to 94 °C was 3 seconds while the time constant for the heater was 1.2 seconds. This value is equal to the time constant of the same chamber with a 250 μm thick top and bottom section.

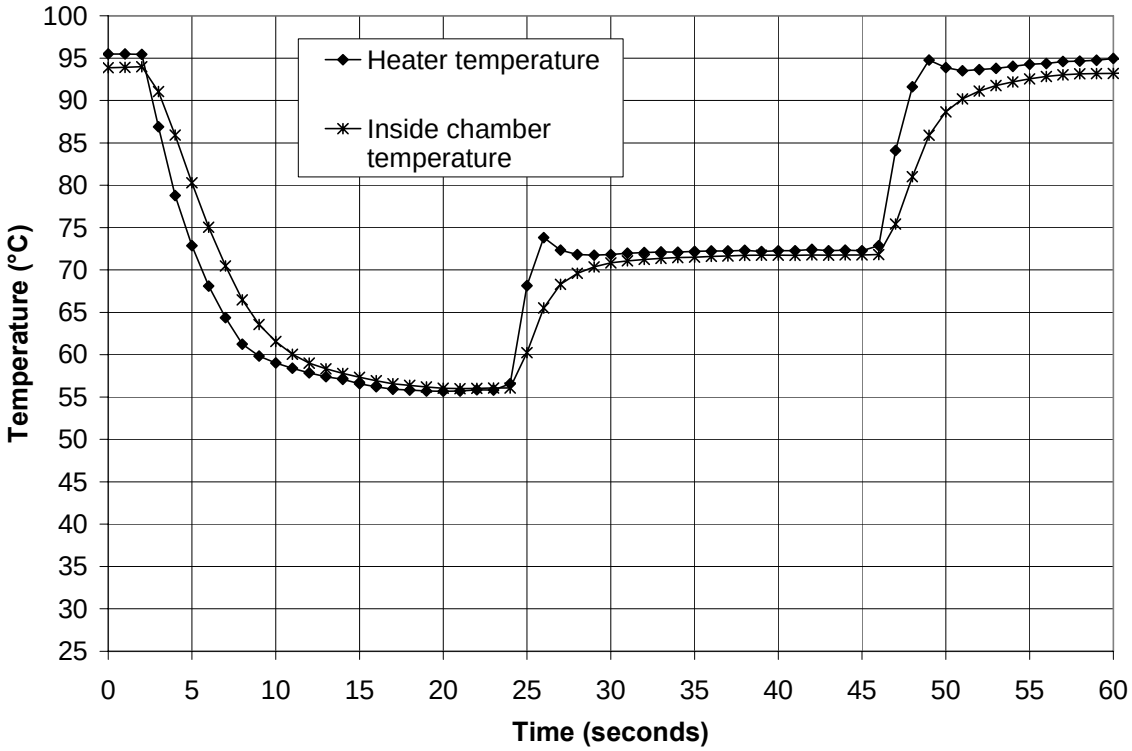

Figure 5.19 Simulated PCR cycle showing 5 mm square microfabricated heater and temperature inside a 3 mm square polycarbonate reaction volume with a 125 µm thick top and bottom section filled with ethylene glycol

A 3 x 3 mm reaction chamber 250 µm thick with a 250 µm thick polycarbonate section bonded to the top and a 125 µm thick section bonded to the bottom was tested to determine if this variation would perform better than the case with a 125 µm thick sheet of polycarbonate bonded to the top and bottom. The performance of this chamber is shown in Figure 5.20.

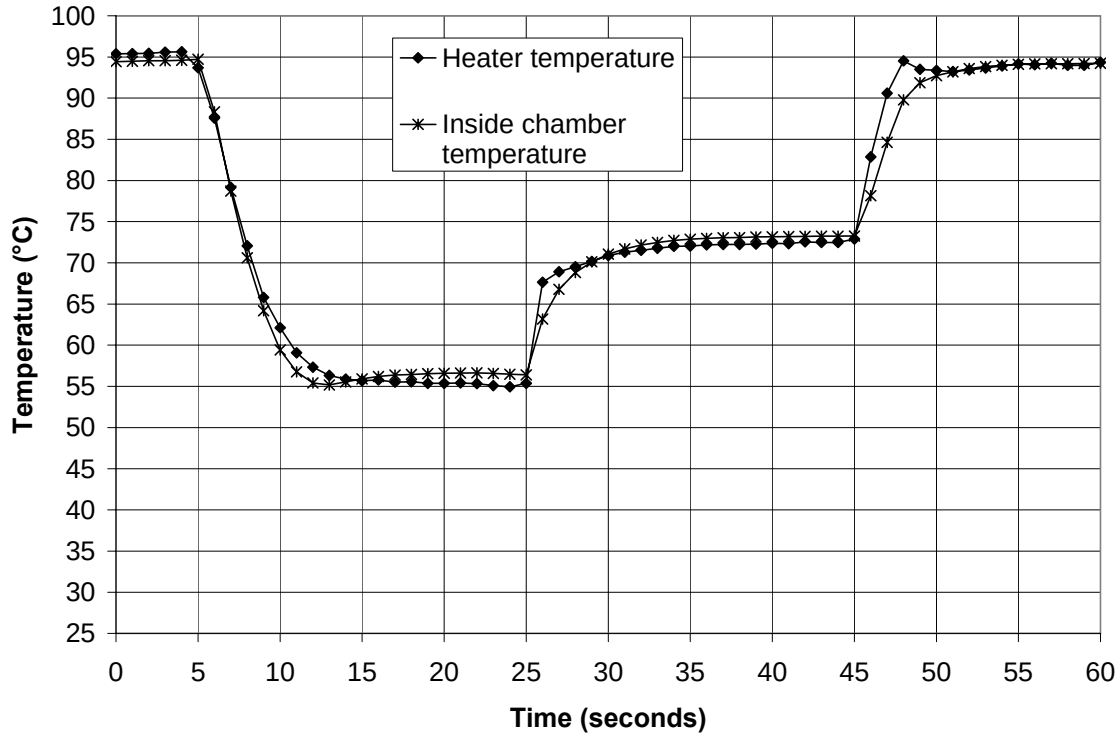

Figure 5.20 Simulated PCR cycle showing 5 mm square microfabricated heater and temperature inside a 3 mm square polycarbonate reaction volume with a 125 μm thick bottom section and a 250 μm thick top section filled with ethylene glycol

The time constant for the reaction chamber during heating between 72 and 94 °C for this case was 2 seconds. The performance of this chamber is superior to any of the chambers tested above. This is clearly seen by comparing the graphs from all of the above analysis and noting the correlation between the heater temperature and the temperature inside the chamber. The microheater showed poor control at the 72 °C setpoint in this case.

5.3.3.1 Thermally bonded polycarbonate chamber sealing

A thermally bonded polycarbonate chamber with a 3 x 3 mm reaction chamber with no sealing on the ends was tested on the microheater to assess its behavior. This

chamber was filled and placed on the microheater at 95 °C. The fluid was immediately pushed out of the central chamber and out to the filling holes.

A thermally bonded polycarbonate chamber with a 3 x 3 mm reaction chamber was sealed with polycarbonate and cyanoacrylate. The surface of the chamber was first cleaned with isopropanol after filling with a 5 % ethylene glycol and water solution dyed blue. Two small pieces of 250 μm thick polycarbonate were cut and bonded to the chamber using cyanoacrylate. The assembly was then placed into a clamp for 5 minutes to strengthen the bond. The chamber was then placed onto the microheater at 95 °C for 600 seconds, 30 PCR temperature cycles with 20 seconds at each temperature, and 300 seconds at 72 °C. The fluid in the central reaction volume was not immediately expelled. An air bubble did form in the middle of the reaction volume however, and did grow. The air bubble initially in the chamber occupied 20 % of the volume and was located on the edge of the chamber. The filling capillaries were completely full for this test. The bubble appeared to grow over the course of the test and upon completion occupied 30 % of the volume and was centrally located. This was problematic because the goal is to keep the PCR solution in the PCR chamber

One of the 3 x 3 mm square polycarbonate reaction chambers was inserted into a vacuum chamber for ten hours prior to filling to assess the effect on bubble formation in the chamber. The chamber was filled with water and sealed with cyanoacrylate. A small air bubble existed in the reaction chamber prior to thermal cycling. The capillaries leading up to the reaction chamber were filled only halfway. The fluid in the reaction chamber was immediately pushed out into the filling capillaries upon placing on the microheater. The difference between this test and the prior one is that the capillaries in

this case were only partially filled while the capillaries in the above case were completely full. This indicates that it is important for this configuration to have the filling capillaries completely full.

Another polycarbonate chamber that was not placed into the vacuum chamber was filled with water. The reaction chamber was filled such that only a small bubble existed in the reaction chamber. The filling capillaries were completely filled with water. The filling holes were then sealed with polycarbonate/cyanoacrylate and the chamber was placed onto the microheater. The fluid in the reaction chamber was not immediately expelled. The chamber was heated at 95 °C for 10 minutes, cycled with 20 second time intervals 30 times, and then heated at 72 °C for 5 minutes. The fluid volume in the reaction chamber decreased during heating at 95 °C while the vapor bubble expanded. During cooling the opposite happened. The volume of fluid in the central reaction chamber appeared to be the same as before thermal cycling after the test. This test showed that a completely full polycarbonate chamber with water could be sealed with polycarbonate and cyanoacrylate.

A polycarbonate chamber of the same type was filled with ethylene glycol to determine the mechanism of bubble formation. Ethylene glycol has a much higher boiling point then water. If the bubbles in the reaction chamber were due to air trapped between the fluid and the polycarbonate, then they should also appear in the ethylene glycol. The chamber was placed onto the microheater at 95 °C. The air bubbles in the reaction chamber did appear.

The results of these tests indicate that trapped air on the polycarbonate surface is liberated during heating. The air forms bubbles that tend to push the fluid in the reaction

chamber. These air bubbles exert a pressure in addition to the pressure created by the air bubble already present in the chamber and the expansion of the fluid. This can be detrimental because the goal is to keep the reaction volume in a stationary location. The best case scenario was for a polycarbonate chamber that had the filling capillaries completely full and a small bubble in the reaction chamber. Glass capillaries do not exhibit this behavior perhaps because of their hydrophilic nature. The water is attracted to the surface and hence expels the air from the capillary upon filling. Fluid placed in them will stay in them during heating as long as they are sealed with mineral oil.

6. SUMMARY, CONCLUSIONS, AND FUTURE WORK

6.1 Summary

The primary objective of this work was to investigate alternative system designs to achieve high speed PCR. A secondary objective was to minimize power consumption. Each of the design alternatives tested had a unique set of features that may be useful for a particular application. Since the focus was on speed and power consumption, much of the description focuses on these parameters. A summary comparison of all of the designs is given in Table 6.1. The microheater was found to yield the fastest cycling with the lowest power consumption, but due to a series of problems with vessel design, definitive PCR results were not obtained in this configuration.

Table 6.1 Comparison of thermocyclers

Heater configuration	Max heating rate (K/s)	Average heating rate (K/s)	Max cooling rate (K/s)	Average cooling rate (K/s)	Max power consumption (W)	Average power over a cycle (W)
TEC with cooling fan	5.2	1.8	6.6	5.8	23.7	11.3
TEC without cooling fan	5.8	2	5.2	4.3	23.7	7.9
Techne themocycler	3.6	2.8	2.0	1.4	264	145
Single fan convective thermocycler	2.0	1.2	1.8	1.2	604	255
Double fan convective thermocycler	4.2	2.6	7.9	5.3	1371	645
Microheater without heat sink	16.7	9.2	7.8	4.0	2.4	0.5
Microheater with heat sink	13.4	11.0	14.6	8.0	2.4	1.0

A listing of the major tasks and accomplishments of the work is given in Sections 6.1.1-6.1.3.

6.1.1 Testing of Peltier thermocyclers

- An independent thermoelectric cooler was tested. Two configurations of this device were tested. The two configurations tested differed in whether the fan on the heat sink was on or off.
- The heat flux produced by the TEC was modeled using the lumped capacitance method. The model was verified by putting the heat flux results into a 2-D heat conduction program.
- A commercially available Peltier thermocycler was tested to assess the heating and cooling rates and power consumption.
- The commercial Peltier device was used to study nucleotide insertion rate and PCR in glass capillaries.

6.1.2 Testing of convective thermocyclers

- Two different convective thermocyclers were tested. One of the convective thermocyclers tested had a single fan. The second convective thermocycler tested had two fans. One of the fans was responsible for flowing air over the heated coil in heating mode. The second fan was used to introduce a cool, high velocity air stream into the vent tube.
- Placing mixing walls into the vent tube and wrapping the outside with insulation provided the most uniform temperature within the vent tube.
- The air velocity in the convective thermocyclers was determined using a control volume approach.

- The lumped capacitance method and a 2-D heat transfer package were used to model the behavior of a polypropylene PCR reaction tube with 10 μL of water in it in the convective thermocycler.
- The lumped capacitance model was used to investigate the behavior of reaction vessels of different geometries and materials in the convective thermal cycler. The effect of different air velocities was also examined.

6.1.3 Testing of a microheater thermocycler

- Microheaters were designed and fabricated based on the power requirements necessary to heat a reaction volume greater than 6 K/s.
- A Wheatstone bridge control system was designed and tested for the microheater.
- Heat treatment was done on the microheater to stabilize the resistance.
- The microheaters were tested to assess the performance under two different conditions. The first condition was with fan cooling only with the heater suspended in air. The second condition was with the heater mounted on top of an aluminum heat sink and with fan cooling.
- 2-D heat transfer software was used to analyze the performance of thermally bonded polycarbonate chambers on the 5 mm square microheater filled with water.
- The pressure rise inside a sealed 5 mm square rigid chamber of depth 250 μm filled 67 % with water and 33 % with air was modeled during heating from ambient to 94 °C.

- Two different types of polycarbonate reaction vessels were tested to determine their efficacy for the PCR reaction. One type of polycarbonate reaction vessel consisted of three sheets of polycarbonate thermally bonded. The other type of polycarbonate chamber was fabricated by drilling a hole into a 2 mm thick sheet of polycarbonate. Some of these chambers were treated with an oxygen plasma etch.

6.2 Conclusions

- PCR is influenced by the ability of the heater to heat the reaction vessel. It was shown in Sections 2.2, 2.4, 3.2, and 4.5 that different heaters have different heating and cooling rates. The average heating rate for the air in convective devices or the surface of the heater for heat conduction devices varied from 1.2 K/s for the single fan convective thermocycler to 11.0 K/s for the microheater with heat sink. The average cooling rate varied from 1.2 K/s for the convective thermocycler to 8.0 K/s for the microheater mounted on a heat sink with fan cooling. The air in the single fan convective thermocycler takes 33 seconds to cool from 94 to 54 °C. The surface of the microheater can cool from 94 to 54 °C in 5 seconds, based on the average cooling rate stated above. The single fan convective thermocycler would spend 16 minutes cooling the air to the setpoint over the course of a 30 cycle PCR reaction while the microheater would only spend 2 minutes cooling to the setpoint over the course of a 30 cycle PCR reaction. This demonstrates the effect that heating and cooling rates have on the time to complete a PCR reaction.

- The results of the modeling of a constant wall thickness polypropylene capillary in the convective thermocycler filled with water shows that the time constant increases from 5 seconds for an 890 μm diameter capillary to 65 seconds for a cylinder diameter of 5 mm with the same wall thickness and air velocity of 1.2 m/s as shown in Section 3.3. 2.12 mm outside diameter spherical reaction vessels made of glass containing an equivalent volume of water and an equivalent wall thickness to a cylindrical reaction vessel of outside diameter 890 μm and inside diameter 400 μm were shown to have time constants 4 times larger then the cylindrical case because of the larger surface area to volume ratio of the cylinder as shown in Section 3.3. The analysis showed that reaction volumes of different geometries for the convective thermocycler have different time constants. Time constants for reaction chambers can be minimized by using capillaries with outside diameters on the order of 900 μm. The advantage of using a convective thermocycler is that different geometry reaction vessels may easily be placed into them.
- Analysis done in Section 5.1 with 2-D finite element analysis showed that the time constant for two nodes, one in the corner and one at the midline, in contact with the reaction fluid at the top of a 5 mm square thermally bonded polycarbonate chamber fabricated from three 250 μm thick sheets centered on the 5 mm square microheater were 4 seconds and 2.5 seconds, respectively. The time constant for two nodes, one in the corner and one at the midline, in contact with the reaction fluid at the top of a 3 mm square thermally bonded polycarbonate chamber fabricated from three 250 μm thick sheets centered on the 5 mm square

microheater were 2.5 seconds and 2 seconds, respectively. Based on these results it was concluded that square microchambers should have perimeters that lie inside of the microheater for greater temperature uniformity.

- The time constant for two nodes, one in the corner and one at the midline, in contact with the reaction fluid at the top of a 3 mm square thermally bonded silicon chamber fabricated from three 250 μm thick sections centered on the 5 mm square microheater were 0.03 seconds and 0.01 seconds, respectively, as analyzed in Section 5.1 with a 2-D heat transfer program. Based on this work, it was concluded that changing the material of the reaction vessel to a material with a higher thermal diffusivity decreased the time constant and provided for uniform heating.
- Based on the PCR time study in Section 2.4.3 it was concluded that the time limiting step in PCR is the polymerase nucleotide insertion rate. An 879 bp segment of DNA could not be copied with a 25 second elongation time and a denaturation and annealing time of 15 seconds. The 879 bp segment could be copied with a 30 second insertion rate, however. This led to the conclusion that the nucleotide insertion rate was 29 bp/s.
- The power consumption of an independent thermoelectric cooler used for PCR can be decreased by 30 % not using a cooling fan on the heat sink with a loss in average cooling of 1.5 K/s, based on the analysis done in Section 2.2. This would amount to 1 minute of time for a 30 cycle PCR reaction. Based on this analysis, the reduction in power consumption warrants not using the fan on the heat sink.

- Air heating rates for the double fan convective thermocycler built in this lab were comparable to the heating rate of the surface of the TEC and consumed 80 times more power on average based on the analysis done in Section 3.2. Convective thermocyclers of the type built in this lab are not capable of low power operation with high heating and cooling rates.
- The microheaters analyzed in Section 4.3.3 fabricated with liftoff and plastic masks suffered delamination. Platinum elements with 30 μm feature size deposited with a thickness of 1000 Å with a 150 Å chrome adhesion layer were pitted, especially at the edges, while 50 μm features were more uniform. The effective resistivity for the 30 μm elements was 3.6 x 10^{-7} Ω-m while the effective resistivity for the 50 μm elements was 2.7 x 10^{-7} Ω-m. The bulk resistivity of platinum is 1.0 x 10^{-7} Ω-m. Edge deformities and pitting influence the resistivity of the deposited platinum.
- A 13 hour heat treatment at 250 °C reduced the resistivity of the temperature probe from 2.7 x 10^{-7} Ω-m to 2.1 x 10-7 Ω-m based on the analysis in Section 4.4. Heat treatment of platinum heaters is necessary to stabilize the resistance.
- The average heating rate for the microheater was 4 times faster then any of the other thermal cycling devices tested as analyzed in Section 4.5. The average cooling rate was 1.5 times faster than any of the other devices tested. The average power for the microheater was 12 % of the power required by its nearest competitor. Microheaters are low power, fast cycling devices.
- The cooling rate of a microheater can be increased by mounting it on a heat sink with no change in average heating performance and double the average cooling

rate, based on the analysis in section 4.5.1. The average power required is doubled from 0.5 W to 1.0 W, however. A heat sink should be used to speed cooling of a microheater.

- The pressure rise during heating from ambient to 94 °C in a rigid, closed 5 mm square thermally bonded reaction volume of height 250 μm filled with water and an air bubble occupying 33% of the reaction volume approaches 100 kPa using an ideal gas mixture model discussed in Section 5.1. Sealing of the reaction vessel is possible with cyanoacrylate and polycarbonate.
- The pressure rise in a square reaction vessel with filling capillaries on the microheater pushes the water out of the main reaction chamber and out into the capillaries, discussed in Section 5.3.3. If the filling capillaries are completely full then some of the reaction will remain in the central reaction volume if the ends of the capillaries are securely sealed. The filling capillaries for the 5 mm square thermally bonded polycarbonate chamber comprised of a middle section of thickness 250 μm had a volume of 6 μL, equal to the central reaction chamber volume. This large volume provides an area for fluid to flow out into during heating unless they are completely full.
- Air bubble formation could be seen in a thermally bonded polycarbonate chamber filled with ethylene glycol on the microheater at 94 °C with the capillaries sealed with cyanoacrylate and polycarbonate, based on the observations described in Section 5.3.3. Air bubbles present in chambers filled with water expanded. Since ethylene glycol has a boiling point of 197 °C negligible ethylene glycol was evaporating. The other source of air in the chamber is air trapped between the

liquid and the chamber surface, air trapped in the polycarbonate, and air within the fluid.

- PCR was routinely completed in glass capillaries with only mineral oil for sealing, discussed in section 5.3.2. One difference between glass and polycarbonate is glass is hydrophilic. Hydrophilic glass capillaries can be sealed with mineral oil and thermal cycled.
- Chambers drilled into polycarbonate without any surface treatment filled with water and sealed with mineral oil did not perform well in cycling tests, while oxygen plasma treated polycarbonate wells filled with water and sealed with mineral oil were able to be thermal cycled without the solution evaporating based on observations discussed in Section 5.3.1. The failure mechanism for the untreated chambers was air bubbles rising to the surface and breaching the oil layer. The shape of the oil-water interface in the well was significantly impacted by the surface treatment. The treated well had a relatively uniform thickness of oil over a largely flat water surface. Oxygen plasma treated polycarbonate chambers sealed with mineral oil can be used for thermal cycling without complete evaporation of the sample.

6.3 Future work

The microheaters show promise for rapid thermal cycling. The microheaters fabricated suffered from delamination problems, especially smaller features. This problem may have been caused by contamination of the e-beam reaction chamber during

evaporation. The resistance of the heaters continued to change even after heat treatment at 250 °C for 13 hours. A longer, hotter heat treatment may be necessary.

The thermally bonded polycarbonate chambers did not perform well in holding the solution in the central reaction chamber. Polycarbonate is an attractive choice for making reaction vessels because it can be bonded in many different ways including tape, glue, and thermally. It can be cut and drilled very easily. Polycarbonate chambers with valves at the inlet and outlet to the chamber could be used to contain the reaction mixture. Another option is to make the volume of the capillaries leading up to the reaction vessel very small so there is no room for the reaction mixture to expand into. Very small filling holes should be utilized to minimize the pressure on the sealing method.

A detection method also needs to be implemented. It was shown in this thesis that it is possible to run PCR with detection reagents in the reaction volume. A detection scheme would involve an illumination source and a fluorescence detector.

A more complete system could be designed that consists of a chip that could be inserted into an array of microheaters. This would involve designing a structure to encase the microheaters and a system to position the reaction chambers on the microchambers and hold them there securely. The control system also needs to be miniaturized. A computer data acquisition unit is currently being used to collect data and provide control. It is possible to implement this control scheme with a microchip. The design needs to move away from plug in power supplies and toward portable battery power.

REFERENCES

Accuratus. (2005). "Accuratus aluminum oxide properties 96 % aluminum oxide." Retrieved March 6, 2005, from http://www.accuratus.com/alumox.html.

Alciatore, D. G. and M. B. Histand (2003). Introduction to Mechatronics and Measurement Systems, McGraw-Hill Higher Education.

Aryee, E., R. Bailey, et al. (2005). "Detection, quantification and genotyping of Herpes Simplex Virus in cervicovaginal secretions by real-time PCR: a cross sectional survey." Virology Journal **2**(61).

Benammar, M. and W. C. Maskell (1989). "Temperature control of thick-film printed heaters." Journal of Physical Engineering: Scientific Instrumentation **22**: 933-936.

Bilitewski, U., M. Genrich, et al. (2003). "Biochemical analysis with microfluidic systems." Analytical and Bionanalytical Chemistry **377**: 556-569.

Cadoret, J.-C., B. Rousseau, et al. (2005). "Cyclic Nucleotides, the Photosynthetic Apparatus and Response to a UV-B Stress in the Cyanobacterium *Synechocystis* sp. PCC 6803." Journal of Biological Chemistry.

Chen, J., W. Musundi, et al. (2005). "Electrokinetically Synchronized Polymerase Chain Reaction Microchip Fabricated in Polycarbonate." Analytical Chemistry **77**: 658-666.

D'Amico, M. L., V. Paiotta, et al. (2002). "A Kinetic Study of the Intercalation of Ethidium Bromide into Poly (A) Poly (U)." Journal of Physical Chemistry B **106**: 12635-12641.

Daniel, J. H., S. Iqbal, et al. (1998). "Silicon microchambers for DNA amplification." Sensors and Actuators A **71**: 81-88.

Draghici, S., P. Khatri, et al. (2005). Identification of genomic signatures for the design of assays for the detection and monitoring of anthrax threats. Pacific Symposium on Biocomputing 2005, World Scientific.

Efunda. (2005). "Efunda polymer material properties." Retrieved July 8, 2005, from http://www.efunda.com/materials/polymers/properties/polymer_datasheet.cfm?MajorID=PC&MinorID=11.

El-Ali, J., I. R. Perch-Nielsen, et al. (2004). "Simulation and Experimental Validation of a SU-8 Based PCR Thermocycler Chip with Integrated Heaters and Temperature Sensor." Sensors and Actuators A **110**: 3-10.

Fermer, C., P. Nilsson, et al. (2003). "Microwave-assisted high-speed PCR." European Journal of Pharmaceutical Sciences **18**: 129-132.

Giani, A., F. Mailly, et al. (2002). "Investigationof Pt/Ti bilayer on SiN_x/Si substrates for thermal sensor applications." Journal of Vacuum Science Technology A **20**(1): 112-116

.

Gill, P. (2005). "DNA as Evidence-The Technology of Identification." The New England Journal of Medicine **352**(26): 2669-2671.

Giordano, B. C., J. Ferrance, et al. (2001). "Polymerase Chain Reaction in Polymeric Microchips: DNA Amplification in Less than 240 Seconds." Analytical Biochemistry **291**: 124-132.

Goodfellow. (2005). "Goodfellow polypropylene material information." Retrieved June 16, 2005, from http://www.goodfellow.com/csp/active/STATIC/E/Polypropylene.HTML.

Gulliksen, A., L. A. Solli, et al. (2005). "Parallel nanoliter detection of cancer markers using polymer microchips." Lab on a Chip **5**: 416-420.

Halverson, R. M., M. W. MacIntyre, et al. (1982). "The Mechanism of Single-Step Liftoff with Chlorobenzene in a Diazo-Type Resist." IBM Journal of Research and Development **26**(5): 590-595.

Hindson, B. J., A. J. Makarewicz, et al. (2005). "APDS: the autonomous pathogen detection system." Biosensors and Bioelectronics **20**: 1925-1931.

Incropera, F. and D. DeWitt (1996). Fundamentals of Heat and Mass Transfer, John Wiley & Sons.

Kermekchiev, M. B., A. Tzekov, et al. (2003). "Cold-sensitive mutants of Taq DNA polymerase provide a hot start for PCR." Nucleic Acids Research **31**(21): 6139-6147.

Klintberg, L., M. Svedberg, et al. (2003). "Fabrication of a paraffin actuator using hot embossing of polycarbonate." Sensors and Actuators A **103**(3): 307-316.

Kopp, M. U., A. J. de Mello, et al. (1998). "Chemical Amplification: Continuous-Flow PCR on a Chip." Science **280**: 1046-1047.

Kovacs, G. (1998). Micromachined Transducers Sourcebook, McGraw-Hill.

Lane, S., J. Everman, et al. (2004). "Amplicon secondary structure prevents target hybridization to oligonucleotide microarrays." Biosensors and Bioelectronics **20**(4): 728-735.

Larsson, A. and H. Derand (2001). "Stability of Polycarbonate and Polystyrene Surfaces after Hydrophilization with High Intensity Oxygen RF Plasma." Journal of Colloid and Interface Science **246**: 214-221.

Lee, D. S., S. Ho Park, et al. (2004). "Bulk-micromachined submicroliter-volume PCR chip with very rapid thermal response and low power consumption." Lab on a Chip **4**: 401-407.

Lee, D. S., C. Y. Tsai, et al. (2004). "A new thermal cycling mechanism for effective polymerase chain reaction in microliter volumes." Microsystem Technologies **10**: 579-584.

LightCycler. (2005). "Technical Aspects of the LightCycler Instrument." Retrieved July 14, 2005, from http://www.roche-applied-science.com/sis/rtpcr/lightcycler/.

Liu, Y., D. Ganser, et al. (2001). "Microfabricated Polycarbonate CE Devices for DNA Analysis." Analytical Chemistry **73**(17): 4196-4201.

Liu, Y., C. Rauch, et al. (2002). "DNA Amplification and Hybridization Assays in Integrated Plastic Monolithic Devices." Analytical Chemistry **74**: 3063-6070.

Loctite. (2000). "Loctite Laboratory Data Sheet, Product 190848." Retrieved August 9, 2005.

Loeffler, J., N. Henke, et al. (2000). "Quantification of Fungal DNA by Using Fluorescence Resonance Energy Transfer and the Light Cycler System." Journal of Clinical Microbiology **38**(2): 586-590.

Lourenco, M. J., J. M. Serra, et al. (1998). "Thin Film Characterization for High Temperature Applications." International Journal of Thermophysics **19**(4): 1253-1265.

Martin, P. M., D. W. Matson, et al. (1998). Fabrication of plastic microfluidic components. Conference on Microfluidics Devices and Systems, Santa Clara, CA, The International Society for Optical Engineering.

Matsubara, Y., K. Kerman, et al. (2004). "On-Chip Nanoliter-Volume Multiplex TaqMan Polymerase Chain Reaction from a Single Copy Based on Counting Fluorescence Released Microchambers." Analytical Chemistry **76**(21): 6434-6439.

Matsubara, Y., K. Kerman, et al. (2005). "Microchamber array based DNA quantification and specific sequence detection from a single copy via PCR in nanoliter volumes." Biosensors and Bioelectronics **20**: 1482-1490.

Melcor. (2005). "Melcor thermal solutions." Retrieved July 23, 2005, from http://www.melcor.com/pdf/MTScat.pdf.

Meldrum, D., H. Evensen, et al. (2000). "Acapella-1K, A Capillary-Based Submicroliter Automated Fluid Handling System for Genome Analysis." Genome Research **10**(1): 95-104.

Moran, M. J. and H. N. Shapiro (1999). Fundamentals of Engineering Thermodynamics, John Wiley & Sons, Inc.

Nagai, H., Y. Murakami, et al. (2001). "Development of a microchamber array for picoliter PCR." Analytical Chemistry **73**(5): 1043-1047

Nagai, H., Y. Murakami, et al. (2000). "High-throughput PCR in silicon based microchamber array." Biosensors & Bioelectronics **16**: 1015-1019.

Nam, H.-M., V. Srinivasan, et al. (2005). "Application of SYBR green real-time PCR assay for specific detection of Salmonella spp. in dairy farm environmental samples." International Journal of Food Microbiology **102**: 161-171.

Nitsche, A., N. Steur, et al. (1999). "Different Real-Time PCR Formats Compared for the Quantitative Detection of Human Cytomegalovirus DNA." Clinical Chemistry **45**(11): 1932-1937.

Pyun, C.-H. and S.-M. Park (1985). Fluorescence Enhancement Mechanisms of Ethidium Bromide by DNA or DNA Base Molecules. The Electrochemical Society Extended Abstracts Fall Meeting, Las Vegas, NV, Electrochemical Society.

Rotron, C. (2005). "Comair Rotron Patriot AC fan." Retrieved July 5, 2005, from http://www.comairrotron.com/images/curves/patriotac3350.pdf.

Rottmayer, R. E. and R. W. Hoffman (1971). "Structure and Intrinsic Stress of Platinum Films." Journal of Vacuum Science Technology A **8**(1): 151-155.

Scheinert, P., B. Behrens, et al. (2005). "Optimizing DNA Amplification Protocols Using the Eppendorf Mastercycler." Retrieved July 6, 2005, from http://www.eppendorfna.com/applications/PCR_appl_protocolsMC.asp.

Selvaganapathy, P. R., E. T. Carlen, et al. (2003). "Recent Progress in Microfluidic Devices for Nucleic Acid and Antibody Assays." Proceedings of the IEEE **91**(6): 954-975.

Shoffner, M. A., J. Cheng, et al. (1996). "Chip PCR. I. Surface passivation of microfabricated silicon-glass chips for PCR." Nucleic Acids Research **24**(2): 375-379.

Vierstraete, A. (2004). "PCR: Polymerase Chain Reaction." Retrieved June 1, 2005, from http://users.ugent.be/~avierstr/principles/pcr.html.

Winter, M. (2005). "Web Elements Periodic Table." Retrieved July 14, 2005, from http://www.webelements.com.

Wittwer, C. T., G. C. Fillmore, et al. (1989). "Automated polymerase chain reaction in capillary tubes with hot air." Nucleic Acids Research **17**(11): 4353-4357.

Yang, J., Y. Liu, et al. (2002). "High sensitivity PCR assay in plastic micro reactors." Lab on a Chip **2**: 179-187.

Ye, M.-Y., X.-F. Yin, et al. (2005). "DNA separation with low-viscosity sieving matrix on microfabricated polycarbonate microfluidic chips." Analytical and Bionanalytical Chemistry **381**: 820-827.

Yoon, D. S., Y.-S. Lee, et al. (2002). "Precise temperature control and rapid thermal cycling in a micromachined DNA polymerase chain reaction." Journal of Micromechanics and Microengineering **12**(6): 813-823.

Zhao, Z., D. Cui, et al. (2002). "An integrated biochip design and fabrication." Proceedings of SPIE-The International Society for Optical Engineering **4936**: 321-326.

Zhao, Z., Z. Cui, et al. (2003). "Monolithically integrated PCR biochip for DNA amplification." Sensors and Actuators A **108**: 162-167.

Zou, Q., Y. Miao, et al. (2002). "Micro-Assembled Multi-Chamber Thermal Cycler for Low-Cost Reaction Chip Thermal Multiplexing." Sensors and Actuators A **102**: 114-121.